Topological Defects in High Density QCD and Other Strongly Interacting Systems

by

Kirk B. W. Buckley

B.Sc., Bishop's University, 1998
M.Sc., The University of British Columbia, 2000

A THESIS SUBMITTED IN PARTIAL FULFILMENT OF
THE REQUIREMENTS FOR THE DEGREE OF

DOCTOR OF PHILOSOPHY

in

THE FACULTY OF GRADUATE STUDIES

(Department of Physics and Astronomy)

We accept this thesis as conforming
to the required standard

THE UNIVERSITY OF BRITISH COLUMBIA

November 27, 2003

Abstract

In this thesis we will examine topological defects that arise in various physical contexts. The main theme of this thesis is the study of matter at high densities and low temperatures. This is important as these are the conditions that are realized in the interior of a neutron star. The first part of this thesis is devoted to the study of topological defects that appear in the color superconducting phase of high density QCD. We will show that unlike the Standard Model at zero density, the Standard Model at large densities supports various types of topological defects. In particular, we will assess the stability of the domain walls at intermediate densities. We will also show that there exists vortices that have a nonzero condensate trapped on the core. The consequence of the nonzero condensate is that it is possible to form stable loops of these strings called vortons. Next, we will examine matter at slightly smaller densities below the point where the color superconducting phase of QCD occurs, where the ground state consists of Cooper pairs of neutrons and Cooper pairs of protons. The presence of an electrically charged proton condensate leads to conventional BCS superconductivity. In this thesis we will demonstrate that the presence of a neutron condensate leads to type-I superconductivity, contrary to the standard picture that the interior of a neutron star exhibits type-II superconductivity. The final part

of this thesis will introduce vortons in the context high temperature superconductivity. These quasiparticles may be important in understanding the nature of the phase transition from the antiferromagnetic state to the superconducting state as the material is doped. In addition, the study of vortons in high temperature superconductivity provides an interesting connection between condensed matter physics and astrophysics/high density QCD.

Contents

Abstract ii

Contents iv

List of Figures vii

Preface viii

Acknowledgements ix

1 Introduction 1

1.1 Topological Defects: A Brief Introduction 4

1.1.1 Domain Walls 5

1.1.2 Strings 7

2 High Density QCD 11

2.1 The CFL phase of high density QCD 12

2.2 K^0-condensation in the CFL phase of high density QCD . . . 16

3 $U(1)_A$ Domain Walls in High Density QCD 20

3.1 Overview 20

3.2 The Effective Potential 21

3.3 Domain wall solutions 26
3.4 Stability analysis of domain walls 28
3.5 Conclusion 37

4 Superconducting K-Strings in High Density QCD 39
4.1 Overview 39
4.2 Superconducting K-strings 42
4.2.1 Topologically stable $U(1)$ strings in $CFL + K^0$ phase . 43
4.2.2 Unstable $SU(2)_I \times U(1)_Y \to U(1)$ strings in $CFL+K^0$ phase 45
4.2.3 K^+-condensation in the core of K^0-strings in $CFL + K^0$ phase 48
4.3 Conclusion 57

5 Drum Vortons in High Density QCD 58
5.1 Overview 58
5.2 K-Vortons 60
5.2.1 Springs vs. Vortons 61
5.2.2 Vortons in the CFL+K^0 phase of high density QCD . . 64
5.3 Domain walls, drum vortons, and Magnus forces 74
5.4 Conclusion 79

6 Neutron Stars as Type-I Superconductors 82
6.1 Overview 82
6.2 Properties of Neutron Stars 83
6.3 Type-II superconductivity vs. precession in neutron stars . . . 88
6.4 Structure of Magnetic Flux Tubes 91

6.5 Vortex-vortex interaction 98
6.6 Critical Magnetic Fields 102
6.7 Conclusion 105

7 Vortons in the $SO(5)$ Model of High T_c Superconductivity . 110
7.1 Motivation 110
7.2 High Temperature Superconductivity 112
7.3 Vortices in the $SO(5)$ theory of high-temperature superconductivity 115
7.4 Vortons in high temperature superconductivity 123
7.5 Conclusion 131

8 Summary and Outlook 137

Bibliography 143

List of Figures

1.1 Domain wall toy potential 6

2.1 QCD phase diagram 19

3.1 Cross section of effective potential for $U(1)_A$ domain walls . . 26
3.2 Profile of $U(1)_A$ domain wall 29
3.3 Potential for stability analysis of $U(1)_A$ domain walls 36

4.1 Critical value of θ_{K^0} for K^+ condensation 52
4.2 Profile of superconducting K-string 55

6.1 Structure of a neutron star 86
6.2 Profile of proton vortex 97

7.1 High temperature superconductivity phase diagram 113

Preface

The work that appears in Chapters 3, 4, 5, 6, and 7 of this thesis is based on Refs. [18, 19, 20, 21, 22] respectively, works on which the author collaborated.

Acknowledgements

I would like to thank several people for their help along the way. I would like to thank my supervisor Dr. Ariel Zhitnitsky for providing a sense of enthusiasm, ideas, and for his patience in answering a seemingly infinite number of questions. I would also like to thank the other members of my supervisory committee, Dr. Janis McKenna, Dr. John Ng, and Dr. Gordon Semenoff, for their help and useful suggestions.

My friends that I have met while at U.B.C. have made my time here very enjoyable. In particular, I would like to thank Mark Laidlaw, Tom Davis, Inaki Olabarrieta, Michael Forbes, Matt Horton, Todd Fugleberg, and Max Metlitski for their input and many interesting conversations about physics. Finally, I am grateful to my family and Lauren Murphy for their constant support and encouragement throughout the course of this work.

Chapter 1

Introduction

It is generally believed that there are no topological defects within the Standard Model of Particle Physics (in the vacuum). This is in contrast with other areas of physics where topological defects are abundant, such as condensed matter physics. A couple of examples of topological defects in condensed matter physics are the quantized Abrikosov magnetic flux tubes in type-II superconductors and the quantized vortex lines in superfluid He. In the early universe, a cosmic string provides another example of a topological defect. Even though it is well known that the Standard Model at zero temperature and chemical potential does not possess any defects due to the trivial topology of the vacuum manifold, it has been realized quite recently [38, 44, 85, 88, 89] that some topological defects (such as domain walls and strings/vortices) may exist within the Standard Model in an unusual environment such as at large baryon density (high density QCD).

The main topic of this thesis is the study of topological defects in matter at high densities and low temperatures. The study of matter under such conditions is motivated by the fact that the inner core of a neutron star is very dense and relatively cold. In particular, it is believed that the typical densities exceed nuclear densities ρ_n, where $\rho_n \sim 10^{14}$ g/cm^3. Densities of this magnitude are extremely huge and are definitely unlike anything that can be

observed on Earth. The product of a large amount of interest in the study of matter at high densities and low temperatures has been the realization that this phase may be very different from our world on Earth [3, 4, 72, 73, 74]. In particular, some of the symmetries that are approximately respected at low densities are broken at large densities. The main part of this thesis will examine the consequence of this symmetry breaking, the formation of topological defects. In this thesis we will also study topological defects in the context of a somewhat less exotic phase of matter, nuclear matter at the nuclear saturation density. The study of defects in this context is also interesting for the physics of neutron stars. Although the observations of neutron stars are constantly improving, it is far from the ideal laboratory in order to test theoretical ideas developed in this thesis. The recently established Cosmology in the Laboratory (COSLAB) program has emerged with the goal of testing theoretical ideas in cosmology and particle physics by doing laboratory experiments in various condensed matter systems [48, 49, 97]. In this thesis we will also apply some of the ideas that are developed to a condensed matter system (high temperature superconductivity). The problem of high temperature superconductivity is an interesting problem in its own right, as well as provides another example of a condensed matter system where some of the ideas explored in this thesis may be tested in the spirit of the COSLAB program.

This thesis is organized as follows. In the rest of this chapter we will give a brief introduction to topological defects. We will also give a couple of examples of topological defects that arise in simple toy models. Chapter 2 will review the basics of QCD at large baryon density, thus setting the stage

for the three subsequent chapters where topological defects are studied in this context. In particular, we will discuss the symmetry breaking pattern of high density QCD. The focus of Chapter 3 is the domain walls that arise when the $U(1)_A$ symmetry is broken in high density QCD. We will examine the stability of these $U(1)_A$ domain walls. In Chapter 4 we will demonstrate that in high density QCD there exists vortices (related to the $U(1)$ symmetry that is broken by K^0 condensation), which we refer to as superconducting K-strings, that have nontrivial core structure with a charged condensate of K^+ mesons trapped on the core. The consequence of the superconducting K-strings discussed in Chapter 4 is that it is now possible to construct loops of such vortices that are classically stable objects called vortons. Vortons in the CFL+K^0 phase of high density QCD are the subject of Chapter 5. Chapter 6 will also deal with physics that is relevant to the interior of a neutron star. However, in this chapter we will be discussing a less exotic phase of matter, neutrons, protons, and electrons in beta equilibrium at relatively high densities. This chapter differs from the material discussed so far, as we are considering densities below the point where the color superconducting phase occurs and above the point where Cooper pairs of protons and neutrons form. We will show that the presence of two condensates (Cooper pairs of protons and neutrons) changes the structure of the magnetic flux tubes (proton vortices). As we will demonstrate, this alteration may have profound consequences as it changes the interaction between adjacent vortices and therefore the boundary between type-I and type-II superconductivity is changed. This means that the conventional picture of a neutron star consisting of a proton superconductor that is a type-II superconductor may have to

be reconsidered. In Chapter 7 we will change directions and introduce the vortons previously discussed in Chapter 5 (in high density QCD) in the context of high temperature superconductivity. In the high temperature superconducting cuprate materials, a phase transition from an antiferromagnetic state to a superconducting state takes place as the hole doping is increased. These vortons may prove to be important quasiparticles that describe the physics when this phase transition occurs. This also provides an interesting connection between the physics of high density baryonic matter and high temperature superconductivity, in the spirit of the COSLAB program.

1.1 Topological Defects: A Brief Introduction

In general, topological defects can arise whenever there is a symmetry that is spontaneously broken. This symmetry breaking may occur in a variety of ways, such as cooling the system through a phase transition. In more technical language, the formation of topological defects is possible when the symmetry breaking results in a set of degenerate ground states with nontrivial topology. Topological defects are time independent finite energy solutions to the classical equations of motion that are stable due to the conservation of some topological charge. In this section we will provide two different examples of topological defects in a couple of toy models. This will be useful in order to give the reader a flavour for what will follow in the rest of this thesis.

1.1.1 Domain Walls

Domain walls can form when a vacuum manifold has two or more disconnected components. To begin, we will consider a real scalar field σ described by the following Lagrangian:

$$\mathcal{L} = \frac{1}{2}\partial_\nu\sigma\partial^\nu\sigma - V(\sigma), \tag{1.1}$$

with the following potential

$$V(\sigma) = \frac{\lambda}{4}(\sigma^2 - \eta^2)^2. \tag{1.2}$$

Upon minimizing the potential $V(\sigma)$ with respect to σ, we see that the vacuum state consists of two disconnected minima at $\sigma = \pm\eta$. We show the potential (1.2) with its degenerate minima at $\sigma = \pm\eta$ in Fig. 1.1. The ground state breaks the discrete symmetry $\sigma \to -\sigma$ (a $\mathbb{Z}_2$ symmetry) under which the original Lagrangian (1.1) was invariant. This is where we encounter our first example of a topological defect. The Euler-Lagrange equations of motion derived from (1.1) have an exact time independent solution given by

$$\sigma(x) = \eta\tanh(\beta x), \qquad \beta = \eta\sqrt{\frac{\lambda}{2}} \tag{1.3}$$

This is a domain wall, as the expectation value of the field σ interpolates from $\sigma(x = -\infty) = -\eta$ to $\sigma(x = +\infty) = +\eta$, with the change occurring in region of space confined to a wall of width $\sim \beta^{-1}$. The $\mathbb{Z}_2$ symmetry remains locally unbroken in the region of width β^{-1}, with a large amount of energy concentrated in this "wall". In three spatial dimensions there are two choices for the domain wall configuration, it is either infinite in extent (σ does not vary in the other two spatial dimensions x, y) or it forms a closed surface (for

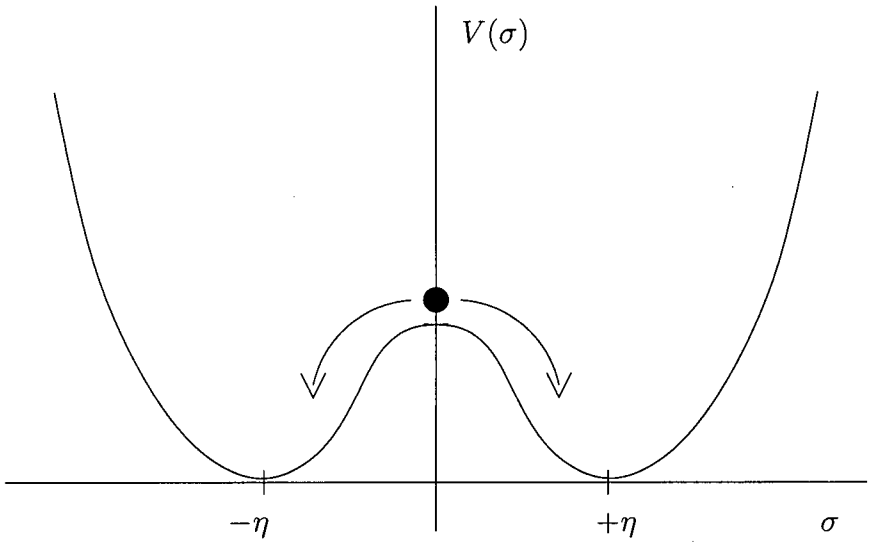

Figure 1.1: The toy potential that is given by Eq. (1.2) is shown above. The vacuum state is degenerate with minima at $\sigma = \pm\eta$. The black dot indicates the unstable symmetric point where the field σ "choose" either $\pm\eta$ as a stable vacuum state. The domain wall solution given by Eq. (1.3) interpolates between the two vacuum states, with $\sigma(-\infty) = -\eta$ and $\sigma(+\infty) = +\eta$.

example, a sphere). The latter case is unstable due to the fact that there is a finite surface tension (or energy per unit area). A domain wall can be formed through the Kibble mechanism [47]: when spontaneous symmetry breaking occurs (for example, when a system is cooled through a phase transition) different uncorrelated regions of space "choose" one of the two degenerate minima of the potential. A domain wall is formed when these regions of space (with different vacuum configurations) coalesce. This domain wall configuration (1.3) cannot relax to either of the two vacuum configurations

($\phi(x) = +\eta$, for example) because this would involve changing the field from $-\eta$ to $+\eta$ over an infinite volume ($x < 0$), which would cost an infinite amount of energy. As was mentioned above, the stability of topological defects can also be seen from the presence of a conserved topological charge. In this case, the conserved current is

$$j^{\mu} = \epsilon^{\mu\nu}\partial_{\nu}\phi \tag{1.4}$$

where $\mu, \nu = 0, 1$ and $\epsilon^{\mu\nu}$ is the antisymmetric symbol in 2 dimensions. The corresponding conserved charge is

$$Q = \int dx j^{0} = \phi(x = +\infty) - \phi(x = -\infty), \tag{1.5}$$

The topological charge of the domain wall solution (1.3) is $Q = 1$, while that of the vacuum $\phi(x) = \pm\eta$ is $Q = 0$. This means that the domain wall configuration cannot relax to either one of the trivial vacuum configurations, as they are in a different topological sector.

A familiar example of a domain wall arises in ferromagnetic systems. Above a certain temperature, called the Curie temperature, a ferromagnet behaves as a paramagnet. In the paramagnetic phase the magnetization at each point is arbitrary. As the system is cooled below the Curie temperature, the symmetry is broken and the spins must choose a particular direction.

1.1.2 Strings

The formation of strings is possible whenever the vacuum manifold is that of a circle (S^1). That is, it possesses one dimensional closed paths that cannot be contracted to a point. Consider a model where the vacuum state breaks a symmetry of the original Lagrangian. Strings are linear defects with the

symmetry restored along the length of the defect. In order to provide a concrete example, we will consider the toy model given in Eqs. (1.1) and (1.2), with the modification that σ is now a complex field. The Lagrangian is now slightly modified from the previous section:

$$\mathcal{L} = \frac{1}{2}\partial_\nu \sigma \partial^\nu \sigma^\dagger - \frac{\lambda}{4}(|\sigma|^2 - \eta^2)^2. \tag{1.6}$$

Now the Lagrangian is invariant under global $U(1)$ transformations, $\sigma \rightarrow e^{i\alpha}\sigma$, with α an arbitrary constant. The potential is no longer the double well potential shown in Fig. 1.1, and now looks like a Mexican hat configuration, with a circle of degenerate minima. The ground state spontaneously breaks this continuous $U(1)$ symmetry, and when this occurs it is possible for σ to have different values of the phase in uncorrelated regions of space, with the magnitude $\langle|\sigma|\rangle = \eta$ the same everywhere. If the phase of $\langle\sigma\rangle$ varies from 0 to 2π as one goes around a closed loop in space, the magnitude of $|\sigma|$ must vanish at some point inside this loop, as the phase is undefined at this point. In three spatial dimensions, regions of space where $\langle|\sigma|\rangle = 0$ will align to form a linear defect, called a global string, where the global $U(1)$ symmetry is restored. Although we cannot obtain an analytical solution of the equations of motion obtained from (1.6) as was possible for the domain wall example above, the string solution has the following form in cylindrical coordinates (r, ϕ, z):

$$\sigma(r, \phi) = \eta f(r)\, e^{in\phi}, \tag{1.7}$$

where n is an integer and $f(r)$ is a solution of the equations of motion obeying the boundary conditions $f(0) = 0$ and $f(\infty) = 1$. The integer n, called the winding number of the string, indicates how many times the phase of the

field σ varies from 0 to 2π as one traverses a loop in physical space. The function $f(r)$ goes from 0 to 1 over a characteristic length ξ scale on the order of $\xi \sim m_\sigma^{-1} \sim (\eta\sqrt{\lambda})^{-1}$, where m_σ is the mass of the scalar field. This can be verified by solving the classical equation of motion numerically with the appropriate boundary conditions.

Examples of global $U(1)$ strings are the quantized vortex lines that appear when superfluid He is rotated. As we mentioned above, another example of strings are the magnetic flux tubes that are present in type-II superconductors when an external magnetic field is applied. These strings are examples of local strings, where a local symmetry (electromagnetism in this case) is broken everywhere except along the length of the string. The string also has a magnetic flux tube along the core that is quantized. One of the main differences between global and local strings is the string tension or energy per unit length. The energy per unit length of a global string is logarithmically divergent, due to the large distance variation of the phase of the scalar field. In practice, this divergent energy is cutoff at some scale, which is set by the size of the system or the distance between strings. This is not the case for local strings. The energy is finite and confined to a thin core, due to the presence of the gauge field which cancels the gradient of the scalar field at large distances. In this thesis we will be discussing both global and local strings.

In addition to the defects described above, there exists a plethora of other types of topological defects. The most well known of these other defects is the t'Hooft-Polyakov monopole that is present in most Grand Unified Theories of particle physics. There also exists hybrid defects, such as domain walls

which are bounded by strings (which we will come to later on in this thesis) and strings which connect monopole-antimonopole pairs. A complete review of topological defects can be found in [96].

Chapter 2

High Density QCD

Recently, there has been a large amount of interest in the study of QCD, the theory of the strong interaction, at large baryon density [3, 4, 73, 74] (for many more references and a nice review, see Ref. [72]). At zero baryon density, QCD is a theory of quarks and gluons which are strongly coupled. It is well known that confinement takes place and the observable particles are colorless hadrons rather than quarks and gluons. If a large external scale such as large temperature or large density is introduced into the problem, one would expect that the correct degrees of freedom would eventually be quarks and gluons due to asymptotic freedom. As one increases the baryon chemical potential the ground state does not consist of nearly free quarks interacting at the Fermi surface, instead the new color superconducting phase appears where the ground state consists of diquark pairs. To explain this phenomenon, let us recall that, in QED, the electron-electron interaction generally repulsive, and superconductivity is a very subtle effect. In the non-Abelian theory of QCD, simple one gluon exchange is always attractive in the color $\overline{3}$ channel. As is well known from the conventional Bardeen-Cooper-Schrieffer theory of superconductivity, an arbitrarily small attractive interaction will lead to the formation of a condensate of Cooper pairs near the Fermi surface. This is what happens in QCD at large baryon density.

The ground state of high density QCD is characterized by a diquark condensate [3, 4, 73, 74], analogous to the condensate of electron Cooper pairs present in a conventional superconductor. This phase of QCD is referred to as the color superconducting phase, due to the fact that the color gauge symmetry is broken, as opposed to the electromagnetic gauge symmetry in BCS superconductivity. The typical chemical potential where this phase is believed to occur is $\mu_c \sim 500$ MeV, which is approximately a few times nuclear density. The gap in the color superconducting state is believed to be on the order of $\Delta \sim 100$ MeV [72]. The transition temperature T_c above which color superconductivity is destroyed is similar to the BCS transition temperature in that $T_c = 0.57\Delta \sim 60$ MeV [17, 71]. Unfortunately, this phase of QCD cannot be realized in any particle accelerator on Earth. The interest in this region of the QCD phase diagram is motivated by the fact that such densities may be realized within the core of compact stars, such as neutron stars [36, 68, 101].

2.1 The CFL phase of high density QCD

In this thesis we will be discussing QCD with $N_f = 3$ flavours of quarks (up, down, and strange) and $N_c = 3$ colors. It is well known that the ground state of $N_f = 3$, $N_c = 3$ QCD exhibits the Cooper pairing phenomenon as in conventional superconductivity [4, 74]. The corresponding condensates in the CFL phase take the approximate form:

$$\begin{aligned} \langle q_{L\alpha}^{ia} q_{L\beta}^{jb} \rangle^* &\sim \epsilon_{\alpha\beta\gamma}\epsilon^{ij}\epsilon^{abc}X_c^\gamma, \\ \langle q_{R\alpha}^{ia} q_{R\beta}^{jb} \rangle^* &\sim \epsilon_{\alpha\beta\gamma}\epsilon^{ij}\epsilon^{abc}Y_c^\gamma, \end{aligned} \tag{2.1}$$

where L and R represent left and right handed quarks, α, β, and γ are the flavour indices, i and j are spinor indices, a, b, and c are color indices, and X_c^γ and Y_c^γ are complex color-flavour matrices describing the Goldstone bosons. The 3×3 matrices X_c^γ and Y_c^γ are $SU(3)$ matrices with the following transformation properties [24]:

$$X \to U_c X U_L^T, \quad Y \to U_c Y U_R^T \tag{2.2}$$

where

$$U_c \in SU(3)_c, \quad U_L \in SU(3)_L, \quad U_R \in SU(3)_R \tag{2.3}$$

This diquark condensate breaks the original symmetry group $SU(3)_c \times SU(3)_L \times SU(3)_R \times U(1)_B \times U(1)_A$ [color gauge symmetry, left and right flavour symmetries, baryonic symmetry, and axial symmetry, respectively] down to the diagonal subgroup $SU(3)_{c+L(R)} \times \mathbb{Z}_2$. This diagonal subgroup tells us that whenever we perform an $SU(3)$ color rotation, we must simultaneously perform left (right) handed flavour rotation. Since color rotations are now linked with flavour rotations, this phase of high density QCD with $N_f = N_c = 3$ is referred to as the color-flavour locked (CFL) phase [4]. Counting the number of broken generators ($(3^2 - 1)$ for each $SU(3)$ and 1 for each $U(1)$), we see that there should be 18 Goldstone bosons (GB). Of these 18 GB, 8 of them are eaten by the Higgs mechanism resulting in the gluons acquiring masses. When electromagnetism is broken, there remains a new "rotated" electromagnetism which is unbroken, similar to the situation in the Standard Model. In the Standard Model, the Higgs vacuum expectation value leaves unbroken a linear combination Q of the weak W_3 boson and Y hypercharge boson. In high density QCD it is a linear combination of the eighth gluon and the photon that forms the new "rotated" electromagnetism, $\tilde{Q} = Q + T_8/\sqrt{3}$. This

leaves ten GB, an octet related to the breaking of $SU(3)$ and two singlets related to $U(1)_B$ and $U(1)_A$. All of these GB [except the one related to $U(1)_B$] are actually pseudo-Goldstone bosons due to the small explicit violation of the symmetry (for example, instantons and finite quark masses). In addition to the Goldstone modes, there are also quark-like quasiparticles that have a minimum excitation energy that is proportional to the superconducting gap Δ and gluons that have a mass on the order of $g\mu$ from the Meissner effect (g is the strong coupling constant). The value of the gap Δ (with 2Δ being the energy required to break a diquark pair) has been calculated at asymptotically large densities where perturbative one-gluon exchange is justified and also at lower densities using phenomenological models. These different approaches yield similar results, with the gap on the order of $\Delta \sim 100$ MeV (for a summary of the different methods that give this result see [72]). The gap Δ in the quark spectrum depends on the chemical potential μ and the strong coupling constant g in the following manner [84];

$$\Delta \sim \frac{\mu}{g^5} \exp\left(-\frac{3\pi^2}{\sqrt{2}g}\right). \tag{2.4}$$

The dependence of the gap on the coupling constant $\Delta \sim e^{-const/g}$ is different from the standard BCS result where $\Delta \sim e^{-const/g^2}$. As explained in Ref. [84], this is due to the fact that the gluon propagator has an infrared divergence at very small scattering angle. The Goldstone bosons are the most relevant degrees of freedom at energies below Δ, as their masses are proportional to the quark masses and are much less than the masses of any other degrees of freedom $m_q \ll \Delta, g\mu$. In QCD at $\mu = 0$ the Goldstone modes resulting from the spontaneous breaking of chiral symmetry are described by the fluctuations of the phase of the chiral condensate, $\langle \bar{\psi}^a_\beta \psi^a_\alpha \rangle = \exp(i\pi^a \lambda^a / f_\pi)$, where

α, β are flavour indices and a is a color index. As the magnitudes of the condensates given by Eq. (2.1) depend on the color index c, one can easily see that these objects are not gauge invariant by themselves. In order to describe the light degrees of freedom in a gauge invariant way, one introduces the color singlet field Σ [24, 86, 87]

$$\Sigma_\gamma^\beta = XY^\dagger = \sum_c X_c^\beta Y_\gamma^{c*}, \tag{2.5}$$

such that the leading terms of the effective Lagrangian in terms of Σ take the form [12]

$$\mathcal{L}_{\text{eff}} = \frac{f_\pi^2}{4}\text{Tr}\left[\nabla_0\Sigma\nabla_0\Sigma^\dagger - v^2\partial_i\Sigma\partial_i\Sigma^\dagger\right] + 2A\left[\det(M)\text{Tr}(M^{-1}\Sigma + h.c.\right], \tag{2.6}$$

$$\nabla_0\Sigma = \partial_0\Sigma + i\left(\frac{MM^\dagger}{2p_f}\right)\Sigma - i\Sigma\left(\frac{M^\dagger M}{2p_f}\right),$$

where the matrix $\Sigma = \exp(i\pi^a\lambda^a/f_\pi)$ describes the octet of Goldstone bosons (pions, kaons, and the eta meson), similar to the zero density case mentioned above. The $SU(3)$ generators λ^a are normalized as $\text{Tr}(\lambda^a\lambda^b) = 2\delta^{ab}$. The quark mass matrix in Eq.(2.6) is given by $M = \text{diag}(m_u, m_d, m_s)$. Finally, we neglect the electromagnetic interactions in the expression (2.6) but keep the isospin violation $\sim (m_d - m_u)$, which is an appropriate approximation for the physically relevant case when the baryon density is not very high [11]. This isospin violation will be crucial for the analysis in Chapter 4. The constants f_π, v and A have been calculated in the leading perturbative approximation and are given by [10, 86, 87]:

$$f_\pi^2 = \frac{21 - 8\ln 2}{18}\frac{\mu^2}{2\pi^2}, \quad v^2 = \frac{1}{3}, \quad A = \frac{3\Delta^2}{4\pi^2}. \tag{2.7}$$

One notices that $v \neq 1$, as expected because Lorentz invariance is not respected at finite chemical potential.

2.2 K^0-condensation in the CFL phase of high density QCD

All of the results that were given in the previous section are valid for QCD with $N_f = 3$ flavours of massless quarks when an $SU(3)$ flavour symmetry is respected. For large values of the chemical potential, this is a valid approximation and the quark mass effects can be ignored as long as $\mu \gg m_s$. As μ is decreased to $\mu = 500$ MeV (the typical density that may be realized inside a neutron star) this approximation breaks down as we now have $m_s \sim \mu$. The phases of the high density quark matter can be very different as the mass of the strange quark m_s is varied. As we have mentioned, for $m_s = 0$ we have the CFL phase of high density QCD. In the opposite extreme, if we consider the case $m_s \to \infty$ the strange quark decouples and the ground state is the so called 2SC phase of high density QCD [3, 73]. In the 2SC phase only the up and down quarks pair to form the diquark condensate. The form of the condensate in the 2SC phase is different from the form given for the CFL phase in Eq. (2.1), with only 4 of the 9 quarks paired. For intermediate values of m_s, one suggestion is that the ground state is the crystalline color superconducting phase [16] where Cooper pairs of quarks have nonzero total momentum. This is called the crystalline phase because condensates with nonzero total momentum spontaneously break translational and rotational invariance, which leads to gaps that vary periodically in space. For a more detailed discussion of the various color superconducting phases of high density QCD as a function of the strange quark mass m_s and chemical potential μ we refer the reader to [2, 72]. There is another possibility which we will

now discuss. Recently, it was realized in [11, 12, 45, 77] that the ground state of the theory may be different from the pure CFL phase for a physical value of the strange quark ($m_s \gg m_u, m_d$): condensation of the K^0 and K^+ mesons would lower the free energy of the system by reducing the strange quark content. Specifically, it has been argued that kaon condensation would occur in the CFL phase if $m_s \geq 60$ MeV [12]. In what follows we consider this special case where kaon condensation occurs. For electrically neutral CFL matter at intermediate densities, it is believed that K^0 condensation would occur [11]. This means that $\Sigma = \mathbf{1}$ is no longer the global minimum of the free energy; instead, some rotated value of Σ describes the ground state in this case. In what follows we consider the realistic case when the isospin symmetry is not exact, $m_d > m_u$ and the chemical potential for electric charge (electrons) is zero, such that K^0 condensation occurs. In order to see how the ground state is altered, we postulate a nonzero expectation value for the field with the same quantum numbers as K^0. If the energy with $\theta_{K^0} \equiv \sqrt{2}K^0/f_\pi \neq 0$ is a global minimum, then kaon condensation does occur. Substituting $\pi^a\lambda^a/f_\pi = \theta_{K^0}(\cos\phi\lambda^6 + \sin\phi\lambda^7)$ (this has the same quantum numbers as K^0) into $\Sigma = \exp(i\pi^a\lambda^a/f_\pi)$, the appropriate expression describing the K^0 condensed ground state can be parameterized as:

$$\Sigma_{K^0} = \begin{pmatrix} 1 & 0 & 0 \\ 0 & \cos\theta_{K^0} & i\sin\theta_{K^0}e^{-i\varphi} \\ 0 & i\sin\theta_{K^0}e^{i\varphi} & \cos\theta_{K^0} \end{pmatrix}, \tag{2.8}$$

where φ describes the corresponding Goldstone mode and θ_{K^0} describes the strength of the kaon condensation. In order to check that the assumption made above that $\langle K^0 \rangle \neq 0$ is correct, we substitute Eq. (2.8) into the static

and spatially constant part of (2.6) and minimize with respect to θ_{K^0} to arrive at [12]:

$$\begin{aligned} \cos\theta_{K^0} &= \frac{m_0^2}{\mu_{\rm eff}^2}, \qquad \mu_{\rm eff} \equiv \frac{m_s^2}{2p_F}, \\ m_0^2 &\equiv a m_u (m_d + m_s), \quad a = \frac{4A}{f_\pi^2} = \frac{3\Delta^2}{\pi^2 f_\pi^2}. \end{aligned} \tag{2.9}$$

We see that K^0 condensation occurs if $m_0 < \mu_{\rm eff}$. The critical value of the strange quark mass where K^0 becomes massless is approximately given by $m_s \gtrsim (24\ m_u)^{1/3}\Delta^{2/3}$. There is some uncertainty in making a definite prediction of the point where K^0 condensation occurs due to the fact that the gap Δ is not precisely known for $\mu = 500$ MeV. However, a reasonable value for the gap is $\Delta \lesssim 100$ MeV, and we know that the quark masses are $m_s \simeq 150$ MeV and $m_u \simeq 5$ MeV. Therefore, according to these estimates we see that K^0 condensation would occur as $m_s > (24\ m_u)^{1/3}\Delta^{2/3}$. If kaon condensation occurs and $\theta_{K^0} \neq 0$, an additional $U(1)$ symmetry is broken.

In Fig. 2.1 we give the basic picture of the QCD phase diagram as a function of temperature T and chemical potential μ. At low temperatures and densities, we have the hadronic phase where quarks and gluons are confined. As the temperature is increased at low densities, we eventually ($T_c \sim 180$ MeV) reach the quark-gluon plasma, where quarks and gluons are deconfined and chiral symmetry is restored. At large densities and low temperatures we have the various color superconducting phases of quark matter. Much less is known about this region of the phase diagram such as the critical chemical potential μ_c where color superconductivity occurs. The reason for this is that unlike finite T QCD, finite μ QCD is not easily placed on the lattice to perform computer simulations, due to the complex nature of the quark

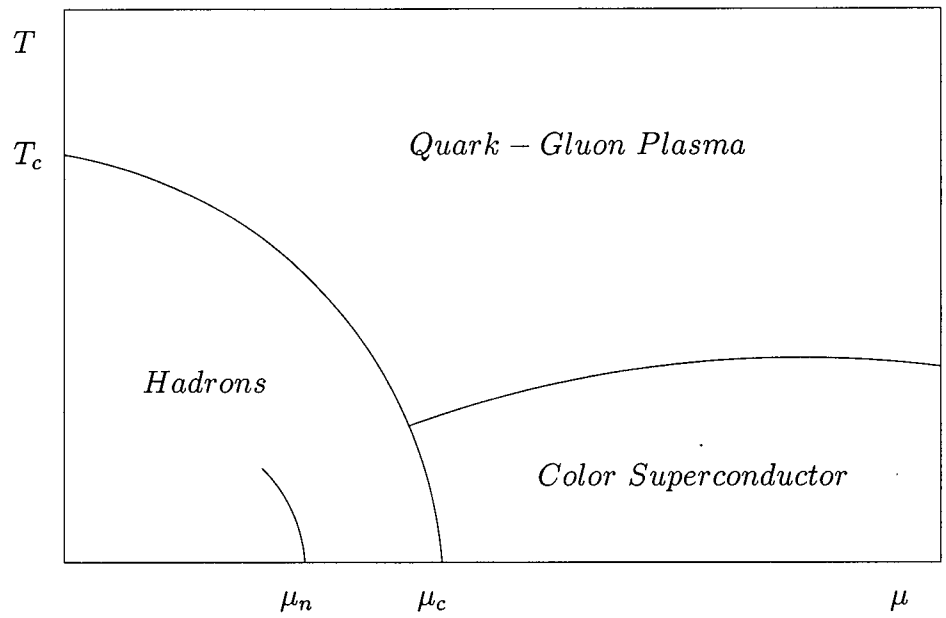

Figure 2.1: In this figure we give a naive picture of the QCD phase diagram as a function of baryon chemical potential μ and temperature T.

determinant. Analytical estimates seem to indicate that $\mu_c \sim 400-500$ MeV. The point μ_n on the phase diagram indicates the nuclear matter saturation density (hadron gas-hadron liquid transition point).

For this thesis the most important aspect of the CFL+K^0 phase of high density QCD is the symmetry breaking pattern. In the next three chapters we will be discussing the consequences of the symmetry breaking, the formation of topological defects.

Chapter 3

$U(1)_A$ Domain Walls in High Density QCD

3.1 Overview

In [88, 89], it was shown that at high densities ($\mu \gg 1$ GeV) there exist domain wall solutions which interpolate between the same vacuum state, in which the $U(1)_A$ phase of the diquark condensate varies between 0 and 2π. This type of domain wall which interpolates between the same vacuum state has been studied before in the context of axion models [96]. It is interesting to note that similar domain wall configurations are present for the zero density case in the large N_c limit and could be present for the physically relevant case of $N_c = 3$ [37], therefore they could be studied at the BNL Relativistic Heavy Ion Collider (RHIC) [83]. Given this, one might ask what happens between these two regions of $\mu = 0$ and $\mu \gg 1$ GeV. The main goal of the present chapter is to discuss the analysis of the classical stability of the $U(1)_A$ domain walls for $\mu \lesssim 1$ GeV. In this chapter we will demonstrate that the $U(1)_A$ domain walls are classically stable down to densities $\mu \simeq 800$ MeV. The main idea is to interpolate between $\mu \gg 1$ GeV (where perturbation theory is justified) and $\mu \simeq \mu_c$ (where instanton calculations lead to a reasonable

description). Ideally, we would like to be able to make definitive statements on the stability of such configurations all the way down from large μ to $\mu_c \sim 500$ MeV, where μ_c is the critical chemical potential above which the color superconducting phase occurs. However, we are unable to make a definitive statement for $\mu_c \lesssim \mu \lesssim 800$ MeV due to a lack of theoretical control in this region. One can only speculate on the behavior in this region.

3.2 The Effective Potential

We will begin by considering the gauge invariant field Σ. Recall from Chapter 2 that the following matrix (given by Eq. (2.5)) which describes the octet of mesons and axial singlet was constructed in [24, 86, 87]:

$$\Sigma_\gamma^\beta = XY^\dagger = \sum_c X_c^\beta Y_\gamma^{c*}. \tag{3.1}$$

If a $U(1)_A$ rotation ($q \rightarrow \exp^{i\gamma_5\alpha/2} q$) of this gauge-invariant field Σ is performed, we see that the fields (2.1) transform as

$$\begin{aligned} X &\rightarrow e^{-i\alpha} X, \\ Y &\rightarrow e^{+i\alpha} Y, \end{aligned} \tag{3.2}$$

and therefore

$$\Sigma \rightarrow e^{-2i\alpha}\Sigma. \tag{3.3}$$

Goldstone's theorem states that there must be a single Goldstone mode η' associated with the breaking of this symmetry. Given this, we can parameterize the field as follows:

$$\Sigma = \Sigma_o \, e^{\rho} \, e^{-i\phi}, \tag{3.4}$$

where the phase $\phi = \eta'/f_{\eta'}$ is defined as a dimensionless field which describes the η' boson, $f_{\eta'}$ is the corresponding decay constant, Σ_o is the vacuum expectation value of the composite field (2.5), and ρ is another dimensionless field which describes the fluctuations of the magnitude of the condensate[1] (analogous to the σ field related to the fluctuations of the $\langle\bar{\psi}\psi\rangle$ chiral condensate). We choose to parameterize the field as e^{ρ} for convenience later on.

In order to construct an effective potential describing the dynamics of the phase of the condensate ϕ as well as the magnitude $|\Sigma|$, there are two types of terms which must be included. The first term which explicitly breaks the $U(1)_A$ symmetry was calculated in [61, 88, 89] by substituting the form of condensates given above into the instanton induced four-fermion Lagrangian [81, 82, 93]:

$$V_{1-\text{inst}}(\rho,\phi) = -a\mu^2\Delta^2\ e^{\rho}\cos\phi, \tag{3.5}$$

where Δ is the value of the gap in the quark spectrum. The perturbative form of the expectation value of the condensate has been used in arriving at this result [84, 88, 89]:

$$\langle|\Sigma|\rangle \equiv \Sigma_o = \frac{9}{8\pi^2}\frac{\mu^4\Delta^2}{g^2}. \tag{3.6}$$

For $N_f = 3$, the dimensionless coefficient a was found to be [61, 89]

$$a = 7\times 10^3\left(\frac{m_s}{\mu}\right)\left(\ln\frac{\mu}{\Lambda_{\text{QCD}}}\right)^7\left(\frac{\Lambda_{\text{QCD}}}{\mu}\right)^9, \tag{3.7}$$

where m_s is the mass of the strange quark. The mass of the corresponding η' boson can be easily calculated by expanding the potential,

$$m_{\eta'} = 2\pi\sqrt{a}\ \Delta. \tag{3.8}$$

[1]The field ρ should not be confused with the familiar ρ meson in QCD.

According to [88, 89], this potential is only under theoretical control when the mass of the η' boson is much less than the typical scale for higher excitations 2Δ, which corresponds to $a \ll 1/\pi^2$. For physical values of the strange quark, this corresponds to a chemical potential of about $\mu \approx 700$ MeV (for $a \sim 1/\pi^2$).

To be able to draw any conclusions about the stability of the domain wall solution for intermediate densities ($\mu_c \lesssim \mu \lesssim 1$ GeV), one must include degrees of freedom which are related to the fluctuations of the absolute value of $|\Sigma|$. We do not know the effective potential in the region of interest; however, for qualitative discussions we shall use a potential derived for asymptotically large μ. The second type of term which must be included in an effective potential description is one which uniquely fixes the magnitude of the condensate. An effective potential for the magnitude of the condensate $|\Sigma|$ was derived in [65] in the perturbative region where the analytical form of the gap is known. This effective potential fixes uniquely the value of the vacuum condensate. The potential is of the Coleman-Weinberg type [26] and is given as follows:

$$\begin{aligned} V_{\rm pert}(|\Sigma|) &= -\left(\frac{2\nu\pi}{\mu}\right)^2 |\Sigma| \left(1 - \ln\frac{|\Sigma|}{\Sigma_o}\right), \\ &= -\frac{\mu^2\Delta^2}{\pi^2} e^{\rho}(1-\rho), \qquad (3.9) \\ \nu &= \sqrt{\frac{8\alpha_s}{9\pi}}, \end{aligned}$$

where $\alpha_s = g^2/4\pi$ is the standard strong coupling constant and the perturbative result of the condensate (3.6) has been used. In all calculations that follow we will assume $\Delta = 100$ MeV as the numerical value for the gap. It

should be noted that the potential (3.9) is justified only in the region

$$\nu \log(|\Sigma|/\Sigma_o) \ll 1. \tag{3.10}$$

Since we are considering $|\Sigma| \approx \Sigma_o$, the use of this effective potential is justified.

We are interested in the region $\mu_c \lesssim \mu \lesssim 1$ GeV, where Eq. (3.9) is not literally correct. Even though the results stated above are not necessarily under theoretical control for $\mu \gtrsim \mu_c$, one can speculate on how the coefficients behave at intermediate densities when $\mu_c \lesssim \mu \lesssim 1$ GeV. Due to the fact that all the same symmetries are present as the chemical potential is lowered until reaching μ_c, we expect the qualitative form of the effective potential (3.5) and (3.9) to remain the same. As the chemical potential is lowered, eventually perturbative calculations which are valid at asymptotically large μ are no longer the correct description and instanton calculations become relevant. One would expect that these calculations must match up at some point. However, the coefficients in front of the potential could possibly be very different in the density region of interest. We will refer to the coefficient in front of the one-instanton potential as β_1 and the coefficient in front of the perturbative potential as β_2. The value of β_1 is essentially fixed by the form of the condensate and by the constituent quark mass. Below the critical chemical potential μ_c at which the chiral phase transition occurs, this coefficient is independent of μ [74]. Therefore, we would expect that β_1 would be some smooth function of μ which reaches its maximum value at $\mu = \mu_c$. At $\mu_c \lesssim \mu \lesssim 1$ GeV, the coefficient β_2 is modified by the formation of instanton-antiinstanton ($I\bar{I}$) molecules [74]. We should also note that the coefficient β_1 can also be estimated from the instanton liquid model [74] using

the average size of instantons as well as requiring a constituent quark mass of about $350 - 400$ MeV.

Combining both terms we have an effective potential which is given by the following:

$$V(\rho, \phi) = -\beta_2 e^{\rho}(1 - \rho) - \beta_1 e^{\rho} \cos\phi. \tag{3.11}$$

The values of the coefficients β_1 and β_2 are known for asymptotically large μ:

$$\beta_1 = a\mu^2\Delta^2, \tag{3.12}$$

$$\beta_2 = \frac{\mu^2\Delta^2}{\pi^2}. \tag{3.13}$$

In Fig. 3.1, we show the cross section of the potential at $\phi = 0, 2\pi$ and $\phi = \pi$ for $\mu = 800$ MeV. Notice that the existence of an absolute minima at $\phi = 0, 2\pi$ and a saddle point at $\phi = \pi$ allows for nontrivial configurations which wind around the barrier at $|\Sigma| = 0$. In the limit $\mu \to \infty$, the parameter $a \to 0$ and the potential has degenerate minima at $|\Sigma| = \Sigma_o$. The kinetic term is given by

$$\frac{|\partial_o\Sigma|^2 - v^2|\partial_i\Sigma|^2}{|\Sigma|^2} = (\partial_o\rho)^2 - v^2(\partial_i\rho)^2 + (\partial_o\phi)^2 - v^2(\partial_i\phi)^2, \tag{3.14}$$

where v is the velocity which is different from 1. The perturbative values for the decay constant f_π and velocity v were calculated in [10]. In order to fix the correct dimensionality, we must multiply the kinetic term by the appropriate powers of the decay constant. The full effective Lagrangian up to two derivatives in the fields is then given by

$$\mathcal{L} = f_\pi^2[(\partial_o\rho)^2 - v^2(\partial_i\rho)^2] + f_\pi^2[(\partial_o\phi)^2 - v^2(\partial_i\phi)^2] - V(\rho, \phi). \tag{3.15}$$

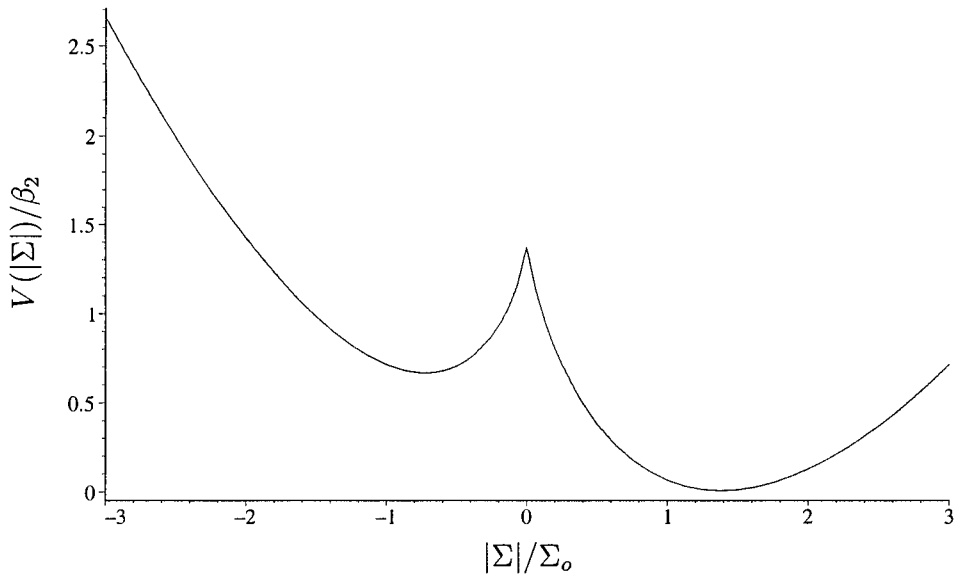

Figure 3.1: The cross section of the effective potential is shown above for $\mu = 800$ MeV. On the left of $|\Sigma| = 0$ the effective potential for $\phi = \pi$ is shown and on the right half $\phi = 0, 2\pi$ is shown.

In the above we have assumed that $f_{\eta'} \simeq f_\rho \simeq f_\pi$. The exact numerical value for f_ρ is not known. However, in the large μ limit $f_{\eta'} \sim f_\rho \sim \mu$ in order to have an appropriate scale for $m_\rho \sim \Delta$ (once again, the ρ field should not be confused with the well known ρ meson in QCD at $\mu = 0$).

3.3 Domain wall solutions

As was done in [88, 89], if we replace the field $|\Sigma| = \Sigma_o e^\rho$ by its vacuum expectation value (which is justified for $\mu \gg 1$ GeV), the resulting potential

is of the sine-Gordon type. The Lagrangian is given by the following:

$$\mathcal{L} = f_\pi^2[(\partial_0\phi)^2 - v^2(\partial_i\phi)^2] - V_{1-\text{inst}}(\phi), \tag{3.16}$$

where the constant term has been dropped. The static domain wall solution to the corresponding equation of motion is well known. Considering a domain wall in the z direction, the solution is given by

$$\phi_o(z) = 4\arctan\left(\exp(-m_{\eta'}z/v)\right), \tag{3.17}$$

where $m_{\eta'}$ is the mass of the η'. This solution interpolates between the same vacuum state; at $z = \pm\infty$ we have $\phi = 0, 2\pi$, respectively. It is well known that this solution is absolutely stable under small perturbations $\phi = \phi_o + \delta\phi$. In other words, the Schrödinger-type equation obtained by varying the field and linearizing the equation of motion,

$$-\partial_z^2\ \delta\phi_n + \frac{m_{\eta'}^2}{v^2}\left(1 - 2\ \text{sech}^2\left(\frac{m_{\eta'}}{v}z\right)\right)\delta\phi_n = \omega_n^2\delta\phi_n, \tag{3.18}$$

has the lowest eigenvalue $\omega_o = 0$ corresponding to $\delta\phi_o = d\phi_o(z)/dz \sim \text{sech}(m_{\eta'}z/v)$. This is just the zero mode which is a result of translational invariance $z \to z + z_o$. Since the lowest eigenvalue is non-negative, the domain wall solution is stable under small perturbations. It turns out that this is the only bound state which is a solution of Eq. (3.18).

In the case in which the replacement $|\Sigma| \to \Sigma_o$ is not done, the solution must be modified. If we want to study a stable solution for μ which is not asymptotically large, we must include fluctuations in ϕ as well as in the ρ direction (*i.e.* the absolute value of Σ). The two equations of motion for

static solutions are given by

$$2f_\pi^2 v^2 \nabla_i^2 \rho = \beta_2\ \rho\ e^\rho - \beta_1\ e^\rho \cos\phi, \tag{3.19}$$

$$2f_\pi^2 v^2 \nabla_i^2 \phi = \beta_1\ e^\rho \sin\phi. \tag{3.20}$$

Although we do not know the exact solution for this set of coupled nonlinear differential equations, if $\beta_1/\beta_2 < 1$ we can approximate the solutions. In this case, the approximate solutions can be parameterized by

$$e^{\rho_o} \approx 1 + \alpha \cos\phi_o, \tag{3.21}$$

$$\phi_o \approx 4 \arctan\left(\exp(-m_{\eta'} z/v)\right), \tag{3.22}$$

where $\alpha \approx \beta_1/\beta_2$. In Fig. 3.2 we show the approximate solution for ϕ_o and ρ_o. Our stability analysis will be based upon these approximate solutions of the equations of motion. Since the above solutions do not correspond to the exact solutions to the equations of motion (minimum energy path which winds around that barrier at $|\Sigma| = 0$), there will be nonzero linear terms when the energy of the system is perturbed about the domain wall solutions ϕ_o and ρ_o. These will be estimated in the following section where the stability analysis is performed.

3.4 Stability analysis of domain walls

Although these domain walls may exist as classically stable objects at large densities, it is not immediately obvious if this is the case at intermediate densities. In order to examine the classical stability of the domain wall configurations in the region $\mu \lesssim 1$ GeV, we must look at how the system

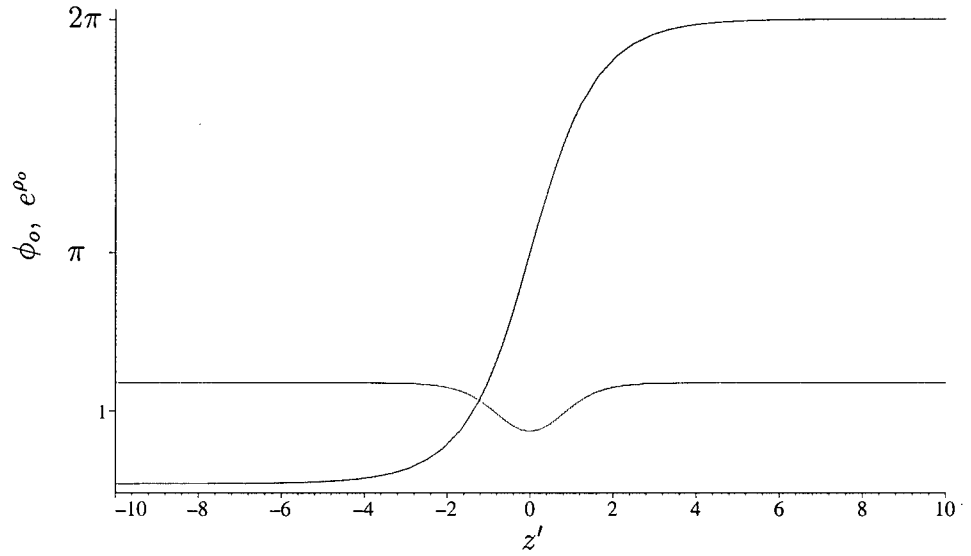

Figure 3.2: In this figure we show the approximate domain wall solution for the fields ϕ_o and ρ_o given by Eq. (3.21) as a function of the dimensionless coordinate $z' = m_{\eta'} z/v$ (defined in Eq. (3.24)). Notice that $\phi_o(-\infty) = 0$ and $\phi_o(+\infty) = 2\pi$, while $e^{\rho_o} \simeq 1$ (therefore $|\Sigma| \simeq \Sigma_o$). We can see that the width of the wall is $\delta'_{\text{wall}} \sim 1$ in these rescaled units.

reacts to small perturbations of the fields. The energy density is given by the following expression:

$$E(\phi,\rho) = \int_{-\infty}^{+\infty} dz[f_\pi^2 v^2 (\nabla\rho)^2 + f_\pi^2 v^2 (\nabla\phi)^2 + V(\phi,\rho)]. \tag{3.23}$$

In order to express all integrals as dimensionless quantities, we will perform the following change of variables:

$$z' = \frac{z}{\lambda}, \quad \lambda = \frac{v}{m_{\eta'}}. \tag{3.24}$$

The energy density is now given by

$$E(\phi,\rho) = \frac{f_\pi^2 v^2}{\lambda}\left[\int dz' \left((\nabla\rho)^2 + (\nabla\phi)^2 + \frac{\lambda^2}{f_\pi^2 v^2}V(\phi,\rho)\right)\right], \tag{3.25}$$

where the derivative is now taken with respect to the dimensionless coordinate z'. We can see that this has the correct dimensions of MeV^3 times the dimensionless integral in square brackets. Following the standard method for analyzing the stability of a classical solution which was briefly described in the previous section, we will expand the fields about their vacuum expectation values:

$$\begin{aligned}\rho &\to \rho_o + \delta\rho,\\ \phi &\to \phi_o + \delta\phi.\end{aligned} \tag{3.26}$$

Next, we substitute Eq. (3.26) into Eq. (3.23) and perform an expansion, neglecting any terms greater that quadratic order in $\delta\rho$ and $\delta\phi$:

$$\begin{aligned} E &\simeq E^{(0)} + E^{(1)} + E^{(2)} \\ &\simeq E(\phi_o,\rho_o) + \gamma\int dz'\ \delta\rho\left(-2\nabla^2\rho_o + \frac{\lambda^2}{f_\pi^2 v^2}\frac{\delta V}{\delta\rho}\Big|_{\phi_o,\rho_o}\right) \\ &+ \gamma\int dz'\ \delta\phi\left(-2\nabla^2\phi_o + \frac{\lambda^2}{f_\pi^2 v^2}\frac{\delta V}{\delta\phi}\Big|_{\phi_o,\rho_o}\right) \\ &+ \gamma\int dz'\ \delta\rho\left(-\nabla^2 + \frac{\lambda^2}{2f_\pi^2 v^2}\frac{\delta^2 V}{\delta\rho^2}\Big|_{\phi_o,\rho_o}\right)\delta\rho \\ &+ \gamma\int dz'\ \delta\phi\left(\frac{\lambda^2}{f_\pi^2 v^2}\frac{\delta^2 V}{\delta\phi\delta\rho}\Big|_{\phi_o,\rho_o}\right)\delta\rho \\ &+ \gamma\int dz'\ \delta\phi\left(-\nabla^2 + \frac{\lambda^2}{2f_\pi^2 v^2}\frac{\delta^2 V}{\delta\phi^2}\Big|_{\phi_o,\rho_o}\right)\delta\phi, \end{aligned} \tag{3.27}$$

where $\gamma = f_\pi^2 v^2/\lambda$. The first term $E^{(0)} = E(\phi_o,\rho_o)$ in the above expansion is the energy density or wall tension of the domain wall. In the case in which

the domain wall solutions given by Eq. (3.21) were the exact solutions to the classical equations of motion, the linear terms $E^{(1)}$ (proportional to $\delta\rho$ and $\delta\phi$) would be zero everywhere. Due to the fact that our solutions are not exact, these must be considered.

First, let us estimate the term which is linear in $\delta\phi$:

$$\delta\phi^{(1)} = \frac{f_\pi^2 v^2}{\lambda} \int dz' \delta\phi \left(-2\nabla^2\phi_o + \frac{\lambda^2}{f_\pi^2 v^2} \beta_1 e^{\rho_o} \sin\phi_o \right). \tag{3.28}$$

We know that $e^{\rho_o} \approx 1 + \rho_o$ and using the fact that ϕ_o is a solution to the equation of motion given by Eq. (3.20) with $\rho = 0$, we have:

$$\begin{aligned} \delta\phi^{(1)} &\approx \frac{f_\pi^2 v^2}{\lambda} \int dz' \, \frac{\lambda^2}{f_\pi^2 v^2} \beta_1 \rho_o \sin\phi_o \delta\phi \\ &\approx \frac{f_\pi^2 v^2}{\lambda} \int dz' \; a \; \pi^2 \sin 2\phi_o \; \delta\phi. \end{aligned} \tag{3.29}$$

This linear term goes like $a\pi^2$ (~ 0.3 for $\mu = 800$ MeV) and the integrand is small compared to the wall tension $E^{(0)}$ and can be neglected. The term which is linear in $\delta\rho$ is:

$$\begin{aligned} \delta\rho^{(1)} = \frac{f_\pi^2 v^2}{\lambda} \int dz' \; \delta\rho \big(-2\nabla^2\rho_o \; &+ \; \frac{\lambda^2}{f_\pi^2 v^2} \beta_2 \rho_o e^{\rho_o} \\ &- \; \frac{\lambda^2}{f_\pi^2 v^2} \beta_1 e^{\rho_o} \cos\phi_o \Big). \end{aligned} \tag{3.30}$$

Using again that $\rho_o \approx (\beta_1/\beta_2)\cos\phi_o$ we see this simplifies to

$$\delta\rho^{(1)} \approx \frac{f_\pi^2 v^2}{\lambda} \int dz' \; \left(-2a \; \pi^2 \delta\rho \nabla^2 (\cos\phi_o) \right). \tag{3.31}$$

Since this term is also proportional to $a\pi^2$, $\delta\rho \ll \rho_o$, and the integral of $\nabla^2(\cos\phi_o)$ is small, we can also neglect this term. The magnitude of the linear term shows how far away we are from the exact solution. This information will be used in what follows for the stability analysis.

Now we consider the most important quadratic term. A similar case involving two coupled scalar fields was looked at in [95] and we will follow the standard procedure presented there closely. If the field configuration is classically stable, the second variation of the energy should be a positive differential operator. This means we must solve the following Schrödinger-type eigenvalue problem:

$$H \begin{pmatrix} \delta\rho \\ \delta\phi \end{pmatrix} = \omega^2 \begin{pmatrix} \delta\rho \\ \delta\phi \end{pmatrix}, \tag{3.32}$$

where H is the operator,

$$H = -\partial_{z'}^2 \mathbf{1} + \frac{\lambda^2}{2f_\pi^2 v^2} U, \tag{3.33}$$

and $\mathbf{1}$ is the 2×2 identity matrix. The potential U is a 2×2 matrix with elements:

$$U_{11} = \beta_2 \, (1 + \rho_o) \, e^{\rho_o} - \beta_1 \, e^{\rho_o} \cos\phi_o, \tag{3.34}$$

$$U_{12} = U_{21} = \beta_1 \, e^{\rho_o} \sin\phi_o, \tag{3.35}$$

$$U_{22} = \beta_1 \, e^{\rho_o} \cos\phi_o. \tag{3.36}$$

If the domain wall solution is a stable one, then the operator H is positive-semidefinite. The eigenvalue equations can be decoupled by diagonalizing the matrix U. We should note that only the potential term has to be diagonalized when looking for negative energy modes, as was done in [95]. The result is

$$U_\pm = \frac{1}{2}\left(a \pm \sqrt{a^2 - 4(ab - b^2 - c^2)}\right), \tag{3.37}$$

where a, b, and c are defined as

$$\begin{aligned} a &= \beta_2 \, (1 + \rho_o) \, e^{\rho_o}, \\ b &= \beta_1 \, e^{\rho_o} \cos\phi_o, \\ c &= \beta_1 \, e^{\rho_o} \sin\phi_o. \end{aligned} \tag{3.38}$$

The operator H now takes the following form:

$$H = \begin{pmatrix} -\partial_{z'}^2 + \frac{\lambda^2}{2f_\pi^2 v^2} U_+ & 0 \\ 0 & -\partial_{z'}^2 + \frac{\lambda^2}{2f_\pi^2 v^2} U_- \end{pmatrix}. \tag{3.39}$$

Since we can immediately see that $U_+ \geq 0$ for all z' due to the fact that $a > 0$, there does not exist any negative eigenvalues corresponding to the first equation in this transformed basis. Looking at the second eigenvalue equation, we have

$$\left(-\partial_{z'}^2 + \frac{\lambda^2}{2f_\pi^2 v^2} U_- \right) \psi_n = \omega_n^2 \psi_n. \tag{3.40}$$

It is a well known theorem of quantum mechanics that there must exist at least one bound-state solution to Eq. (3.40). Due to the fact that our domain wall solution should be invariant under translations in space $z' \to z' + z'_o$, there should be a corresponding zero mode in the spectrum of Eq. (3.40). In the high density limit, we recover the familiar sine-Gordon equation and we know that there is only one bound state in the spectrum of Eq. (3.18). If the exact solution to the equations of motion (3.19) and (3.20) were known, one would expect to see a corresponding mode with a vanishing eigenvalue in the spectrum of Eq. (3.40). As the density is lowered ($\beta_1 \leq \beta_2$) and the saddle point at $\phi = \pi$ is still present, one would expect the appearance of a mode with a negative eigenvalue corresponding to instability of the domain

wall. Due to the fact that there still must be a zero mode in the spectrum, the zero mode would become the first excited state of Eq. (3.40) and the lowest mode would have some negative eigenvalue $\omega_0^2 < 0$ corresponding to the instability of the domain wall. The problem of stability analysis now reduces to determining the eigenvalues corresponding to the bound states of Eq. (3.40). The appearance of an additional bound state in the spectrum as the chemical potential is lowered will be the first sign that the system is approaching the point of instability.

Since the solution corresponding to Eq. (3.21) is not the exact solution but does represent a path which winds around the barrier at $|\Sigma| = 0$, it is quite possible that the zero mode could show up in the spectrum with a small nonzero eigenvalue. It would show up as a true zero mode only when the exact solution to the equation of motion is substituted into Eqs. (3.38).

Although the potential U_- is nontrivial, we will use a variational approach in order to determine the upper bounds on ω_0^2 and ω_1^2. In choosing a trial wave function, we make the observation that the potential U_- is quite similar to the same potential which arises when analyzing the stability of the sine-Gordon soliton, Eq. (3.18). We will pick our normalized trial wave function accordingly:

$$\psi_0 = \sqrt{\frac{\sigma}{2}}\,\mathrm{sech}(\sigma z'), \tag{3.41}$$

with σ being the variational parameter. Note that this trial wave function satisfies the required boundary conditions $\psi_o(z' = \pm\infty) \to 0$. For the first excited state, we must pick an odd function of z. We will choose the properly normalized function

$$\psi_1 = \sqrt{\frac{3\sigma}{2}}\tanh(\sigma z')\,\mathrm{sech}(\sigma z'). \tag{3.42}$$

Applying the variational principle, we must calculate

$$E_n^{(2)}(\sigma) = \frac{f_\pi^2 v^2}{\lambda} \langle \psi_n | \left(-\partial_{z'}^2 + \frac{\lambda^2}{2 f_\pi^2 v^2} U_- \right) | \psi_n \rangle, \tag{3.43}$$

and minimize this quantity with respect to σ to obtain an upper bound $E_n^{(2)}(\sigma)$ on the energy of the n^{th} state. The integral given by Eq. (3.43) must be performed numerically.

We now have the framework in place in order to test the stability of our domain wall configurations. Setting $\mu \sim 800$ MeV and $m_s \sim 100$ MeV, we see that the ratio of the coefficients is $\beta_1/\beta_2 \approx 0.3$. In this case, the linear terms (3.29) and (3.31) are small and the solutions given by Eq. (3.21) are valid approximations to the exact solutions. In Fig. 3.3, we show the effective Schrödinger potential $U_{\text{eff}} = \lambda^2 U_-/(2 f_\pi^2 v^2)$ for $\mu = 800$ MeV. For the above choice of parameters, the wall tension given by Eq. (3.25) is

$$E^{(0)}(\phi_o, \rho_o) \approx 17.48 \frac{f_\pi^2 v^2}{\lambda}. \tag{3.44}$$

For the trial wave functions given in Eqs. (3.41) and (3.42), the following results for the two bound states of Eq. (3.40) were obtained:

$$\begin{aligned} E_0^{(2)}(\sigma_{\text{min}}) &\leq -0.016 \frac{f_\pi^2 v^2}{\lambda}, \\ E_1^{(2)}(\sigma_{\text{min}}) &\leq +1.163 \frac{f_\pi^2 v^2}{\lambda}. \end{aligned} \tag{3.45}$$

From this, we can see that $E_1^{(2)} \gg E_0^{(2)}$ and both of these quantities are much less the wall tension given by Eq. (3.44). Even though the ground state energy seems to be negative, due to the fact that $E_1^{(2)} \gg E_0^{(2)}$ we can associate this mode with the zero mode. The small nonzero eigenvalue is actually an artifact of our approximations. The appearance of a negative mode is merely

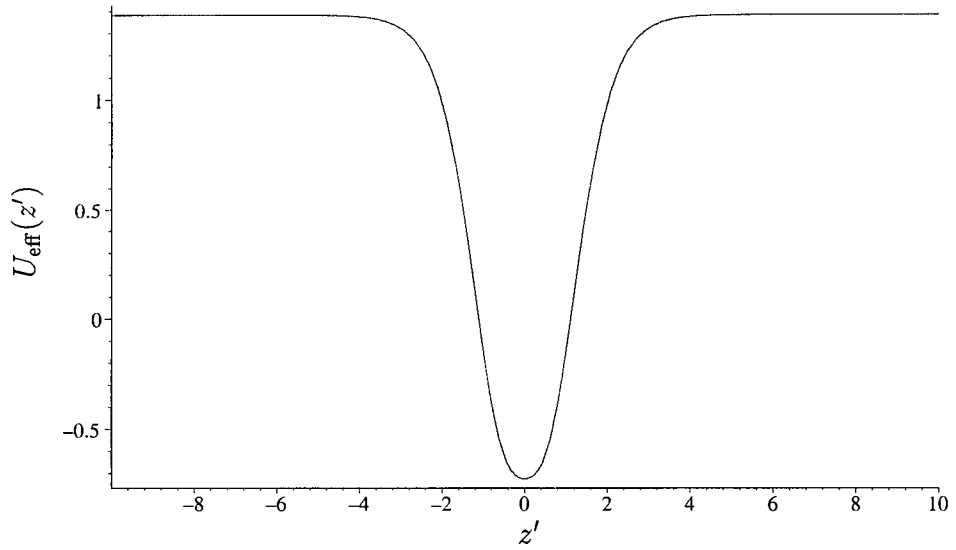

Figure 3.3: This figure shows the effective Schrödinger potential $U_{\text{eff}}(z') = (\lambda^2/2f^2v^2)U_-(z')$ as a function of the dimensionless coordinate z' where U_- is given by Eq. (3.37). The presence of a negative eigenvalue in the spectrum of this potential is indicative of the instability of the classical domain wall solution. The effective potential is shown in this figure for $\mu = 800$ MeV.

a consequence of the approximate solutions (3.21) as discussed above. This identification can be verified by increasing the chemical potential. When the above calculations are repeated as the chemical potential is increased, we see that the energy $E_0^{(2)} \to 0$. This result is expected due to the fact that the $|\Sigma|$ field can be integrated out as μ increases and the sine-Gordon type theory is recovered. As μ is increased, we also see that the eigenvalue of the first excited state ω_1 increases towards the maximum value of U_{eff}. Eventually, as μ is increased further, there is no longer a first excited bound state in the

spectrum. The calculation of $E_0^{(2)}$ and $E_1^{(2)}$ was done with the variational functions chosen to be different from Eqs. (3.41) and (3.42). The results obtained were the same order of magnitude as stated above (3.45). This supports our interpretation of the $E_0^{(2)}$ state as the would-be translational mode if exact solutions are known. The magnitudes of the linear terms (3.29) and (3.31) are approximately the same order of magnitude of $E_0^{(2)}$, which supports our interpretation of $E_0^{(2)}$ as the zero mode.

3.5 Conclusion

In this chapter we presented an analysis of the classical stability of $U(1)_A$ domain walls [88, 89]. Naively one would expect that decreasing μ from $\mu \gg 1$ GeV (when the calculations are under control [88, 89]), we would inevitably face the situation in which the domain walls become unstable objects due to the fast growth of the coefficient β_1 (3.11). This expectation may not necessarily be correct due to the even faster growth of the coefficient β_2 (3.11) which receives contributions from the formation of $I\bar{I}$ molecules as well as perturbative contributions.

What we have actually demonstrated is that the domain wall solution remains classically stable down to $\mu \simeq 800$ MeV. In order to assess the stability of the domain walls for $\mu_c \lesssim \mu \lesssim 800$ MeV, one must explicitly include the $I\bar{I}$ contribution in the effective potential (which is expected to be the dominant contribution at $\mu \sim \mu_c$ [74]). This would hopefully lead to $\beta_1/\beta_2 < 1$, ensuring the classical stability of the $U(1)_A$ domain walls. Unfortunately, due to the lack of information in this region we cannot generalize our results

to below 800 MeV to μ_c. However, we can argue that the $U(1)_A$ domain walls remain classically stable down to $\mu \gtrsim \mu_c$ due to the faster growth of the coefficient β_2 compared to β_1 as μ is decreased. The ratio β_1/β_2 may be very sensitive to changes in the instanton size distribution or the various form factors. This is a difficult problem and unfortunately we do not know how to estimate such contributions for a small chemical potential.

We should remark here that the stability of the $U(1)_A$ domain wall implies a classical stability of the $U(1)_A$ strings [38], which become the edge of the domain walls. It remains to be seen whether these topological defects will have any impact on the physics of neutron stars and other compact stellar objects with high core density μ.

Chapter 4

Superconducting K-Strings in High Density QCD

4.1 Overview

As we discussed in Chapter 2, the nonzero diquark condensate in the CFL phase of high density QCD breaks various symmetries that are respected at zero baryon density. Specifically, both the exact $U(1)_B$ and the approximate axial $U(1)_A$ symmetries of QCD are spontaneously broken, leading to the formation of $U(1)_A$ and $U(1)_B$ global strings described in [38]. The main global property of the strings, the string tension $\alpha_{\rm str}$, has been calculated in [38] with the result $\alpha_{\rm str} \sim 2\pi v^2 f_\pi^2 \ln R$. The decay constant $f_\pi \sim \mu$ is set by the chemical potential μ in dense QCD, $v^2 \simeq 1/3$ is the velocity of Goldstone modes in this media, and R is an upper cutoff determined by the environment of the string (for example, the presence of other strings).

If, in addition to the CFL phase, K^0-condensation also occurs as argued in [11, 12, 45, 77] and reviewed in Chapter 2, then the hypercharge symmetry $U(1)_Y$ is also spontaneously broken. If this is the case, the formation of one more type of strings related to the spontaneously broken $U(1)_Y$ global symmetry is possible [38]. The string tension $\alpha_{\rm str}$ in this case behaves similarly

to $U(1)_A$ and $U(1)_B$ global strings, and is determined by the corresponding decay constant $f_\pi \sim \mu$. The next step in studying $U(1)_Y$ strings was undertaken in [44] where it was demonstrated that the internal core structure of the $U(1)_Y$ string could be very different from the $U(1)_A$ and $U(1)_B$ global strings described earlier in [38]. It was argued that the relevant symmetry may not be restored in the core. In most known cases, particularly in magnetic vortices in a conventional superconductor, the $U(1)_{EM}$ symmetry is restored inside the core. If this is the case, the $U(1)_Y$ string becomes superconducting with the core having a K^+ condensate. It has been known for quite a while that this unusual behavior may occur in the the theory of cosmic strings and in quantum field theory in general [42, 100]. Experiments with ^3He have provided a concrete example of vortices with nontrivial core structure in nature. Under certain conditions the vortices in the superfluid $^3He - B$ phase of ^3He have a core that is filled with the $^3He - A$ phase (see [76] for a review). High temperature superconductors [7, 103] and two component Bose-Einstein condensates [63] provide other examples of this phenomena. However, this behavior of the vortex core is considered an exception rather than a common phenomenon in physics.

The $U(1)_Y$ strings might be phenomenologically relevant objects realized in nature (presumably in neutron stars). In this chapter we will analyze the core structure of $U(1)_Y$ strings in detail. First, we will explain the phenomenon of a core transition in the interior of the vortices qualitatively, using some analytical estimates. We will then go on to make quantitative estimates for the phenomenologically relevant parameters in the CFL+K^0 phase when the core transition does occur.

The fact that there should be some kind of phase transition in the string core as a function of the external parameters can be understood from the following simple arguments. If the up and down quark mass difference $m_d - m_u$ is relatively large, then there would only be a $U(1)$ (rather than $SU(2)_I$) symmetry which is broken. The standard topological arguments suggest that in this case, the K^0-string would be a topologically stable configuration with the restoration of the corresponding $U(1)$ symmetry inside the core. If $m_d - m_u$ is exactly zero then the $SU(2)_I$ symmetry is exact and symmetry arguments suggest that both of the K^0 and K^+ fields condense. In this case no global stable strings are possible. From these two limiting cases, it is clear that there should be some intermediate region that somehow interpolates (as a function of $m_d - m_u$) between the two. We will now describe the way this interpolation works. For relatively large $m_d - m_u$ nothing unusual happens. The K^0-string is normal, K^0 is condensed outside the core and the symmetry is restored inside the core. At some finite magnitude of $m_d - m_u$, an instability arises through the condensation of the K^+-field inside of the core of the string. As the magnitude of $m_d - m_u$ decreases, the size of the core becomes larger and larger with nonzero values for both the K^0 and the K^+ condensates inside the core. Finally, at $m_d = m_u$ the core of the string (with nonzero K^0 and K^+ condensates) fills the entire space, in which case the meaning of the string is completely lost, and we are left with the situation where the $SU(2)_I$ symmetry is exact: no stable strings are possible.

Given this argument, we would expect that there must be some transition region where the $SU(2)_I$ symmetry is broken and K^+-condensation will occur inside the core. The point at which this occurs will be estimated in this chap-

ter. We will show that K^+-condensation only occurs above a certain point $\theta_{K^0} > \theta_{\rm crit}$, with $\theta_{\rm crit}$ given by $\sin(\theta_{\rm crit}/2) \simeq$ constant $(\Delta/m_s)\sqrt{(m_d - m_u)/m_s}$, where $\Delta \sim 100$ MeV is the superconducting gap and m_s is the strange quark mass. This analytical calculation, along with a numerical solution, allows us to describe the region in parameter space where this phenomenon certainly happens.

4.2 Superconducting K-strings

We will begin by considering global K^0-strings when they are topologically stable. This case corresponds to the approximation when the splitting between K^0 and all other degrees of freedom is relatively large so that in our effective Lagrangian description we can neglect all fields except K^0. After this we will analyze the situation when the K^0 and K^+ masses are degenerate such that the K^0-strings become unstable. Finally, we will introduce a small explicit isospin violation into our description $\sim (m_d - m_u)$ in order to analyze the stability/instability issue for the physically relevant case. The important global characteristic of the K^0-string, the string tension $\alpha_{\rm str}$, is determined to logarithmic accuracy by the pion decay constant $\alpha_{\rm str} \sim f_\pi^2$ as discussed in [38], and it is not sensitive to the internal structure of the core. The subject of this chapter is the analysis of the core structure of the K^0-strings.

4.2.1 Topologically stable $U(1)$ strings in $CFL + K^0$ phase

We start by considering the following effective field theory which describes a single complex K^0 field. In order to describe K^0 condensation, we will use the following effective Lagrangian (obtained from Eq. (2.6)

$$\mathcal{L}_{\text{eff}}(K^0) = |(\partial_0 + i\mu_{\text{eff}})K^0|^2 - v^2|\partial_i K^0|^2 - m_0^2|K^0|^2 - \lambda|K^0|^4. \tag{4.1}$$

The parameters in Eq. (4.1) are defined in Eqs. (2.7) and (2.9). We neglect all other degrees of freedom at this point. If $\mu_{\text{eff}} > m_0$ the kaon field acquires a nonzero vacuum expectation value $\langle K^0 \rangle = \eta/\sqrt{2}$ where

$$\eta^2 = \frac{\mu_{\text{eff}}^2 - m_0^2}{\lambda} = \frac{\mu_{\text{eff}}^2}{\lambda}(1 - \cos\theta_{K^0}). \tag{4.2}$$

For $\mu_{\text{eff}} > m_0$ it is more convenient to represent the effective Lagrangian in the familiar form of a Mexican hat type potential:

$$\begin{aligned} \mathcal{L}_{\text{eff}} = |\partial_0 K^0|^2 \;&+\; i\mu_{\text{eff}}(\partial_o \bar{K}^0)K^0 - i\mu_{\text{eff}}\bar{K}^0(\partial_o K^0) \\ &-\; v^2|\partial_i K^0|^2 - \lambda\left(|K^0|^2 - \frac{\eta^2}{2}\right)^2. \end{aligned} \tag{4.3}$$

This is a textbook Lagrangian with a spontaneously broken global $U(1)$ symmetry which admits topologically stable global string solutions. As is well-known, global strings are solutions of the time independent equation of motion. The time independent equation of motion for K^0 is given by:

$$v^2\nabla^2 K^0 \;=\; 2\lambda\left(|K^0|^2 - \frac{\eta^2}{2}\right)K^0. \tag{4.4}$$

For the K^0-string solution we will make the following ansatz:

$$K^0_{\text{string}} \;=\; \frac{\eta}{\sqrt{2}} f(r) e^{in\phi}, \tag{4.5}$$

where n is the winding number of the string (we will take $n = 1$ in what follows), ϕ is the azimuthal angle in cylindrical coordinates, and $f(r)$ is a yet to be determined solution of Eq. (4.4) which obeys the boundary conditions $f(0) = 0$ and $f(\infty) = 1$. Substituting this ansatz into Eq. (4.4), we arrive at the following ordinary differential equation:

$$\frac{1}{r}\frac{d}{dr}\left(r\frac{df(r)}{dr}\right) - \frac{f(r)}{r^2} = \frac{\mu_{\rm eff}^2(1-\cos\theta_{K^0})}{v^2}(f(r)^2-1)f(r), \tag{4.6}$$

where we have replaced $\lambda\eta^2 \to \mu_{\rm eff}^2(1-\cos\theta_{K^0})$ according to Eq. (4.2). Although a numerical solution of this equation is possible, the most important part of this section is an analytical analysis and, therefore, we prefer to take a variational approach. We follow [42, 104] and assume a solution of the form:

$$f(r) = 1 - e^{-\beta r}, \tag{4.7}$$

with the variational parameter β. Minimizing the energy with respect to β, the result is [104]:

$$\beta_{\rm min}^2 = \frac{89}{144}\frac{\mu_{\rm eff}^2}{v^2}(1-\cos\theta_{K^0}). \tag{4.8}$$

This result was compared with the exact numerical solution of (4.6) and is a reasonable approximation. From this equation we see that a typical string core radius is given by $r_{\rm core} \sim 1/\beta_{\rm min} \sim v/\mu_{\rm eff}(\sin\theta_{K^0}/2)$ and it becomes smaller when $\mu_{\rm eff}$ gets larger. The first important lesson of this simple exercise is the observation that the global string is stable and the $U(1)$ symmetry is restored inside of the core, $f(r=0) = 0$, as expected. The second important lesson is the observation that the core size becomes large when $\theta_{K^0} \to 0$.

4.2.2 Unstable $SU(2)_I \times U(1)_Y \to U(1)$ strings in $CFL + K^0$ phase

Our next task is an analysis of the K^0-string when isospin is an exact symmetry (*i.e.* $m_u = m_d$) and the symmetry pattern breaking is $SU(2)_I \times U(1)_Y \to U(1)$. We know that the K^0-string is unstable, based on topological arguments. We want to analyze the stability issue in detail to understand this phenomenon on a quantitative level.

To simplify things we start with the effective Lagrangian which only includes a single complex kaon doublet $\Phi = (K^+, K^0)$. As discussed in [12], this approach is justified to discuss kaon condensation in the CFL phase if all other degrees of freedom are much heavier. As before (see Eqs. (4.1,4.3)) we can represent the effective Lagrangian in the form of a Mexican hat type potential,

$$\begin{aligned}\mathcal{L}_{\rm eff}(\Phi) = |\partial_o \Phi|^2 \ , \ + \ & i\mu_{\rm eff}(\partial_o \bar{\Phi}^{\rm T})\Phi - i\mu_{\rm eff}\bar{\Phi}^{\rm T}(\partial_o \Phi) \\ - \ & v^2 |\partial_i \Phi|^2 - \lambda \left(|\Phi|^2 - \frac{\eta^2}{2} \right)^2 . \end{aligned} \tag{4.9}$$

All parameters are defined in the same way as in (2.9,4.2,4.3) and the Φ field acquires a nonzero vacuum expectation value of the form

$$\langle \Phi \rangle = (0, \frac{\eta}{\sqrt{2}}). \tag{4.10}$$

The time independent equations of motion for K^0 and K^+ are given by:

$$v^2 \nabla^2 K^+ = 2\lambda(|K^+|^2 + |K^0|^2 - \frac{\eta^2}{2})K^+, \tag{4.11}$$

$$v^2 \nabla^2 K^0 = 2\lambda(|K^+|^2 + |K^0|^2 - \frac{\eta^2}{2})K^0. \tag{4.12}$$

For the K^0-string solution we will make the following ansatz:

$$K^0_{\text{string}} = \frac{\eta}{\sqrt{2}} f(r) e^{in\phi}, \quad K^+ = 0, \tag{4.13}$$

where $f(r)$ is the solution of Eq. (4.6) with the boundary conditions $f(0) = 0$ and $f(\infty) = 1$. From topological arguments we know that although the solution (4.13) satisfies the equation of motion (4.11, 4.12), it is an unstable solution. The source of instability can be seen as follows. We follow the standard procedure and expand the energy in the K^0-string background to quadratic order in K^+ and K^0 modes:

$$E(K^0 = K^0_{\text{string}} + \delta K^0,\ K^+) \approx E_{\text{string}} + \delta E. \tag{4.14}$$

We know that the K^0-string itself is a stable configuration, therefore, the δK^0 modes cannot have negative eigenvalues which would correspond to the instability. Therefore, we concentrate only on the "dangerous" modes related to K^+ fluctuations, in which case δE is given by:

$$\delta E = \int d^2r \left(v^2 |\nabla K^+|^2 + \mu^2_{\text{eff}} (1 - \cos\theta_{K^0})(f(r)^2 - 1)|K^+|^2 \right), \tag{4.15}$$

where $f(r)$ is the solution of Eq. (4.6) with the boundary conditions $f(0) = 0$ and $f(\infty) = 1$. If δE is a positive quantity, then the K^0-string is absolutely stable and the K^+ modes do not destroy the string configuration. If δE is negative, this means that this is a direction in configuration space where the K^0-string decays. Following [43], the K^+ field can be expanded in Fourier modes:

$$K^+ = \frac{\eta}{\sqrt{2}} \sum_m g_m(r) e^{im\phi}. \tag{4.16}$$

Now we have the K^+ field in terms of the dimensionless Fourier components $g_m(r)$. Setting $m = 0$ in the above expansion in order to analyze the lowest

energy δE_0 contribution in (4.15), we arrive at:

$$\delta E_0 = \frac{\eta^2}{2}\int d^2r \left(v^2(\frac{\partial g_0(r)}{\partial r})^2 + \mu_{\rm eff}^2(1-\cos\theta_{K^0})(f^2(r)-1)g_0^2(r)\right). \quad (4.17)$$

In order to have dimensionless coordinates and fields, we will perform the following change of variables, $\tilde{r} = \gamma r$, where $\gamma \equiv \mu_{\rm eff}/v$. This change of variables sets the string width in $f(\tilde{r})$ to be $\tilde{r}_{\rm core} \sim 1$. Equation (4.17) now reads:

$$\delta E_0 = \frac{\eta^2 v^2}{2}\int d^2\tilde{r}\, g_0(\tilde{r})\hat{O}g_0(\tilde{r}), \quad (4.18)$$

where

$$\begin{aligned} \hat{O} &= -\frac{1}{\tilde{r}}\frac{d}{d\tilde{r}}(\tilde{r}\frac{d}{d\tilde{r}}) + \lambda'(f^2(\tilde{r})-1), \quad (4.19)\\ \lambda' &= (1-\cos\theta_{K^0}). \end{aligned}$$

The problem is reduced to the analysis of the two-dimensional Schrödinger equation for a particle in an attractive potential $V(r) = -\lambda'(1-f^2(\tilde{r}))$ with $f(\tilde{r})$ being the solution of Eq. (4.6) with the boundary conditions $f(0) = 0$ and $f(\infty) = 1$. This potential is negative everywhere and approaches zero at infinity. We know from standard quantum mechanics [53] that for an arbitrarily weak potential well there is always a negative energy bound state in one and two spatial dimensions; in three dimensions a negative energy bound state may not exist. For the two dimensional case (the relevant problem in our case) the lowest energy level of the bound state is always negative and exponentially small for small λ'. One should note that our specific potential $V(r) = -\lambda'(1-f^2(\tilde{r}))$ which enters (4.19) is not literally the potential well, however one can always construct the potential well V' such that its

absolute value is smaller than $|V(r)|$ everywhere, *i.e.* $|V'| < |V(r)|$ for all r. For the potential well V' we know that the negative energy bound state always exists; when V' is replaced by V it makes the energy eigenvalue even lower. Therefore, the operator (4.19) has always a negative mode regardless of the local properties of the function $f(r)$. As a consequence, the string (4.5) is an unstable solution of the classical equation of motion. We expected this result from the beginning from topological arguments. The instability manifests itself in the form of a negative energy bound state solution of the corresponding two-dimensional Schrödinger equation (4.18) regardless of the magnitudes of the parameters.

4.2.3 K^+-condensation in the core of K^0-strings in $CFL + K^0$ phase

The issue of the stability or instability of K^0-strings reviewed in the previous section is highly sensitive to the degree of symmetry present in the Lagrangian describing the K^0/K^+ system. If the $SU(2)_I$ symmetry is strongly broken, the K^0-strings will be absolutely (topologically) stable as discussed in subsection 4.2.1. If the $SU(2)_I$ symmetry remains unbroken, the K^0-strings will always be unstable as discussed in subsection 4.2.2. We will now introduce an explicit symmetry breaking parameter δm^2 into (4.9) that is fixed by the original Lagrangian (2.6) such that our simplified version of the system (only

$\Phi = (K^+, K^0)$ fields are taken into account) has the form[1]

$$\begin{aligned} \mathcal{L}_{\text{eff}}(\Phi) &= |\partial_0\Phi|^2 + i\mu_{\text{eff}}(\partial_o\bar{\Phi}^{\text{T}})\Phi - i\mu_{\text{eff}}\bar{\Phi}^{\text{T}}(\partial_o\Phi) \\ &- v^2|\partial_i\Phi|^2 - \lambda\left(|\Phi|^2 - \frac{\eta^2}{2}\right)^2 - \delta m^2\Phi^\dagger\tau_3\Phi, \qquad (4.20) \\ \delta m^2 &\equiv \frac{a}{2}m_s(m_d - m_u), \end{aligned}$$

We anticipate that, as the symmetry breaking parameter δm^2 in Eq. (4.20) becomes sufficiently large, a stable K^0-string with a restored $U(1)$ symmetry in the core, $f(r = 0) = 0$, must be reproduced, as discussed in subsection 4.2.1. When the symmetry breaking parameter δm^2 in becomes sufficiently small, one should eventually reach a point where the K^+ instability occurs, and it is energetically favorable for a K^+ condensate to form inside the core of the string.

In this subsection we calculate the critical value of θ_{K^0} when the K^+ instability occurs, and a K^+ condensate does form in the string core. In addition to this, we will obtain an estimate of the absolute value of the K^+-condensate at the center of the core of the string ($r = 0$). In order to determine if K^+-condensation occurs within the core of K^0-strings, we would

[1]In addition to the mass splitting proportional to the difference $m_d - m_u$, there is also a splitting due to electromagnetic effects, $\delta m^2_{EM} \sim \alpha_{EM}\Delta^2/(8\pi)$. As we have already mentioned, the electromagnetic contribution becomes important at very large chemical potential [11]. However, this correction can be neglected for the present work since we are not considering large chemical potentials and it only amounts to a 10% correction, $\delta m_{EM}/\delta m \sim 0.1$. In order to remain self-consistent, we neglect all electromagnetic contributions throughout this chapter.

like to solve the set of coupled differential equations

$$v^2\nabla^2 K^+ = 2\lambda(|K^+|^2 + |K^0|^2 - \frac{\eta^2}{2})K^+ + \delta m^2 K^+, \quad (4.21)$$

$$v^2\nabla^2 K^0 = 2\lambda(|K^+|^2 + |K^0|^2 - \frac{\eta^2}{2})K^0 - \delta m^2 K^0. \quad (4.22)$$

with the appropriate boundary conditions. We will follow a different approachto gain a deeper understanding of the phenomenon of K^+-condensation. In order to verify our quantitative picture of the way the instability manifests itself as the $SU(2)_I$ symmetry is restored, we will linearize Eq. (4.21) about the K^0-string solution given by Eqs. (4.5) and (4.7). The linearized equation reads:

$$\frac{d^2K^+}{dr^2} + \frac{1}{r}\frac{dK^+}{dr} - \frac{\delta m^2}{v^2}K^+ = 0. \quad (4.23)$$

We recognize Eq. (4.23) as the modified Bessel equation of order 0. Given this, we can immediately write down the solution for asymptotically large distances, where this approximation is justified, $K^+ \sim K_0(\delta m r/v)$. This asymptotic solution verifies the qualitative picture sketched earlier, the width of the condensate on the core of K^0-string grows as $1/\delta m$ and fills all space as $\delta m \to 0$. We are mainly interested in the *critical values* of the parameters when K^+-condensation starts to occur inside the core. In this case we can treat K^+ field as a small perturbation in the K^0 background field. Such an approach is not justified when K^+-condensation is already well-developed in which case both fields K^0 and K^+ must be treated on the same footing. However, this approach is quite appropriate when one studies the transition from the phase where K^+ background field is zero to the region where it becomes nonzero.

To begin, we will expand the energy in the constant K^0-string background

to quadratic order in K^+:

$$E \approx E_{\text{string}} + \delta E, \tag{4.24}$$

where δE is given by:

$$\begin{aligned}\delta E = \int d^2r \left(v^2|\nabla K^+|^2 \right. &+ \mu_{\text{eff}}^2(1-\cos\theta_{K^0})\cdot(f^2(r)-1)|K^+|^2 \\ &\left. + \frac{a}{2}m_s(m_d-m_u)\,|K^+|^2\right). \end{aligned}\tag{4.25}$$

If δE is a positive quantity, then the K^0-string is stable and K^+ condensation does not occur inside the core of the string. If δE is negative, this means that it is energetically favorable for K^+ condensation to occur inside the core of the string. We follow the same procedure as before keeping the most "dangerous" mode to arrive at:

$$\begin{aligned}\delta E = \frac{\eta^2}{2}\int d^2r \left(v^2(\frac{\partial g_0(r)}{\partial r})^2 \right. &+ \mu_{\text{eff}}^2(1-\cos\theta_{K^0})\cdot(f^2(r)-1)g_0^2(r) \\ &\left. + \frac{a}{2}m_s(m_d-m_u)g_0^2(r)\right). \end{aligned}\tag{4.26}$$

In dimensionless variables this expression can be represented as follows

$$\delta E = \frac{\eta^2 v^2}{2}\int d^2\tilde{r}\; g_0(\tilde{r})[\hat{O}+\epsilon]g_0(\tilde{r}), \tag{4.27}$$

where

$$\begin{aligned}\hat{O} &= -\frac{1}{\tilde{r}}\frac{d}{d\tilde{r}}(\tilde{r}\frac{d}{d\tilde{r}}) + (1-\cos\theta_{K^0})(f^2(\tilde{r})-1), \\ \epsilon &\equiv \frac{a}{2}\frac{m_s(m_d-m_u)}{\mu_{\text{eff}}^2}.\end{aligned}$$

The only difference between this expression and Eq. (4.18) describing the instability of the string in case of exact isospin symmetry is the presence of the

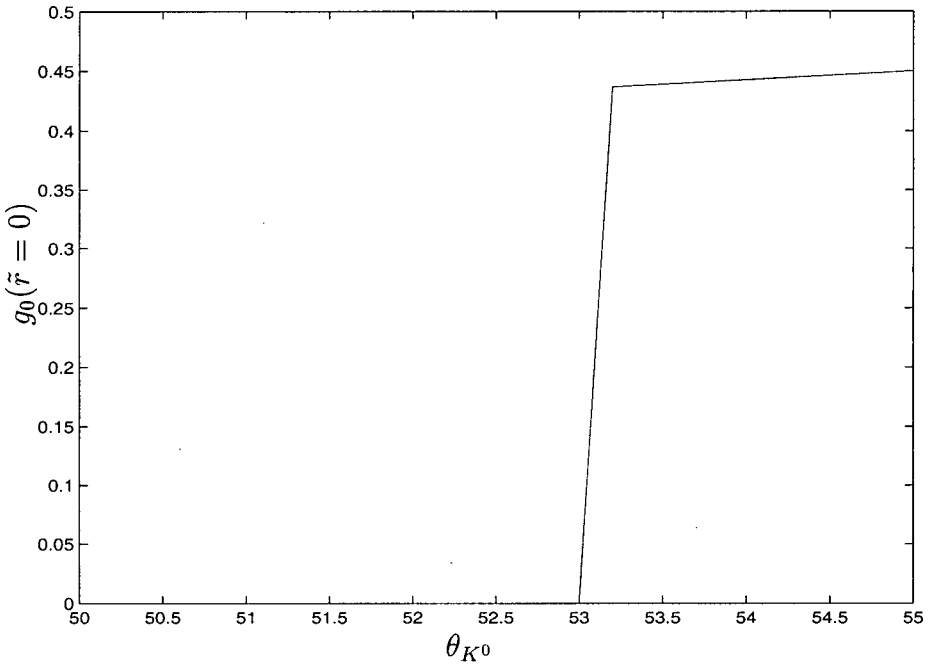

Figure 4.1: In this figure we plot the the value of the K^+-condensate at the centre of the K^0-string $g_0(\tilde{r}=0)$ as a function of the kaon condensation angle θ_{K^0}. From this graph, we can see that K^+-condensation occurs at $\theta_{K^0} \gtrsim 53^o$.

term $\sim \epsilon$ in Eq. (4.27). The problem of determining when K^+-condensation occurs is now reduced to solving the Schrödinger type equation $\hat{O}g_0 = \hat{E}g_0$. From the previous discussions we know that $\hat{E}$ for the ground state is always negative. However, to insure the instability with respect to K^+-condensation one should require a relatively large negative value *i.e.* $\hat{E} + \epsilon < 0$. It can not happen for arbitrary weak coupling constant $\sim (1 - \cos\theta_{K^0})$ when θ_{K^0} is small. However, it does happen for relatively large θ_{K^0}. To calculate the

minimal critical value $\theta_{\rm crit}$ when K^+-condensation develops, one should calculate the eigenvalue $\hat{E}$ as a function of parameter θ_{K^0} and solve the equation $\hat{E}(\theta_{\rm crit}) + \epsilon = 0$. As we mentioned earlier, for very small coupling constant $\lambda' = (1 - \cos\theta_{K^0}) \to 0$ the bound state energy is negative and exponentially small, $\hat{E} \sim -e^{-\frac{1}{\lambda'}}$. However, for realistic parameters of μ, Δ, m_s, m_u, m_d the parameter ϵ is not very small and we expect that in the physical region of parameter space the bound state energy $\hat{E}$ is the same order of magnitude as the potential energy $\sim \lambda'$. In this case we can estimate $\theta_{\rm crit}$ from the following conditions $-\hat{E}(\theta_{\rm crit}) \sim \lambda' \sim (1 - \cos\theta_{\rm crit}) \sim \epsilon$ as

$$\sin\frac{\theta_{\rm crit}}{2} \sim {\rm const}\frac{\Delta}{\pi f_\pi}\sqrt{\frac{m_s(m_d - m_u)}{\mu_{\rm eff}^2}} \sim {\rm const}\frac{\Delta}{m_s}\sqrt{\frac{(m_d - m_u)}{m_s}}, \qquad (4.28)$$

where we have neglected all numerical factors in order to explicitly demonstrate the dependence of $\theta_{\rm crit}$ on the external parameters. The limit of exact isospin symmetry, which corresponds to $m_d \to m_u$ when the string becomes unstable, can easily be understood from the expression (4.28). Indeed, in the case that the critical parameter $\theta_{\rm crit} \to 0$ becomes arbitrarily small, the K^+ instability would develop for arbitrarily small $\theta_{K^0} > 0$. The region occupied by the K^+ condensate at this point is determined by the behavior of lowest energy mode g_0 at large distances, $g_0(\tilde{r} \to \infty) \sim \exp(-\hat{E}\tilde{r})$ with the core size $\tilde{r}_{\rm core} \sim (m_d - m_u)^{-1} \to \infty$ as expected.

In order to make a quantitative, rather than qualitative, estimate of the critical value $\theta_{\rm crit}$ when $\hat{E}(\theta_{\rm crit}) + \epsilon = 0$, we discretize the operator $\hat{O}$ and solve the problem numerically, with the boundary conditions $g_0(\infty) = 0$ and $g_0(0) =$ constant. Varying the condensation angle θ_{K^0}, we see that a negative eigenvalue $\hat{E} + \epsilon < 0$ appears when $\theta_{K^0} > \theta_{\rm crit} \approx 53^o$. The following

parameters were used: $m_u = 5$ MeV, $m_d = 8$ MeV, $m_s = 150$ MeV, $\mu = 500$ MeV, and $\Delta = 100$ MeV which gives $\epsilon \equiv am_s(m_d - m_u)/(2\mu_{\rm eff}^2) \simeq 0.1$. In Fig. 4.1 we show a plot of $g_0(\tilde{r} = 0)$ as a function of θ_{K^0}. One can see that the transition from no K^+-condensation is reached at about $\theta_{\rm crit} \approx 53^o$. Note that there is an abrupt point at which K^+-condensation occurs inside the core. The transition to the K^+-condensed core corresponds to a jump at $\theta_{\rm crit}$. The finite slope on the plot at this point is due to the discretization of the θ_{K^0} variable. In Fig. 4.2 we plot the functions $f(\tilde{r})$ (related to the K^0-string by (4.5)) and $g_0(\tilde{r})$ (related to the K^+ condensate by (4.16)) as a function of the rescaled coordinate $\tilde{r}$. One can see that the K^+ condensate falls off over the same distance scale as the K^0-string reaches its vacuum expectation value. We should note that the solution to the above Schrödinger equation does not give us the overall normalization of the function $g_0(\tilde{r})$. We have estimated the overall normalization of $g_0(\tilde{r})$ by minimizing the total energy of the system using a variational approach. We have demonstrated above that K^+ condensation might occur in the core of K^0-strings if some conditions are met. We have also explained how this phenomenon depends on the external parameters and derived the equation $\hat{E}(\theta_{\rm crit}) + \epsilon = 0$, the solution of which allows us to calculate the critical parameters when K^+ condensation starts to occur. All these discussions were quite general because they were based on the symmetry and topological properties of the system rather than on a specific form of the interaction. However, the numerical estimates presented above were derived by using a concrete form of the effective Lagrangian (4.20) describing the lightest degrees of freedom, K^+ and K^0. To formulate the question of how sensitive our numerical results are when the form of

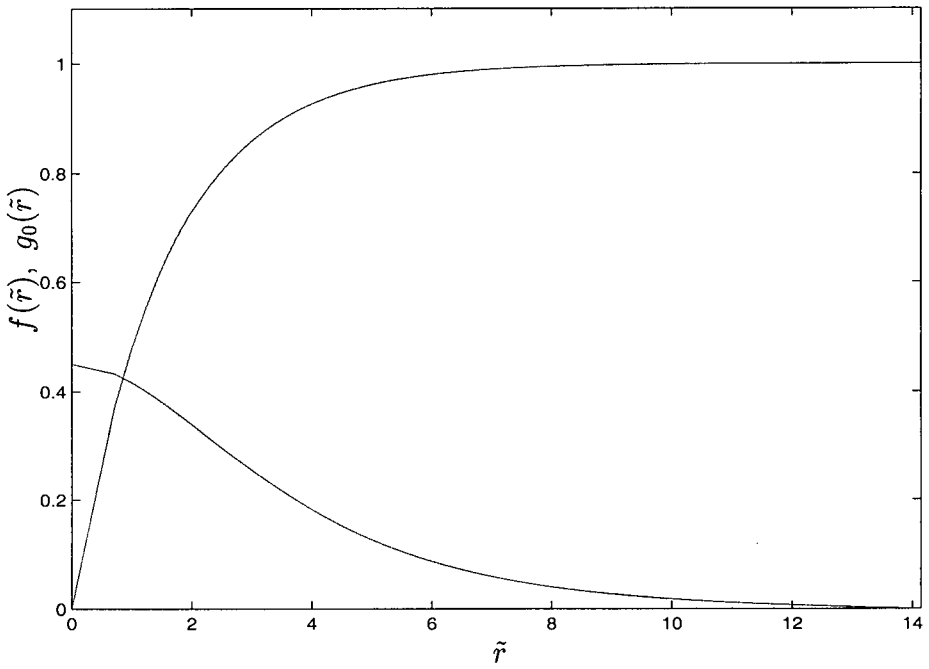

Figure 4.2: In this figure we plot the functions $f(\tilde{r})$ and $g_0(\tilde{r})$ as a function of the dimensionless rescaled coordinate $\tilde{r} \equiv \mu_{\rm eff} r/v$. The function $f(\tilde{r})$ is the line that approaches 1 for large $\tilde{r}$ in the graph above, while $g_0(\tilde{r})$ approaches 0 at large $\tilde{r}$.

the potential changes in a more specific way, let us remind the reader that the effective Lagrangian describing the Goldstone modes can be represented in many different forms as long as the symmetry properties are satisfied. The results for the amplitudes describing the interaction of the Goldstone particles do not depend on the specific representation used. A well-known example of this fact is the possibility of describing the π meson properties by using a linear σ model as well as a nonlinear σ model (and many other models

which satisfy the relevant symmetry breaking pattern). The results remain the same if one discusses the local properties of the theory (for example, the $\pi - \pi$ scattering length) when the π meson is considered as a small quantum fluctuation rather than a large background field . It may not be the case when π represents a large background field in which case some numerical difference between different representations of the effective Lagrangian may occur. Roughly speaking, the source of the difference is an inequality $\pi(x) \neq \sin \pi(x)$ for large global background fields such as a string solution which is the subject of this chapter.

Having this in mind, we repeated similar numerical estimates discussed above for the original effective Lagrangian (2.6) where Goldstone fields represented in the exponential form rather than in form determined by the effective Lagrangian (4.20). As before, in these estimates we considered exclusively K^+ modes which are the energetically lowest modes and which can potentially destabilize the system presented by the background field of the K^0-string. This approximation is justified as long as the K^+ field is the lowest massive excitation in the system where a K^0 condensate develops. Also, the typical size of the core must be larger than the inverse gap Δ^{-1}, *i.e.* $r_{\text{core}} \simeq v/\mu_{\text{eff}} \gg \Delta^{-1}$ in order to maintain color superconductivity inside the core. We assume that this is the case. Our numerical results suggest that the critical parameters are not very sensitive to the specific form of the Lagrangian such that θ_{crit} is close to our previous numerical estimates. Therefore, the real world (with our parameters $\theta_{K^0} \simeq 70^o$) case corresponds to $\theta_{K^0} > \theta_{\text{crit}}$ and a K^+ condensate does develop inside the core of the K^0-strings.

4.3 Conclusion

We have demonstrated that, within the CFL+K^0 phase of QCD, K^+ condensation does occur within the core of global K^0 strings if some conditions are met, *i.e.* $\theta_{K^0} > \theta_{\text{crit}}$. We have presented two estimates for θ_{crit}; an analytical one which gives a qualitative explanation of the phenomenon, as well as numerical one for the physically relevant parameters realized in nature. Our results suggest that if a CFL+K^0 phase is realized in nature, it is likely that K^0 strings form together with K^+ condensation inside the core, in which case the strings become superconducting K-strings. In the next chapter we will explore one of the consequences of K^+ condensation in the core of K^0-strings.

Chapter 5

Drum Vortons in High Density QCD

5.1 Overview

In this chapter we will examine the consequence of the presence of a nonzero K^+-condensate trapped on the core of the superconducting K-strings described in the previous chapter. In addition to the pioneering work of Witten [100] where strings with nontrivial core structure were first introduced, subsequent studies demonstrated that the presence of a condensate localized on the string may lead to the classical stability of superconducting string loops [27, 42]. The first class of superconducting string loops, called "springs", were characterized by a nonzero spacelike current [27, 42]. It is well known that a loop of a normal global string with no condensate in the core is unstable in the vacuum (as the energy of the loop is proportional to the length). Upon formation the loop will shrink and eventually disappear through the emission of particles. The hope was that if there is a persistent superconducting current trapped on the string, then this current could in turn balance the string tension and prevent the loop from shrinking. Such a configuration would have a total energy $E \sim \alpha_{\rm str} L + J^2 L$, where $\alpha_{\rm str}$ is the string tension

(or energy per unit length), $J \sim 1/L$ is the current, and L is the length of the loop. Since the energy in the global string is linear in L and the energy due to the current goes like $1/L$, there should exist a classically stable configuration for nonzero length $L_{\min}$. However, it was found that springs do not exist in a large region of parameter space, due to the fact that as the loop shrinks the current becomes larger, quenching the value of the condensate on the string [31, 42]. Physically, the current acts as a positive mass squared term in the Lagrangian therefore decreasing the size of the condensate in the core. In most cases the maximum current which can occur before the condensate is quenched is less than the current which is needed to stabilize the string loop. Thus, although such defects, called springs, may become stable configurations (due to the special fine tuning), this is usually not the case.

A more general type of topological defect was introduced by Davis and Shellard in [30, 32, 33] which has two types of conserved charges trapped on the string worldsheet. The first is a topological charge which had been included the analysis of springs, and the second is a Noether charge. he difference with the previous case is that a more general solution is "stationary" but not "static"; rather it has an explicit time-dependent phase $e^{i\omega t}$. This factor leads to a conserved charge trapped on the core, and the configuration can be stabilized due to the conservation of the corresponding charge. The time-dependent configuration becomes the lowest energy state in the sector with a given nonzero charge. A similar idea was advocated by Coleman [25] in his construction of Q-balls, stable objects with a time-dependent wave function. This class of objects generally possess nonzero angular momentum and charge, which lead these quasiparticles to be referred to as vortons. It is

interesting to note that numerical simulations performed recently in Ref. [55] seem to confirm the classical stability of these vortons. In this chapter we will apply these ideas to superconducting K-strings, as previously described in Chapter 4, to construct vortons in the CFL+K^0 phase of high density QCD. One difference between our case and that of other theories where vortons are present is the appearance of a domain wall. Our K-vortons have a domain wall [85] which stretches across the surface of the vorton like a soap bubble. This particular type of vorton (with an attached domain wall) was recently discussed within the linear sigma model at nonzero temperature [23]. We should note that we will not be addressing the issue of vorton formation in this chapter. Rather, we will assume that there is some nonzero probability for the formation of such topological defects when the CFL+K^0 phase occurs. We refer the reader to [62] for a detailed study on vorton formation. Furthermore, there are many other issues that will not be addressed in the present chapter. These include; finite temperature effects, estimates of the lifetime of a vorton, weak interactions with the electrons present in the CFL+K^0 phase, and EM interactions with the electric and magnetic fields present in neutron stars. Some of these topics (along with many useful references) can be found in chapters 5 and 8 of the book by Vilenkin and Shellard [96] where they have been discussed in a cosmological/high energy physics setting.

5.2 K-Vortons

Building on the idea of superconducting K-strings discussed in Chapter 4, we will proceed to show that superconducting string loops can exist as classically

stable objects which are supported by the presence of two conserved charges that become trapped on the string worldsheet. These quasiparticles have been widely discussed in the context of cosmology [23, 27, 30, 31, 32, 33, 42, 100]. In our case, high density QCD, we have the benefit of having an effective Lagrangian that contains parameters that have already been calculated.

5.2.1 Springs vs. Vortons

Shortly after the pioneering paper of Witten [100] on superconducting strings, there was much interest in the idea that superconducting strings loops could be supported by the presence of persistent currents [27, 31, 42]. We will consider a large loop of string of radius $R \gg \delta$, where δ is the string thickness, so that curvature effects can be neglected. The z-axis is defined along the length of the string, varying from 0 to $L = 2\pi R$ as one goes around the loop. The superconducting current can be described by including a phase in the K^+ field, $K^+ \rightarrow K^+ e^{ikz}$. Following [100], we define a charge N, which is topologically conserved:

$$N = \oint_C \frac{dz}{2\pi} \left(\frac{d\alpha}{dz} \right) = kR, \tag{5.1}$$

where the path C is defined along the string loop and $\alpha = kz$ is the phase. Since the field must be single valued as one goes around the loop, k can be interpreted as a winding number density $k = N/R$, with N constrained to be an integer. If N is an integer then it cannot change continuously. This means that there is a persistent current associated with the conserved quantity N. The only way that N can unwind is through a tunneling process whereby the condensate is quenched to down to zero on the string, allowing the winding

number to decrease from N to $N-1$ [14].

The energy of this configuration has the form:

$$\begin{aligned} E &= \alpha_{\rm str} L + v^2 k^2 L \Sigma \\ &= \alpha_{\rm str} L + (2\pi)^2 v^2 \frac{N^2}{L} \Sigma \end{aligned} \tag{5.2}$$

where $\alpha_{\rm str}$ is the K-string tension, the winding number density k is expressed in terms of the conserved charge N, (5.1), and the quantity Σ is defined as the integral of $|K^+|^2$ over the string cross section[1]

$$\Sigma \equiv \int_{\times} d^2 r |K^+|^2. \tag{5.3}$$

This energy has a nontrivial minimum with respect to the loop length L, thus it was originally believed that springs are stable semi-topological defects.

However, later on it was realized that the spring cannot carry arbitrarily large currents or winding number densities $k = N/R$. The addition of the z-dependent phase acts as an effective positive mass-squared term in the Lagrangian:

$$\delta \mathcal{L} = -v^2 |\partial_z K^+|^2 = -v^2 k^2 |K^+|^2. \tag{5.4}$$

As a loop with a conserved nonzero charge N (defined at the moment of loop formation) shrinks to reach the energetically favorable length, k increases, the effective mass squared of K^+ on the string core also increases hence decreasing the strength of the condensate inside the core. Eventually it may no longer be energetically favorable for K^+ to condense inside the string core, and superconductivity on the string will be destroyed with $|K^+|$ quenched

[1]The quantity Σ should not be confused with the matrix Σ^β_γ introduced in Chapter 2 that describes the octet of Goldstone bosons.

down to 0 on the string. In most models discussed in the context of cosmology [31, 42], quenching occurs before the spring reaches its equilibrium length and hence no stable configurations exist.

However, this is not the end of the story. As Davis and Shellard originally pointed out there exists a more general type of topological defect which is stabilized by angular momentum [30, 32, 33]. These types of objects are referred to as vortons and have been widely discussed in the context of cosmology and cosmic strings (see [96] for a review and [54] for recent work). As well as the topological charge present in the spring configurations discussed previously, vortons also have a conserved Noether charge on the string core. The amount of charge present on the string is proportional to the parameter ω in the time dependent phase $K^+ \to K^+ e^{-i\omega t}$. The addition of this phase leads to a nonzero Noether charge given by:

$$Q = \int d^3 r j^0 = \omega L \Sigma. \tag{5.5}$$

The addition of a time dependent phase also contributes to the effective mass squared of the K^+ field as in (5.4), only having the opposite sign:

$$\delta \mathcal{L} = |\partial_0 K^+|^2 = +\omega^2 |K^+|^2. \tag{5.6}$$

Yet ω enters the energy with the same sign as k:

$$\begin{aligned} E &= \alpha_{\rm str} L + (v^2 k^2 + \omega^2) \Sigma L \\ &= \alpha_{\rm str} L + (2\pi)^2 v^2 \frac{N^2}{L} \Sigma + \frac{Q^2}{\Sigma L}, \end{aligned} \tag{5.7}$$

and therefore the energy still has a nontrivial minimum with respect to L.

Thus, from (5.6) we see that a nonzero ω will counteract the quenching effect of k, increasing the value of the condensate on the string (anti-quenching)

as the string loop shrinks [32]. As discussed in [32], when the loop shrinks $\omega/(vk)$ tends to 1, meaning that at the equilibrium length the quenching and anti-quenching effects approximately cancel each other out, leaving a stable vorton behind.

Note that the results discussed above do not rely on whether the condensate on the string is electrically charged. As Davis and Shellard originally pointed out [32], the stability of the vortons is purely mechanical and not electromagnetic in origin. The reason is simple, a vorton with nonzero N and Q has nonzero angular momentum. The fact that the vorton is spinning and angular momentum is conserved leads to the classical stability of these objects. Therefore, the addition of electromagnetic effects should not change the qualitative behavior that will be discussed below, and therefore we neglect the electromagnetic contribution in the present chapter.

5.2.2 Vortons in the CFL+K^0 phase of high density QCD

In order to describe our K-vortons, we expand the full effective Lagrangian given by (2.6) to fourth order in the K^0 and K^+ fields. We expect that this Lagrangian captures the essential physics of the K^0 and K^+ mesons because

it respects all of the relevant symmetries:

$$\begin{aligned}\mathcal{L} &= \frac{1}{6f_\pi^2}((\bar{K}^0\overleftrightarrow{D_\mu}K^0)^2+(\bar{K}^+\overleftrightarrow{D_\mu}K^+)^2+(\bar{K}^+\overleftrightarrow{D_\mu}K^0)(\bar{K}^0\overleftrightarrow{D_\mu}K^+)\\ &+ (\bar{K}^+\overleftrightarrow{D_\mu}K^+)(\bar{K}^0\overleftrightarrow{D_\mu}K^0))+|D_\mu K^0|^2+|D_\mu K^+|^2\\ &- m_0^2|K^0|^2-m_+^2|K^+|^2+\frac{m_0^2}{6f_\pi^2}|K^0|^4+\frac{m_+^2}{6f_\pi^2}|K^+|^4\\ &+ \frac{(m_0^2+m_+^2)}{6f_\pi^2}|K^0|^2|K^+|^2 \end{aligned} \tag{5.8}$$

where the covariant derivative is defined by:

$$\begin{aligned} D_0 &\equiv (\partial_0 - i\mu_{\text{eff}}), \quad D_i \equiv v\partial_i,\\ \bar{\phi}_1\overleftrightarrow{D_\mu}\phi_2 &\equiv \bar{\phi}_1(D_\mu\phi_2)-(\overline{D_\mu\phi_1})\phi_2,\\ (\overline{D_0\phi_1}) &\equiv (\partial_0+i\mu_{\text{eff}})\bar{\phi}_1, \quad (\overline{D_i\phi_1})\equiv v\partial_i\bar{\phi}_1 \end{aligned} \tag{5.9}$$

and the masses are given by:

$$m_0^2 = am_u(m_s+m_d), \quad m_+^2 = am_d(m_s+m_u) \tag{5.10}$$

It is necessary to keep the fourth order terms involving derivatives such as $\partial_0 K^+, \partial_i K^+$ in (5.8) for a discussion of vortons (the reason for this will become apparent in the following). The effective Lagrangian given in (5.8) will be used throughout the rest of this chapter. If one neglects the fourth order terms with derivatives $\sim \mu_{\text{eff}} \neq 0$ only, the Lagrangian (5.8) reduces to Eq. (4.20).

Recall from Chapter 4 that the superconducting strings can be described using the following time independent ansatz:

$$K^0_{\text{string}}(r,\phi) = \frac{\eta'}{\sqrt{2}}f(r)e^{i\phi}, \tag{5.11}$$

$$K^+_{\text{cond}}(r) = \frac{\sigma}{\sqrt{2}}g(r), \tag{5.12}$$

where $\eta'/\sqrt{2} = \sqrt{(\mu_{\rm eff}^2 - m_0^2)/(2\lambda_0)}$ is different from the vacuum expectation value for the field $\langle\Phi\rangle = \eta/\sqrt{2}$ (see (4.20)) by the size of the symmetry breaking term $\sim \delta m^2$, ϕ is the azimuthal angle in cylindrical coordinates, $\sigma/\sqrt{2}$ is the value of the condensate on the string core, and $f(r)$ and $g(r)$ are solutions to the equations of motion which obey the boundary conditions $f(0) = 0$, $f(\infty) = 1$ and $g'(0) = 0$, $g(\infty) = 0$. This configuration is the one described above where the field K^0 vanishes at the center of the string and goes to its vacuum expectation value at ∞, with a nonzero K^+ condensate that exists only on the string core. The functions $f(r)$ and $g(r)$ can be approximated by the following functions which obey the appropriate boundary conditions:

$$\begin{aligned} f(r) &\approx (1 - e^{-\beta r}), \\ g(r) &\approx e^{-\kappa r}(1 + \kappa r), \end{aligned} \tag{5.13}$$

where $\beta \simeq \sqrt{\mu_{\rm eff}^2 - m_0^2}$ and $\kappa \simeq \delta m$ are the approximate inverse widths of the string core and condensate respectively. In addition, the value of the condensate at the center of the string can be estimated by substituting the approximate solutions (5.11) and (5.13) into the Hamiltonian and minimizing the energy with respect to the parameter σ.

In order to describe a vorton in our case, we will add a time and z dependent phase in the standard form to the string-condensate solution (5.11) presented in the previous section:

$$\begin{aligned} K^0 &= K^0_{\rm string}(r, \phi), \\ K^+ &= K^+_{\rm cond}(r)\, e^{-i\omega t + ikz}. \end{aligned} \tag{5.14}$$

Recall that z is defined as the coordinate which runs along the length of the

string and varies from 0 to $L = 2\pi R$ as one goes around a loop of radius R. The loop is assumed to be large, $R \gg \delta$ (δ is the typical string thickness), so that we can neglect curvature effects and consider a straight string.

We can substitute these expressions into the original Lagrangian (5.8) and obtain the Lagrangian describing the dynamics in the two transverse dimensions:

$$\begin{aligned} \mathcal{L} &= -v^2|\partial_i K^0|^2 - v^2|\partial_i K^+|^2 + M_0^2|K^0|^2 + M_+^2|K^+|^2 \\ &- \lambda_0|K^0|^4 - \lambda_+|K^+|^4 - \zeta|K^0|^2|K^+|^2 \end{aligned} \tag{5.15}$$

where i runs over x, y. The parameters of Eq. (5.15) are given by:

$$\begin{aligned} M_0^2 &= \mu_{\text{eff}}^2 - m_0^2, \quad M_+^2 = \tilde{w}^2 - v^2k^2 - m_+^2 \\ \lambda_0 &= \frac{4\mu_{\text{eff}}^2 - m_0^2}{6f_\pi^2}, \quad \lambda_+ = \frac{4(\tilde{w}^2 - v^2k^2) - m_+^2}{6f_\pi^2}, \\ \zeta &= \frac{(\tilde{w} + \mu_{\text{eff}})^2 + 4\tilde{w}\mu_{\text{eff}} - v^2n^2 - m_+^2 - m_0^2}{6f_\pi^2} \end{aligned}$$

where

$$\tilde{w} = \omega + \mu_{\text{eff}} \tag{5.16}$$

is the effective frequency of K^+ field. In simplifying (5.8) to (5.15) we have ignored all fourth order terms in fields which have derivatives in x, y directions since these variations change the profile (as a function of r) of the string itself, but do not influence the effects that are the main subject of this work – the formation of a closed loop of the string, a vorton.

It is important to note that fourth order couplings in (5.15) are strongly dependent on ω and k. This property is what distinguishes our model from the models considered in the context of cosmology [31]. However, the main

feature of the time-dependent ansatz (5.14) which leads to the existence of stable vortons does not depend on these small differences; it remains the same as discussed earlier in different models in the cosmological context [31]. This is because the stability of vortons is not related to the specific properties of the Lagrangian, but rather it is guaranteed by the conservation of topological charge (5.1) and the Noether charge:

$$\begin{aligned} Q &= \int d^3 r j^0 \\ &\simeq \frac{L}{2} \int d^2 r \ |K^+|^2 \left[2(\omega + \mu_{\rm eff})\right] \\ &\simeq L\tilde{w}\Sigma. \end{aligned} \tag{5.17}$$

which reduces to the expression (5.5) with the replacement $\omega \to \tilde{w} = \omega + \mu_{\rm eff}$. In the above expression we have omitted higher order terms[2] in derivatives and/or fields to simplify the expression for the charge Q (5.17). The presence of time dependence leads to a configuration with nonzero conserved Noether charge. Vortons have been referred to as semi-topological defects [30] due to the fact that they are partially stabilized by topology and partially stabilized by the presence of a conserved Noether charge, similar to Q-balls [25].

The K^+/K^0 string loops in our model are always charged and this charge has to be taken into account when studying their dynamics. In particular, even if the K^+ field originally has no explicit time dependence, i.e $\omega = 0$ and $\tilde{w} = \mu_{\rm eff}$, explicit time dependence will appear in the process of the loop

[2] As we have already mentioned these higher order terms in the effective description lead to some difference in the definition of the fields. In particular, we could define the fundamental field K^+ as the phase of Σ^β_γ (2.5) or we could define K^+ as $\sin(K^+)$ etc. We do not expect that this ambiguity can change the qualitative results which follow.

shrinking to preserve the Noether charge that was present at the moment of formation.

We will now proceed to study what values $\tilde{w}$ and k can assume. These values are clearly not arbitrary since the masses and the couplings in the Lagrangian (5.15) depend on $\tilde{w}$ and k. Thus, for the vorton to exist, $\tilde{w}$ and k must not destroy the K^+ condensate of the superconducting K^0/K^+ string. The constraints on the parameters in (5.15) which guarantee superconductivity have been discussed in detail by [42] and can be stated as follows:

1. It must be energetically favorable for K^0 to condense in the vacuum, *i.e.* $\langle K^0 \rangle \neq 0$. This guarantees that the $U(1)_Y$ symmetry is spontaneously broken and a K^0 string can form.

2. It must be energetically unfavorable for K^+ to condense in the vacuum, *i.e.* in vacuum $\langle K^+ \rangle = 0$. This guarantees that K^+ does not condense outside the string and is bound to the string core. This constraint requires that the effective mass squared of K^+ must be positive off of the string core.

3. It must be energetically favorable for K^+ condensation to occur on the string core. A necessary condition for this is that the effective mass squared of K^+ must be negative inside the string core.

4. A sufficient condition for 3. is that total energy associated with K^+ condensation inside the string core must be negative.

The first 3 constraints can be summarized in terms of the parameters (5.16)

as:

$$\begin{aligned} &1.\quad \frac{M_0^4}{\lambda_0} > \frac{M_+^4}{\lambda_+} \\ &2.\quad \frac{\zeta}{2\lambda_0} M_0^2 > M_+^2 \\ &3.\quad M_+^2 > 0 \end{aligned} \tag{5.18}$$

Notice that the approximate degeneracy between K^0 and K^+ implies that $M_+^2 \simeq M_0^2$ and therefore

$$\tilde{w}^2 - v^2 k^2 - m_+^2 \approx \mu_{\text{eff}}^2 - m_0^2. \tag{5.19}$$

Our calculations support this estimate of the allowed values of ω and k (25 MeV$\lesssim \tilde{w} \lesssim$45 MeV). The upper limit on $\tilde{w}$ has to do with the fact that for large values of $\tilde{w}$ the parameters M_+^2 and ζ break the degeneracy between the K^0 and K^+ fields. Moreover, the increase of M_+^2 and ζ with $\tilde{w}$ cannot be cancelled out simultaneously by an increase in k. Thus for large $\tilde{w}$, ζ becomes too large and the energy associated with a K^+ condensate in the core is no longer negative.

The total energy of this field configuration can also be computed from (5.8). The energy is given as usual by the integral of the T^{00} component of the energy-momentum tensor:

$$\begin{aligned} E &= L \int d^2r (v^2 |\partial_i K^0|^2 + v^2 |\partial_i K^+|^2 - M_0^2 |K^0|^2 \\ &- M_+'^2 |K^+|^2 + \lambda_0 |K^0|^4 + \lambda_+' |K^+|^4 + \zeta' |K^0|^2 |K^+|^2) \end{aligned} \tag{5.20}$$

where the coefficients are given by:

$$\begin{aligned} M_0^2 &= \mu_{\rm eff}^2 - m_0^2, \quad \lambda_0 = \frac{4\mu_{\rm eff}^2 - m_0^2}{6f_\pi^2}, \\ M_+'^2 &= \mu_{\rm eff}^2 - \omega^2 - v^2k^2 - m_+^2, \\ \lambda_+' &= \frac{4(\mu_{\rm eff}^2 - \omega^2 - v^2k^2) - m_+^2}{6f_\pi^2}, \\ \zeta' &= \frac{8\mu_{\rm eff}^2 - \omega^2 - v^2k^2 - m_+^2 - m_0^2}{6f_\pi^2} \end{aligned} \tag{5.21}$$

In the case when $\omega = k = 0$ one reproduces the energy for the string obtained from Eq. (4.20). The part of the energy (5.20) associated with a single K^0 vortex of length L without a condensate in the center (terms involving only K^0 in (5.20)) is given to logarithmic accuracy as:

$$E_{K^0} = 2\pi R\,(\pi\eta'^2 v^2 \ln(\beta\Lambda)), \quad \eta'^2 = \frac{\mu_{\rm eff}^2 - m_0^2}{\lambda_0} \tag{5.22}$$

where β is the inverse width of the string's core introduced in the ansatz (5.13) and Λ is a long distance cutoff which is introduced in order to control the logarithmic divergence which appears due to the large distance variation of the phase. The cutoff is typically the distance between strings or the radius of curvature, and since we will be considering loops of strings in this chapter, the natural correspondence to make is $\Lambda \simeq R$. The additional energy of the K^+ condensate in the core of the string (due to the nonzero values of ω, k) has the following leading term behavior:

$$\begin{aligned} E_{K^+} &\simeq L(\omega^2 + v^2k^2)\Sigma \\ &\simeq \frac{Q^2}{2\pi R\Sigma} + \frac{2\pi v^2 N^2 \Sigma}{R}, \end{aligned} \tag{5.23}$$

where we expressed ω, k in terms of the conserved charges Q, N. Note that this is only an approximate expression for the energy of the condensate and

that we have neglected various higher order terms in K^0, K^+ in Eq. (5.20) as well as in the definition of the charge Q (5.17). As we mentioned earlier, these higher order terms reflect the ambiguity in the description of solitons using the effective Lagrangian approach when $K^0/f_\pi \sim 1$. These terms effectively play a role by determining the magnitude of the K^+ condensate in the core represented by the parameter Σ in our calculations. Once the presence of a K^+ condensate is established, these terms can change some numerical results, but we do not expect that these terms can change our qualitative results because the existence of vortons is based on conservation of charges rather than on the specific properties of the field representations used in this chapter. In other words, once the parameters are such that a K^+ condensate forms in the core of the vortex, the vorton can also form. We use the simplest possible expressions for the relevant parameters in order to illuminate the fact that stability occurs for a nonzero value of R. Thus, as discussed before, the total energy $E = E_{K^0} + E_{K^+}$ has a minimum with respect to R at which a stable vorton exists. With our parameters it happens at R_0 given by,

$$(2\pi R_0)^2 \simeq \frac{Q^2 + (2\pi)^2 v^2 N^2 \Sigma^2}{\pi \Sigma \eta'^2 v^2 \ln(\beta\Lambda)}. \tag{5.24}$$

At this point in our discussion the size of the vortons is not constrained in any way; they could be arbitrarily large, similar to cosmic string vortons. However, when an explicit symmetry breaking term is taken into account, the vorton size cannot be arbitrarily large. Rather, the size will be constrained by the strength of an additional force due to the domain wall attached to the string, as we will discuss in the next section.

One should emphasize at this point that the source of this stability is

purely mechanical, and not related to the electromagnetic interactions. This is in contrast with the suggestion made in [44], where it was mentioned that it may be possible to have classically stable K-vortons in high density QCD due to a persistent superconducting current trapped on the string. As we have demonstrated above, the source of the vorton stability has a quite different origin. We expect that the maximum electromagnetic current which can occur in the system (before the K^+ condensate is quenched) is less than the current which is required to stabilize the string loop, as it was demonstrated to happen in most cases [42] and [31] where a similar problem was previously analyzed.

The stability of the vortons can also be demonstrated explicitly in a different way. As Davis and Shellard originally pointed out, the source of this stability is purely mechanical. The presence of time dependence in (5.14) allows the vortons to spin and carry angular momentum. The conservation of angular momentum is reflected by the conservation of the topological and Noether charges, N and Q respectively. We can easily calculate the approximate angular momentum carried by a vorton from the energy-momentum tensor obtained from (5.8)

$$M^{ij} = \int d^3r (x^i T^{0j} - x^j T^{0i}). \tag{5.25}$$

The angular momentum carried by a single vorton (5.14) is approximately:

$$M \simeq 2\pi R^2 k \ \tilde{w}\Sigma. \tag{5.26}$$

The direction of M is perpendicular to the surface formed by the vorton. From the expression (5.26) for the angular momentum, we can see that that $M \sim N \cdot Q$ is proportional to the classically conserved quantities N and Q.

Although our K^+ field is electrically charged, we have not mentioned or included interactions with electromagnetic gauge field. We expect that the quantitative results discussed above would be slightly different upon including a gauge field, with the qualitative behavior remaining unchanged. Qualitatively, we expect that the electromagnetic interactions would enhance that stability of the vortons because the electromagnetic charge of the K^+ condensate trapped in the core gives an additional contribution $\sim Q^2/R$ and prevents the vortons from shrinking.

5.3 Domain walls, drum vortons, and Magnus forces

In the previous section we have demonstrated that loops of superconducting K-strings, called vortons, can exist as classically stable objects due to the fact that charges and currents are trapped on the string core. We will now include a brief discussion of other effects that are important in order to have a correct description of vortons in the CFL+K^0 phase of high density QCD.

Up to this point, we have not included terms in the Lagrangian that explicitly break the $U(1)_Y$ symmetry. If the weak interactions are taken into account, there is a small piece which must be added to the effective Lagrangian (5.8) which explicitly breaks the $U(1)_Y$ symmetry [85]:

$$\delta\mathcal{L} = -V(\varphi) = f_\pi^2 m_{\rm dw}^2 \cos\varphi, \tag{5.27}$$

where φ is the phase of K^0 and $m_{\rm dw}$ will be given below. As described in full detail in Ref. [85], this leads to the formation of domain walls, with

the phase φ varying from 0 to 2π across the wall (the same vacuum state exists on both sides of the wall, similar to the $U(1)_A$ domain walls in Chapter 3). Consequently, this leads a domain wall being attached to every string. Therefore, as one encircles the string at large distances from the core the phase variation from 0 to 2π is not uniform but is sandwiched inside a domain wall of width $m_{\rm dw}^{-1}$, with $m_{\rm dw}^{-1}$ set by the coefficient of the explicit symmetry breaking term. We will simply state the results of Son [85] here without going into details. The domain wall tension $\alpha_{\rm dw}$ (energy per unit area) is given by:

$$\begin{aligned} \alpha_{\rm dw} &= 8 v f_\pi^2 m_{\rm dw}, \\ m_{\rm dw}^2 &= \frac{162\sqrt{2}\pi}{21 - 8\ln 2}\frac{G_F}{\alpha_s}\cos\theta_c \sin\theta_c m_u m_s \Delta^2, \end{aligned} \tag{5.28}$$

where G_F is the Fermi constant, θ_c is the Cabibbo angle, and α_s is the strong coupling constant. The inverse mass $m_{\rm dw}^{-1}$ is approximately the width of the domain wall. Son calculates $m_{\rm dw} \sim 50$ keV for physical values of the relevant parameters [85]. If the size of the domain wall is greater than the thickness, $R \gg m_{\rm dw}^{-1}$ for a circular domain wall of radius R, then the total energy of this configuration can be approximated as:

$$E_{\rm dw} \simeq \pi R^2 \alpha_{\rm dw} \tag{5.29}$$

Since every string must be attached to a domain wall, the vortons discussed in the previous section will have a domain wall stretched across their surface like a soap bubble. Similar configurations have been recently studied in the linear sigma model at nonzero temperature [23] and have been referred to as "drum vortons". In the case that there is no domain wall attached to

the vorton, the minimization of the energy with respect to R leads to the result that $k = N/R = \text{const}$ for the chiral case $vk = \omega$, independent of R. Therefore, the vorton could have an arbitrarily large size. The presence of the domain wall will lead to an upper bound on the radius of these vortons. Now that we have an approximate expression to the domain wall contribution to the energy, we can add Eqs. (5.22), (5.23), and (5.29) to arrive at an expression for the total energy of a circular drum vorton of radius R which is valid for $R \gg m_{\rm dw}^{-1}$:

$$\begin{aligned} E &= E_{K^0} + E_{K^+} + E_{\rm dw} \\ &= 2\pi^2 R\, \eta^2 v^2 \ln(\beta R) + \pi R^2 \alpha_{\rm dw} \\ &+ \frac{1}{R}\left(\frac{Q^2}{2\pi\Sigma} + 2\pi v^2 N^2 \Sigma\right). \end{aligned} \tag{5.30}$$

This expression must be minimized with respect to R to find the size of these classically stable objects. This problem is quite complicated because of a number simplifications we have made in Eq. (5.30). In particular, Eq. (5.29) is not literally valid for relatively small $R_0 \sim m_{\rm dw}^{-1}$ when equilibrium is reached (see below).

We will now estimate the typical size of a vorton. We start with relatively small charges Q, N (and correspondingly R) when the domain wall contribution can be neglected, and equilibrium is reached at R_0 given by Eq. (5.24). We slowly increase Q and N so that the domain wall contribution becomes of the same order of magnitude as the string-related terms. This happens when $Q, N \sim f_\pi/m_{\rm dw} \gg 1$. The size of the configuration at this point $R_0 \sim Q/f_\pi \sim m_{\rm dw}^{-1}$ reaches the magnitude of the domain wall width, *i.e.* $(50\ \text{keV})^{-1}$, which is much larger than any QCD-related scale of the prob-

lem. If one increases Q and N further, the first term in Eq. (5.30) becomes irrelevant, and equilibrium is achieved when $R_0^3 \sim Q^2/(\Sigma\alpha_{\rm dw})$ at which point the energy of the configuration $E \sim Q^{4/3}\alpha^{1/3}$ grows too fast with Q. We would expect that such a large configuration will decay to smaller vortons, conserving the charges Q and N and decreasing the total energy. Therefore, one expects that the maximum vorton size is related to the weak interactions which set the typical vorton scale to be $m_{\rm dw}^{-1}$.

There exists an additional force which may further stabilize the vortons. This is the Magnus force, which arises when a global string moves through a Lorentz-noninvariant fluid. We naturally have such a background, since we are working at nonzero chemical potential, which breaks Lorentz invariance. The corresponding expression has been derived in Ref. [34] where it was demonstrated that in the language of the Goldstone boson such a background corresponds to a time dependent phase of the order parameter. In our notations this phase takes the form $\sim e^{i\mu_{\rm eff}t}$. If vorton moves with velocity $\vec{v}$ through this fluid, the force exerted on the vorton per unit length:

$$\vec{F} = 2\pi\gamma\eta^2\mu_{\rm eff}\ \vec{v}\times\vec{m}, \tag{5.31}$$

where γ is the standard relativistic factor and $\vec{m}$ is the circulation vector of unit magnitude, $|\vec{m}| = 1$, which points in the direction of the string. If the velocity vector $\vec{v}$ is perpendicular to the plane formed by the vorton, then there will be a Magnus force present which points outward, further stabilizing the vorton. This will in turn increase the size of the vorton. If the vorton moves in the opposite direction, the Magnus force points inward, which decreases the size of the vorton.

Finally, the issue of quantum stability of vortons has not been addressed in this chapter. In the pure current case ($Q = 0, N \neq 0$), the instanton solution has been explicitly constructed and the lifetime calculated analytically [14]. The decay mechanism is a quantum mechanical tunneling process where the condensate goes to zero on the core, allowing the winding number to decrease from N to $N - 1$. However, the vortons discussed here have nonzero Q, N so the results obtained in [14] do not apply. In spite of this fact, we expect that the vortons in high density QCD discussed in this chapter are long lived due to the approximate "chiral" relation (5.19) which must be satisfied in order to have superconducting strings. However, at the moment we cannot make any definitive statements on the lifetime of the vortons discussed in this chapter. In order to make such estimations we need to understand the vorton interactions, which were completely ignored in this work. To understand the dynamics of vortons we need to know: first of all, the interaction of the Goldstone particles with the vorton. This would allow us to calculate the corresponding cross section which is important for the analysis of the frictional force acting on a moving vorton. Secondly, the same interaction would allow us to estimate the Goldstone mode production by the vorton. This knowledge is essential for the study of the Goldstone boson radiation from moving vortons. Finally, the interaction is essential for studying such issues as the typical lifetime of a vorton, the typical behavior of vortons when they can join/disjoin with each other and absorb/emit the Goldstone bosons. The quantum numbers (N, Q, M) should be conserved in all the processes mentioned above. Unfortunately, none of these questions can be answered at this point.

5.4 Conclusion

In this chapter we have demonstrated that loops of superconducting K-strings, called K-vortons, can exist as classically stable objects within the CFL+K^0 phase of high density QCD. The main mechanism which stabilizes these superconducting K-string loops is the presence of charge and current trapped on the string. The main difference between these vortons and vortons within other models is the presence of a domain wall which is stretched across the surface. These domain walls set up an upper bound on the allowable vorton size, which is $m_{\rm dw}^{-1}$, in contrast with cosmic vortons where the size of the vortons could be arbitrarily large.

The most intriguing aspect of these vortons is their ability to carry angular momentum due to the presence of nonzero charge and current trapped in the core. Moreover, the vortons are very efficient carriers of the angular momentum. In order to simplify our estimates in what follows, we will use Λ_{QCD} as the typical scale of the problem. It could be any of dimensional parameters (or their combination) discussed above such as $\mu_{eff}, \Delta, k, \omega, f_\pi, ..$ etc. As we demonstrated above, the angular momentum carried by a single vorton of size L is $M \sim \Lambda_{QCD}^2 L^2$ (see Eq. (5.26)), and grows proportional to the area L^2 up to a maximal possible size, which is $\bar{L} \sim m_{\rm dw}^{-1}$. The parameter $m_{\rm dw}$ has a characteristic scale of the weak interactions, and it is three order of magnitudes smaller than Λ_{QCD}. At the same time, the energy of the vorton scales linearly with the size, $E \sim \Lambda_{QCD}^2 L$ as long as $L \leq \bar{L} \sim m_{\rm dw}^{-1}$. Therefore, the angular momentum per energy scales as $M/E \sim L$ for $L \leq \bar{L} \sim m_{\rm dw}^{-1}$. A typical straight vortex (not a vorton) is expected to carry the angular momentum according to the relation $M \sim \Lambda_{QCD} L$ and $E \sim \Lambda_{QCD}^2 L$, such

that $M/E \sim \Lambda_{QCD}^{-1}$. Therefore, according to our estimates the vortons are much more efficient carriers of the angular momentum than regular straight vortices. In addition to this, the larger the vorton, the more efficient it becomes at carrying angular momentum. However, as explained above there is a maximum vorton size before they become unstable; it is $\bar{L} \sim m_{\rm dw}^{-1}$.

Therefore, one should expect that most of the vortons in the core of a neutron star would be the same typical size, which is $\bar{L} \sim m_{\rm dw}^{-1}$. As discussed above, the vorton's ability to carry angular momentum efficiently makes it an important dynamical degree of freedom. In particular, vortons might be the key elements for the explanation of phenomenon such as glitches. The glitches that have been observed in neutron stars are periodic jumps in the rotational frequency of the star, with $\Delta\Omega/\Omega \sim 10^{-6}$. The same vortons might be important objects for other problems such as describing the dynamics of the electromagnetic fields in the core of a neutron star (as vortons are positively charged configurations due to a K^+ condensate trapped in the vortex). The vortons could be important for discussions of transport properties, as well as problems related to the cooling of the system. This is due to the fact that a vorton is a relatively large configuration with fields correlated over large distances (in QCD units). The cross-section for the particle scattering by strings, could be very large [5], and could influence the cooling of the system. Finally, vortons may be the only possible defects that can carry angular momentum in the crystalline superconducting phase [16]. Indeed, in this phase it is quite difficult (if possible at all) to construct a regular straight vortex which can carry the angular momentum. To conclude, we believe that the physics of vortons could prove to be interesting for compact

astrophysical objects such as neutron stars.

Chapter 6

Neutron Stars as Type-I Superconductors

6.1 Overview

The study of compact astrophysical objects such as neutron stars is very interesting as the underlying physics is extremely diverse. A complete physical description of neutron stars draws on various subfields of physics ranging from general relativity to high density quark matter. Up to this point in this thesis, we have focused on the consequences of the realization of the color superconducting CFL+K^0 phase of high density QCD in the inner core of a neutron star. Although this is a very realistic possibility [36, 68, 101], the observational evidence that the density exceeds the critical density ($\mu > \mu_c \sim 500$ MeV) is far from conclusive [99]. In this chapter we will change directions slightly and consider baryonic matter at slight smaller densities, where the system is made up mainly of neutrons with a small amount electrons and protons in beta equilibrium. At these densities the protons form Cooper pairs and Bose condense to give an electromagnetic superconductor. We will demonstrate that the presence of the additional neutron Cooper pairs may result in type-I superconductivity rather than the

conventional picture of type-II superconductivity. Before we begin this discussion, we will give a quick summary of some of the properties of neutron stars.

6.2 Properties of Neutron Stars

Neutron stars are some of the most interesting objects in the observable universe (see the classic textbook by Shapiro and Teukolsky [79] and Ref. [41] for a recent review). They are extremely dense stars with densities on the order of $\rho \sim 10^{15}$ g/cm^3. The typical radius is believed to be approximately $R \sim 10$ km, with a mass just over a solar mass $M \sim 1.4 M_\odot$. The first radio pulsars was discovered in 1967, which were quickly identified as rotating neutron stars. The term radio pulsar comes from the fact that the rotational and magnetic axes are misaligned and therefore they emit dipole radiation in the form of radio waves. The magnetic fields that are present are extremely large, with $B \sim 10^{15}$ G. Pulsars can be rotating extremely fast, with periods, $P = 2\pi/\Omega$, ranging from 1.5 ms to 8.5 s. The rotational rate of neutron stars decreases as a function of time due to the electromagnetic torque that it experiences. One of the interesting aspects of pulsars are the glitches, which are sudden jumps or increases in the rotational rate. The size of these glitches varies, with $\Delta P/P$ ranging from 10^{-8} to 10^{-6}. It is believed that glitches originate below the crust of the star, deep in the extremely dense interior.

In the interior of a neutron star the most important particle physics process is inverse β-decay. This is a weak interaction process where an electron

and a proton are converted into a neutron and a neutrino:

$$e^- + p \rightarrow n + \nu$$

This process is kinematically forbidden unless the electron energy is large enough to balance the mass difference between the proton and the neutron ($m_n - m_p = 1.29$ MeV). The reverse reaction can also occur, known as β-decay, can also occur,

$$n \rightarrow e^- + p + \overline{\nu}.$$

However, this reaction cannot occur if the density is large enough that all the electron energy levels in the Fermi sea are filled up to the one that the emitted electron would fill. This means that the inverse β-decay process is effective in converting electrons and protons into neutrons (plus neutrinos) above some critical density. As we go deeper into a neutron star, the density increases and therefore more and more proton/electrons pairs are converted into neutrons. This means that the nuclei become more and more neutron rich. The excess neutrinos that are produced in inverse β-decay are responsible for various transport properties. Neutrinos provide the primary mechanism for neutron star cooling.

We will now briefly summarize the various phases of matter that are thought to exist inside of a neutron star. The outer crust is a solid region made up of a Coulomb lattice of heavy nuclei and a gas of relativistic degenerate electrons. The densities in this region are thought to be less than $\rho \lesssim 10^{11}$ g/cm^3. As we go deeper into the interior of a neutron star, we reach the region known as the inner crust, which consists of a lattice of neutron-rich nuclei along with superfluid neutrons (the excess neutrons are

the result of inverse β-decay) and an electron gas ($\rho \lesssim 10^{14}$ g/cm^3). The next phase is the neutron liquid above the nuclear saturation density, which is composed mainly of neutrons together with a small amount of protons and normal electrons, with typical densities less than the critical density where the color superconducting phase of quark matter occurs (discussed in Chapter 2). There is some evidence that in the inner core of a neutron star [36, 68, 101] the color superconducting state (with $\rho > \rho_c$) may be realized, although this issue is highly controversial [99]. In this chapter we are interested in the physics that takes place in the neutron liquid state of nuclear matter, with 10^{14} g/cm$^3 \lesssim \rho < \rho_c$. In Fig. 6.1 we give a picture of the different phases inside a neutron star and the volume that they occupy. At the bottom of the diagram *Quarks*? indicates the possibility of having a quark matter core which is in the color superconducting state.

As we have just described, the neutron liquid phase consists mainly of neutrons with a small amount of proton and electrons in beta equilibrium. We know from BCS theory that since there is an attractive interaction present (the strong nuclear force) we would expect Cooper pairs of neutrons and protons to form for states near the Fermi surface. This can occur as long as the thermal energy kT is smaller than the gap parameter Δ (the gap in the excitation spectrum, with 2Δ the energy cost to separate a pair). From theoretical calculations, it is expected that the typical gap is $\Delta \sim 1-3$ MeV [8, 58]. The temperature of a neutron star is relatively low ($kT \sim 1$ keV), therefore we would expect BCS pairing of neutrons and proton in the interior of a neutron star. In the inner crust, where there is an excess of free neutrons, it is believed that neutrons form $^1S_0$ states leading to superfluidity in the

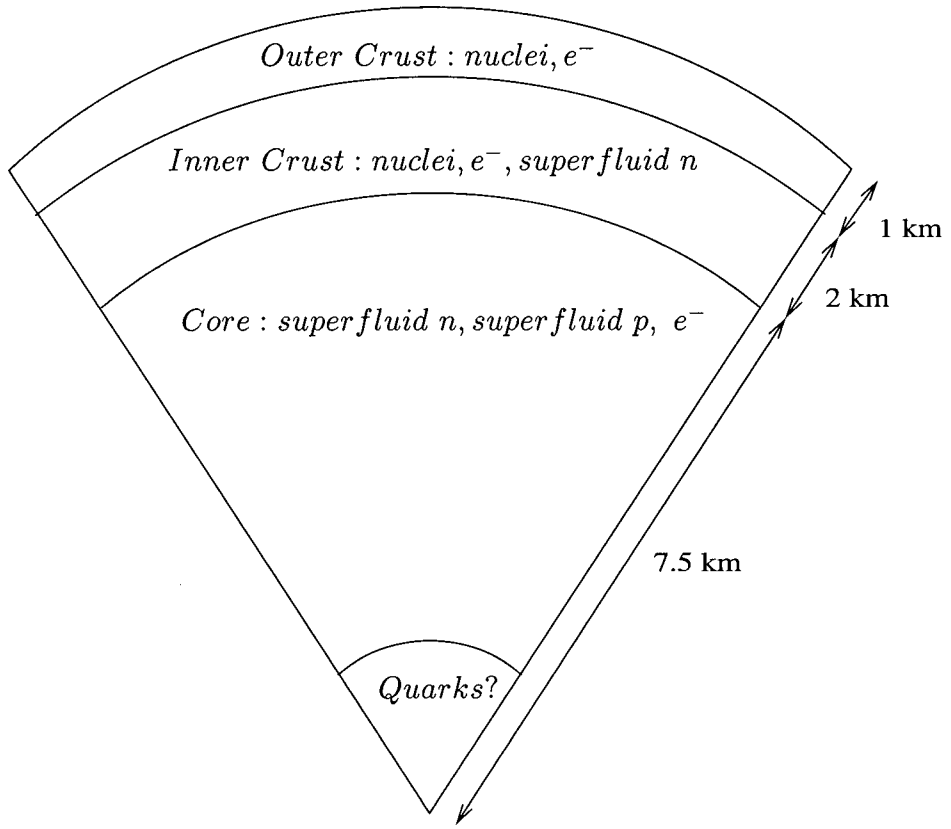

Figure 6.1: In this figure we sketch the structure of a neutron star.

lattice of neutron rich nuclei. In the neutron liquid phase where there are no longer any nuclei present, only free neutrons and protons, it is expected that the neutrons are now paired in a $^3P_2$ state which Bose condense to give a superfluid state [8, 58]. Additionally, since the free protons also interact via the strong nuclear force, the states near the Fermi surface pair to form $^1S_0$ states. This leads to an electromagnetic superconductor, as we have a system that consists of Cooper pairs with electric charge $2|e|$.

It is generally believed that the proton superconductor exhibits type-II

superconductivity. This means that at low values of an external magnetic field there are no magnetic flux tubes present in the superconductor (*i.e.* $H < H_{c1}$, where H_{c1} is the critical magnetic field where it is energetically favorable to form a single magnetic flux tube in a superconducting sample). As the magnetic field is increased above H_{c1}, a stable vortex lattice of magnetic flux tubes forms, with the number of flux tubes proportional to the total magnetic field. Eventually, as the field is increased further ($H \geq H_{c2}$), the vortices (that are filled with a normal non-superconducting core) fill the entire sample resulting in the destruction of superconductivity everywhere. In contrast, type-I superconductivity differs from type-II in that there is no intermediate state where a stable vortex lattice forms. Typically type-I/II behavior is determined by considering the Landau-Ginzburg parameter $\kappa = \lambda/\xi$, where λ is the London penetration depth and ξ is the coherence length. The London penetration depth is the typical scale over which the magnetic field goes to zero inside the superconducting region. The coherence length ξ is the typical size of the region in which superconductivity is destroyed inside the cores of vortices. The values for the London penetration depth and the coherence length inside a neutron star are estimated to be $\lambda \sim 80$ fm and $\xi \sim 30$ fm. These lead to a Landau-Ginzburg parameter that is $\kappa > 1/\sqrt{2}$ such that type-II superconductivity occurs. As we will discuss in the following section, recent observations have indicated that this picture may not necessarily be correct.

6.3 Type-II superconductivity vs. precession in neutron stars

Recently, it was pointed out by Link [56] that observations of long period precession [91] may be inconsistent with the standard picture of the interior of a neutron star. In the conventional picture, the extremely dense interior is mainly composed of neutrons, with a small amount of protons and electrons in beta equilibrium. The neutrons form $^3P_2$ Cooper pairs and Bose condense to a superfluid state, while the protons form $^1S_0$ Cooper pairs and Bose condense to give a superconductor. It is generally believed that the proton superconductor is a type-II superconductor, which means that it supports a stable lattice of magnetic flux tubes in the presence of a magnetic field. This belief is based on simple estimates of the coherence length and the London penetration depth which unambiguously imply type-II superconductivity. In addition, the rotation of a neutron star causes a lattice of quantized vortices to form in the superfluid neutron state, similar to the observed vortices that form when superfluid He is rotated fast enough. The axis of rotation and the axis of the magnetic field are not aligned. This, coupled with the fact that the two different types of vortices interact quite strongly lead to the suggestion that the observed long period precession may require reexamining the picture of type-II superconductivity inside neutron stars [56] that follows from the standard analysis when only a single proton field is considered. If one takes into account that Cooper pairs of neutrons are also present in the system and they interact strongly with the proton Cooper pairs, the proton superconductor may actually be type-I, even when a naive analysis

that only includes the degrees of freedom related to the protons seems to indicate type-II behavior. If this scenario is realized in nature, this means that the interior of a neutron star would exhibit the Meissner effect and therefore would not support a stable lattice of magnetic flux tubes. This would resolve the apparent discrepancy [56] between the observation of long period precession [91] and the typical parameters of the neutron stars which naively suggest type-II superconductivity. In the following chapter we will provide a detailed analysis showing that the interior of a neutron star may in fact be a type-I superconductor.

As we have already mentioned, for accepted estimates of the proton correlation length ξ and the London penetration depth λ, the distant proton vortices repel each other leading to formation of a stable vortex lattice. Inside the core of these vortices, the proton condensate vanishes, and the core is filled with normal protons resulting in the restoration of the broken $U(1)_{EM}$ symmetry. This is the standard picture realized in conventional type-II superconductors. However, there are many situations where this picture will be qualitatively modified. For example, if there is a second component (such as a neutron component in our specific case), it may be energetically favourable for the cores of vortices to be filled with a nonzero condensate of this second component [96, 100]. There are numerous examples of physical systems where this phenomena occurs: superconducting cosmic strings in cosmology, magnetic flux tubes in the high T_c superconductors, Bose-Einstein condensates, superfluid ^3He, and high baryon density quark matter [7, 44, 63, 96, 97, 100, 103]. The case of high density quark matter has already been discussed in Chapters 4 and 5 of this thesis. Given this, one might

guess that such nontrivial vortex structure may be present in the core of a neutron star where we have another example of a two component system. We shall argue in what follows that if the interaction between the proton and neutron Cooper pairs is approximately equal (a precise condition of this "approximately" will be derived below), the vortex-vortex interaction will be modified and the system will be a type-I superconductor where the magnetic field is completely expelled from the bulk.[1] The main assumption that we are making is that the interactions between the proton and neutron Cooper pairs are approximately equal, leading to an approximate $U(2)$ symmetry. We believe that this assumption is justified by the original isospin $SU(2)$ symmetry of the neutrons and protons. The result of this is that the proton vortices or magnetic flux tubes have nontrivial core structure. The superfluid density of the neutrons is larger in the vortex core than at spatial infinity. In addition, the size of the vortex core and the asymptotic behavior of the proton condensate is modified due to the additional neutron condensate. The most important result of these effects is that the interaction between distant proton vortices may be attractive in a physical region of parameter space leading to type-I behavior: destruction of the proton vortex lattice and expulsion of the magnetic flux from the superconducting region of the neutron star.

[1] In reality, the magnetic field must be present in the neutron star interior. This picture may be realized in nature is through the formation of domains of superconductor matter and normal matter.

6.4 Structure of Magnetic Flux Tubes

We start by considering the following effective Landau-Ginzburg free energy that describes the a two component Bose condensed system. In our system, we have a proton condensate described by ψ_1 and a neutron condensate described by ψ_2. The ψ_1 field with electric charge e (which is actually twice the fundamental charge of the proton) interacts with the gauge field $\mathbf{A}$, with $\mathbf{B} = \nabla \times \mathbf{A}$. The two dimensional free energy reads (we neglect the dependence on third direction along the vortex so that $\mathcal{F}$ measure the free energy per unit length):

$$\mathcal{F} = \int d^2r \, (\frac{\hbar^2}{2m}(|(\nabla - \frac{ie}{\hbar c}\mathbf{A})\psi_1|^2 + |\nabla\psi_2|^2) + \frac{\mathbf{B}^2}{8\pi} + V(|\psi_1|^2, |\psi_2|^2)) \quad (6.3)$$

Here we have moved the effective mass difference of the proton and neutron Cooper pairs onto the interaction potential V. In the free energy given above, we have ignored the term coupling the proton and neutron superfluid velocities, which gives rise to the Andreev-Bashkin effect [6], as it is not important in our discussion. We have also ignored the fact that the neutron condensate has a nontrivial ${}^3P_2$ order parameter as only the magnitude of the neutron condensate is relevant to the effect described below.

The free energy (6.3) is invariant under a $U(1)_1 \times U(1)_2$ symmetry associated with respective phase rotations of fields ψ_1 and ψ_2, which corresponds to the conservation of the number of Cooper pairs for each species of particles. Moreover, we know that the free energy (6.3) describes particles interacting via the strong nuclear force and, therefore, must be approximately invariant with respect to the $SU(2)$ isospin symmetry. Thus, we will assume that the interaction potential V can be approximately written

as $V(|\psi_1|^2, |\psi_2|^2) \approx U(|\psi_1|^2 + |\psi_2|^2)$. In reality this symmetry is explicitly slightly broken, and the potential V has a minimum at $|\psi_1|^2 = n_1, |\psi_2|^2 = n_2$, where the bulk proton and neutron superfluid densities n_1 and n_2 are both nonzero. Hence in the ground state, $\langle|\psi_i|^2\rangle = n_i$, $i = 1, 2$, and both $U(1)$ symmetries are spontaneously broken. In order to give the details of our calculations, we will use the following standard ϕ^4-type potential:

$$V(|\psi_1|^2, |\psi_2|^2) = -\mu_1|\psi_1|^2 - \mu_2|\psi_2|^2 + \frac{a_{11}}{2}|\psi_1|^4 + \frac{a_{22}}{2}|\psi_2|^4 + a_{12}|\psi_1|^2|\psi_2|^2 \quad (6.4)$$

where μ_i is the chemical potential of the i^{th} component and a_{ij} is proportional to the scattering length between the i^{th} and j^{th} components. The small explicit $U(2)$ violation is parameterized as follows, $\mu_1 = \mu - \delta\mu$, $\mu_2 = \mu + \delta\mu$, and $\delta\mu/\mu \ll 1$. Also, the scattering lengths a_{ij} are approximately equal, $a = a_{11} \approx a_{22}$ and $a_{12} = a - \delta a$, with $\delta a/a \ll 1$. The chemical potential is fixed by calculating the densities far away from the vortex, $n_i = \langle|\psi_i|^2\rangle$, $i = 1, 2$. The densities n_i can be calculated by minimizing Eq. (6.4) with respect to $|\psi_i|^2$.

$$n_1 = \frac{a_{22}\mu_1 - a_{12}\mu_2}{a_{11}a_{22} - a_{12}^2} \simeq \frac{\mu}{2a} - \frac{\delta\mu}{\delta a}, \quad (6.5)$$

$$n_2 = \frac{a_{11}\mu_2 - a_{12}\mu_1}{a_{11}a_{22} - a_{12}^2} \simeq \frac{\mu}{2a} + \frac{\delta\mu}{\delta a}. \quad (6.6)$$

An important quantity for the analysis that follows will be the ratio of proton density to neutron density, $\gamma \equiv n_1/n_2$. A typical value of γ in the core of a neutron star is $1 - 5\%$, therefore we will often use the limit $\gamma \ll 1$ in our discussion.[2] The Landau-Ginzburg equations of motion that follow from the

[2]One should remark here that the strong deviation of γ from 1 does not imply a large difference in the interaction between different species of particles.

free energy (6.3) are:

$$\frac{\hbar^2}{2m}(\nabla - \frac{ie}{\hbar c}\mathbf{A})^2\psi_1 = (-\mu_1 + a|\psi_1|^2 + (a-\delta a)|\psi_2|^2)\psi_1, \quad (6.7)$$

$$\frac{\hbar^2}{2m}\nabla^2\psi_2 = (-\mu_2 + a|\psi_2|^2 + (a-\delta a)|\psi_1|^2)\psi_2, \quad (6.8)$$

$$\frac{\nabla \times (\nabla \times \mathbf{A})}{4\pi} = \frac{-ie\hbar}{2mc}[\psi_1^*(\nabla - \frac{ie}{\hbar c}\mathbf{A})\psi_1 - h.c] \quad (6.9)$$

We will now investigate the structure of the proton vortices, which exist due to the spontaneous breaking of the $U(1)_1$ symmetry. Such vortices are characterized by the phase of the ψ_1 field varying by an integer multiple of 2π as one traverses a contour around the core of the vortex. By continuity, the field ψ_1 must vanish in the center of the vortex core. Up to this point, it has been assumed that the neutron order parameter ψ_2 will remain at its vacuum expectation value in the vicinity of the proton vortex. As we have already remarked, this is not the case in many similar systems. Actually, it can be shown by using the equations of motion obtained from the free energy (6.3) that for most potentials V, which are approximately invariant under the $SU(2)$ symmetry, it is *impossible* for the ψ_2 field to remain constant when the ψ_1 field varies in space. On the other hand, from an energetic point of view, given that the potential V can be written approximately as $V \approx U(|\psi_1|^2 + |\psi_2|^2)$, one can argue (based on the results of Chapter 4) that it may be favorable for the ψ_2 field to increase its magnitude in the vortex core to compensate the decrease in the magnitude of ψ_1.

Anticipating nontrivial behavior of the neutron field ψ_2, we will adopt the following cylindrically symmetric ansatz for the fields describing a proton vortex with a unit winding number:

$$\psi_1 = \sqrt{n_1}\, f(r)\, e^{i\theta}, \quad \psi_2 = \sqrt{n_2}\, g(r), \quad \mathbf{A} = \frac{\hbar c}{e}\frac{a(r)}{r}\,\hat{\theta} \quad (6.10)$$

where (r, θ) are the standard polar coordinates. Here we assume that the proton vortex is sufficiently far from any rotational neutron vortices, so that any variation of ψ_2 is solely due to the proton vortex. The functions f, g, and a obey the following boundary conditions: $f(0) = 0$, $f(\infty) = 1$, $g'(0) = 0$, $g(\infty) = 1$, $a(0) = 0$, and $a(\infty) = 1$. We see that the fields ψ_1 and ψ_2 approach their vacuum expectation values at $r = \infty$.

The London penetration depth λ and the coherence length ξ of the proton superconductor will be introduced in the standard fashion:

$$\lambda = \sqrt{\frac{mc^2}{4\pi e^2 n_1}}, \tag{6.11}$$

$$\xi = \sqrt{\frac{\hbar^2}{2mn_1 a}}. \tag{6.12}$$

We wish to find the asymptotic behavior of fields ψ_1, ψ_2 and $\mathbf{A}$ far from the proton vortex core, as this will determine whether distant vortices repel or attract each other. The asymptotic behavior can be found analytically by expanding the fields defined in (6.10):

$$f(r) = 1 + F(r), \quad g(r) = 1 + G(r), \quad a(r) = 1 - rS(r) \tag{6.13}$$

so that far away from the vortex core, $F, G, rS \ll 1$ and $F, G, S \to 0$ as $r \to \infty$. This allows us to linearize the equations of motion (6.7,6.8,6.9) corresponding to the free energy (6.3) far from the vortex core to obtain:

$$(\frac{\partial^2}{\partial r^2} + \frac{1}{r}\frac{\partial}{\partial r}) \begin{pmatrix} F \\ G \end{pmatrix} = \mathbf{M} \begin{pmatrix} F \\ G \end{pmatrix}, \tag{6.14}$$

$$S'' + \frac{1}{r}S' - \frac{1}{r^2}S = \frac{1}{\lambda^2}S, \tag{6.15}$$

where all derivatives are with respect to r and the matrix $\mathbf{M}$ mixing the fields F and G is,

$$\mathbf{M} = \frac{4m}{\hbar^2} \begin{pmatrix} a & a - \delta a \\ a - \delta a & a \end{pmatrix} \begin{pmatrix} n_1 & 0 \\ 0 & n_2 \end{pmatrix} \tag{6.16}$$

Here we assume that $(rS)^2 \ll F, G$, *i.e.* the superconductor is not in the strong type-II regime (this is justified since we are only attempting to find the boundary between type-I and type-II superconductivity). The solution to Eq. (6.15) is known to be:

$$S = \frac{C_A}{\lambda} K_1(r/\lambda) \tag{6.17}$$

where K_1 is the modified Bessel function and C_A is an arbitrary constant. The remaining equation (6.14) can be solved by diagonalizing the mixing matrix $\mathbf{M}$. In previous works the influence of the neutron condensate on the proton vortex was neglected, which formally amounts to setting the off-diagonal term M_{12} in Eq. (6.16) to 0. In that case, one can assume that the neutron field remains at its vacuum expectation value, *i.e.* $G = 0$, to obtain,

$$F = C_F K_0(\sqrt{2}r/\xi) \tag{6.18}$$

where K_0 is the modified Bessel function. It is estimated that $\lambda \sim 80$ fm and $\xi \sim 30$ fm, which leads to $\kappa = \lambda/\xi \sim 3$ for the Landau-Ginzburg parameter. For conventional superconductors, if $\kappa > 1/\sqrt{2}$, distant vortices repel each other leading to type-II behavior. This is the standard picture of the proton superconductor in neutron stars that is widely accepted in the astrophysics community.

However, the standard procedure described above is inherently flawed since the system exhibits an approximate $U(2)$ symmetry, and therefore the

couplings a_{ij} are approximately equal $a_{11} \approx a_{22} \approx a_{12}$. This makes the mixing matrix $\mathbf{M}$ nearly degenerate. The general solution to Eq. (6.14) is:

$$\begin{pmatrix} F \\ G \end{pmatrix} = \sum_{i=1,2} C_i K_0(\sqrt{\nu_i} r)\ \mathbf{v_i} \tag{6.19}$$

where ν_i and $\mathbf{v_i}$ are the eigenvalues and eigenvectors of matrix $\mathbf{M}$, and C_i are constants to be calculated by matching to the solution of the original nonlinear equations of motion. We would like to introduce the parameter ϵ (which measures the asymmetry between the proton and neutron Cooper pairs) defined in the following way:

$$\epsilon = (a_{11}a_{22} - a_{12}^2)/a_{ij}^2 \simeq 2\frac{\delta a}{a}. \tag{6.20}$$

In the limit $\gamma = n_1/n_2 \ll 1$ and $\epsilon = 2\delta a/a \ll 1$ one can estimate the eigenvalues and eigenvectors of the matrix $\mathbf{M}$ as:

$$\nu_1 \simeq \frac{2\epsilon}{\xi^2}, \quad \mathbf{v_1} \simeq \begin{pmatrix} -1 \\ \gamma \end{pmatrix}, \tag{6.21}$$

$$\nu_2 \simeq \frac{2}{\gamma\xi^2}, \quad \mathbf{v_2} \simeq \begin{pmatrix} 1 \\ 1 \end{pmatrix}. \tag{6.22}$$

The physical meaning of the solution (6.19) is simple: there are two modes in our two component system. The first mode describes fluctuations of the relative density (concentration) of the two components and the second mode describes fluctuations of the overall density of the two components. Notice that $\nu_1 \ll \nu_2$, and hence the overall density mode has a much smaller correlation length than the concentration mode. Therefore, far from the vortex core, the contribution of the overall density mode can be neglected, and one

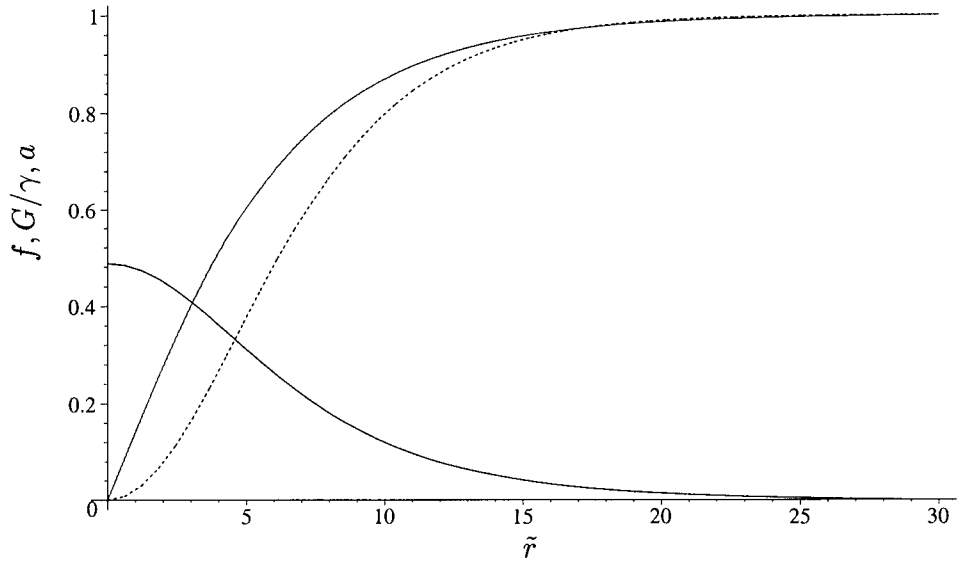

Figure 6.2: In this figure we show the functions $f(\tilde{r})$, $G(\tilde{r})/\gamma$, and $a(\tilde{r})$ (defined in Eqs. (6.10,6.13)) as a function of the dimensionless radial coordinate $\tilde{r} = r/\xi$. The dotted line corresponds to $a(\tilde{r})$, the solid line approaching 1 at large $\tilde{r}$ corresponds to $f(\tilde{r})$, and the solid line approaching 0 at large $\tilde{r}$ corresponds to $G(\tilde{r})/\gamma$.

can write:

$$\begin{pmatrix} F \\ G \end{pmatrix} (r \to \infty) \simeq C_1 K_0(\sqrt{2\epsilon} r/\xi) \cdot \begin{pmatrix} -1 \\ \gamma \end{pmatrix} \tag{6.23}$$

The most important result of the above discussion is that the distance scale over which the proton and neutron condensates tend to their vacuum expectation values near a proton vortex is of order $\xi/\sqrt{\epsilon}$ - the correlation length of the concentration mode. Since $\epsilon \ll 1$, this distance scale can be much larger than the proton correlation length ξ, which is typically assumed to be the radius of the proton vortex core. The appearance of the concentration mode

agrees with the arguments presented earlier, supporting the picture that the neutron condensate will increase its magnitude slightly in the vortex core, while the proton condensate will decrease its magnitude to 0 in the centre of the core. We note should that in the limit $\epsilon = 0$, the size of the proton vortex core becomes infinite, and the vortex is thereby destroyed. This agrees with our intuition, as $\epsilon \to 0$ the only symmetry that is spontaneously broken is the $U(1)_2$ symmetry (since $\mu_2 > \mu_1$) and therefore the formation of $U(1)_1$ vortices is not possible.

We have also verified numerically the results described above by solving the equations of motions (6.7,6.8,6.9). Our numerical results support the analytical calculations given above. Namely, we find that the magnitude of the neutron condensate is slightly increased in the vortex core, the radius of the magnetic flux tube is of order λ, and the radius of the proton vortex core is of order $\xi/\sqrt{\epsilon}$. In Fig. 6.2 we show the numerical solution of the profiles of the proton vortex ($f(\tilde{r})$), neutron condensate ($G(\tilde{r})/\gamma$), and $a(\tilde{r})$ (related to the gauge field through Eq. (6.13)) as a function of the dimensionless radial coordinate $\tilde{r} = r/\xi$, where ξ is the coherence length (6.12). We have used $\kappa = 3$, $n_1/n_2 = 0.05$, and $\epsilon = 0.02$ in this numerical solution.

6.5 Vortex-vortex interaction

Now that we know the approximate solution for the proton vortex, we will proceed to look at the interaction between two widely separated proton vortices. If the interaction between two vortices is repulsive, it is energetically favorable for the superconductor to organize an Abrikosov vortex lattice with

each vortex carrying a single magnetic flux quantum. As the magnetic field is increased, more vortices will appear in the material. This is classic type-II behavior. If the interaction between two vortices is attractive, it is energetically favorable for n vortices to coalesce and form a vortex of winding number n. This is type-I behavior. Typically, the Landau-Ginzburg parameter $\kappa = \lambda/\xi$ is introduced. In a conventional superconductor, if $\kappa < 1/\sqrt{2}$ then the superconductor is type-I and vortices attract. If $\kappa > 1/\sqrt{2}$ then vortices repel each other and the superconductor is type-II. As mentioned above, the typical value for a neutron star is $\kappa \sim 3$, so we would naively expect that the proton superfluid is a type-II superconductor.

We expect that a similar classification should remain in effect for the proton vortices described above. However, in such an analysis the coherence length ξ should be replaced by the actual size of the proton vortices $\delta \sim \xi/\sqrt{\epsilon}$. Therefore, we will define a new Landau-Ginzburg parameter for our case,

$$\kappa_{np} = \frac{\lambda}{\delta} = \sqrt{\epsilon}\frac{\lambda}{\xi}. \tag{6.24}$$

We expect type-I behavior with an attractive force between vortices if $\kappa_{np} \ll 1$ and type-II behavior if $\kappa_{np} \gg 1$. For relatively small ϵ this argument would immediately suggest that for the typical parameters of a neutron star type-I superconductivity is realized (rather than the naively assumed type-II superconductivity). In what follows we will present different arguments supporting this claim.

In order to make this qualitative discussion more concrete, we will present two different calculations supporting our claim that for the typical parameters of a neutron star the proton superconductor may be type-I rather than type-II. First of all, we follow the method suggested originally in [90] to cal-

culate the force between two widely separated vortices. The methods of [90] were subsequently applied in [60] to the case similar to ours, the interaction of two widely separated vortices that have nontrivial core structure. In these papers, the force between two widely separated vortices is calculated by using a linearized theory with point sources added at the location of the vortices. The point sources in the linearized theory are chosen to produce fields matching the long distance asymptotics of the original theory. Therefore, we expand the free energy (6.3) up to quadratic order in the fields F, G, and $\mathbf{A}$ introduced in the previous section, eliminating the phase of ψ_1 field in favor of the longitudinal component of $\mathbf{A}$, to produce a noninteracting free energy:

$$\mathcal{F}_{free} = \int d^2r \left[\frac{\hbar^2}{2m}(n_1(\nabla F)^2 + n_2(\nabla G)^2) + \frac{1}{8\pi}((\nabla \times \mathbf{A})^2 + \frac{1}{\lambda^2}\mathbf{A}^2) + 2an_1^2F^2 + 4(a-\delta a)n_1n_2FG + 2an_2^2G^2 \right] \tag{6.25}$$

Following [60, 90], we must also add the source terms for each field to model the vortices:

$$\mathcal{F}_{source} = \int d^2r(\rho F + \tau G + \mathbf{j}\cdot\mathbf{A}). \tag{6.26}$$

The solutions to the equations of motion following from $\mathcal{F}_{free}$ coupled to the sources can be obtained in the same manner as was done in [60]. The equations of motion resulting from $\mathcal{F}_{free} + \mathcal{F}_{source}$ are:

$$(\nabla^2 - \mathbf{M}) \begin{pmatrix} F \\ G \end{pmatrix} = \frac{m}{\hbar^2} \begin{pmatrix} \rho/n_1 \\ \tau/n_2 \end{pmatrix}, \tag{6.27}$$

$$\nabla^2\mathbf{A} - \frac{1}{\lambda^2}\mathbf{A} = 4\pi\mathbf{j} \tag{6.28}$$

where $\mathbf{M}$ is the same mixing matrix given in Eq. (6.16). Since we are

interested in the asymptotic behavior, we will choose the the first eigenvalue/eigenvector solution (6.21) that diagonalizes $\mathbf{M}$. Therefore, the asymptotic field solutions are given by Eqs. (6.17,6.23):

$$F \simeq -G/\gamma \simeq -C_1 K_0(\sqrt{2\epsilon}r/\xi), \quad \mathbf{A} \simeq \frac{\hbar c}{e\lambda} C_A K_1(r/\lambda)\, \hat{\theta} \tag{6.29}$$

Following [60], we require that (6.29) are solution of the equations of motion (6.27) and (6.28). The source solutions can immediately be written down when we compare Eqs. (6.27) and (6.28) with the following Bessel equations:

$$(\nabla^2 - \mu^2) K_0(\mu x) = -2\pi\, \delta(\mathbf{x}) \tag{6.30}$$

$$(\nabla^2 - \mu^2) \frac{x_j}{x} K_1(\mu x) = \frac{2\pi}{\mu}\, \partial_j \delta(\mathbf{x}) \tag{6.31}$$

The source solutions that solve the equations of motion along with (6.29) are:

$$\rho \simeq -\tau \simeq \frac{1}{2}\Big(\frac{\hbar c}{e\lambda}\Big)^2 C_1 \delta^2(\mathbf{r}), \quad \mathbf{j} \simeq -\frac{\hbar c}{2e} C_A \nabla \times (\delta^2(\mathbf{r})\hat{z}) \tag{6.32}$$

Since the equations of motion corresponding to $\mathcal{F}_{free}$ coupled to $\mathcal{F}_{source}$ are linear, the two-vortex solution can be considered as the sum of two single vortices at positions $\mathbf{r}_1$ and $\mathbf{r}_2$. To calculate the vortex-vortex interaction energy, we use ansatz $(F, G, \mathbf{A}) = (F_1 + F_2, G_1 + G_2, \mathbf{A_1} + \mathbf{A_2})$ $(\rho, \tau, \mathbf{j}) = (\rho_1 + \rho_2, \tau_1 + \tau_2, \mathbf{j_1} + \mathbf{j_2})$ in $\mathcal{F}_{free} + \mathcal{F}_{source}$ and subtract off the energy of each isolated vortex. The notation $1, 2$ indicates that these are functions of $\mathbf{r} - \mathbf{r}_{1,2}$. Using the equations of motion (6.27,6.28) the interaction energy can be written as

$$\mathcal{F}_{int} = \int d^2r (\mathbf{j_1} \cdot \mathbf{A_2} + \rho_1 F_2 + \tau_1 G_2) \tag{6.33}$$

Substituting the asymptotic field solutions (6.29,6.32) into the interaction energy given above, the integration can be done as in [60] to obtain the

following expression for the interaction energy per unit vortex length of two widely separated parallel vortices:

$$U(d) \simeq \frac{2\pi\hbar^2 n_1}{m}(C_A^2 K_0(d/\lambda) - C_1^2(1+\mathcal{O}(\gamma))K_0(\sqrt{2\epsilon}d/\xi)) \tag{6.34}$$

where $d = |\mathbf{r}_1 - \mathbf{r}_2| \to \infty$ is the separation between the two vortices. We see that if the first term in U dominates as $d \to \infty$ then the potential is repulsive, otherwise, if the second term dominates the potential is attractive. In other words, if $\sqrt{\epsilon}\lambda/\xi < 1/\sqrt{2}$, then vortices attract each other and the superconductor is type-I; otherwise, vortices repel each other and the superconductor is type-II. This confirms our original qualitative argument that $\kappa_{np} = \lambda/\delta = \sqrt{\epsilon}\lambda/\xi$ should be considered as an effective Landau-Ginzburg parameter, which determines the boundary between the type-I and type-II proton superconductivity. In terms of the parameters of our theory, we have

$$\kappa_{np} = \frac{mc}{\sqrt{\pi}\hbar}\frac{\sqrt{\delta a}}{e} \tag{6.35}$$

In this case we see that the type-I/II behavior is controlled in part by the degree of symmetry breaking (proportional to δa). Our numerical estimates (see conclusion) suggest that $\kappa_{np} < 1/\sqrt{2}$, and therefore, the system is a type-I superconductor.

6.6 Critical Magnetic Fields

Our second check that for relatively small ϵ the superconductor in neutron stars may be type-I is based on the calculation of the critical magnetic fields. Usually one calculates the critical magnetic fields H_c and H_{c2}. These are the

physically meaningful fields above which the superconductivity is destroyed in type-I and type-II superconductors respectively. If $H_c > H_{c2}$ then the superconductor is type-I, otherwise, the superconductor is type-II.

First, we will calculate the critical magnetic field H_c. This is defined as the point at which the Gibbs free energy of the normal phase is equal to the Gibbs free energy of the superconducting phase. In other words, as the external magnetic field H is increased above H_c, it is energetically favorable for the superconducting state to be destroyed macroscopically. The Gibbs free energy in the presence of an external magnetic field H is:

$$g(H,T) = f(B,T) - \frac{BH}{4\pi} \tag{6.36}$$

where H is the external magnetic field, B is the magnetic induction, and T denotes temperature. The quantity $f(B,T)$ is the integrand of the free energy density (given by Eq. (6.3)) over a superconducting sample. For the superconducting state where $\langle|\psi_1|^2\rangle = n_1$, $\langle|\psi_2|^2\rangle = n_2$, and $B = 0$ (Meissner effect), the Gibbs free energy is

$$g_s(H,T) = -\frac{\mu^2}{2a} - \frac{(\delta\mu)^2}{\delta a} - \delta a\left(\frac{\mu}{2a}\right)^2, \tag{6.37}$$

where we expressed the result in terms of the parameters of Eq. (6.3). We also replaced the densities $(n_1+n_2) \to \mu/a$ and $(n_2-n_1) \to 2\delta\mu/\delta a$ in terms of the same parameters by neglecting small factors $\sim \delta a/a$. For the normal state, we have $\langle|\psi_1|^2\rangle = 0$, $\langle|\psi_2|^2\rangle = (\mu+\delta\mu)/a$, and $B = H$. The Gibbs free energy is:

$$g_n(H,T) = -\frac{H}{8\pi} - \frac{\mu^2}{2a} - \frac{\mu\delta\mu}{a} \tag{6.38}$$

As H_c is defined as the point at which $g_s(H_c) = g_n(H_c)$, we can solve for the critical field. Equating the free energies of the normal and superconducting

state, we find

$$H_c = \sqrt{8\pi\delta a}\left(\frac{\mu}{2a} - \frac{\delta\mu}{\delta a}\right) \to n_1\sqrt{8\pi\delta a}, \tag{6.39}$$

where at the final stage we used the equation for n_1 in the superconducting phase expressed in terms of the original parameters (6.5).

Now we will proceed to calculate H_{c2}. This is the critical magnetic field below which it becomes energetically favorable for a microscopic region of the superconducting state to be nucleated, with the normal state occurring everywhere else in space. In order to calculate H_{c2}, we follow the standard procedure and linearize the equations of motion for ψ_1 about the normal state with $\langle|\psi_1|^2\rangle = 0$ and $\langle|\psi_2|^2\rangle = (\mu + \delta\mu)/a$. The linearized equation of motion reads,

$$\frac{\hbar^2}{2m}\left(-i\nabla - \frac{e}{\hbar c}\mathbf{A}\right)^2\psi_1 = \omega\psi_1, \tag{6.40}$$

$$\omega = (\mu + \delta\mu)\frac{\delta a}{a} - 2\delta\mu. \tag{6.41}$$

This is simply a Schrödinger equation for a particle in a magnetic field, with an energy of ω. This is a standard quantum mechanics problem and the solution can immediately be written down in the form of Landau levels. The first Landau level is the ground state energy of $\epsilon_0(H) = \hbar|e|H/2mc$. Therefore, if $\omega < \epsilon_0$, then only the trivial solution with $\psi_1 = 0$ is possible. The critical field H_{c2} is defined as the point at which $\omega = \epsilon_0(H_{c2})$. This is given as

$$H_{c2} = \frac{2mc}{\hbar|e|}[(\mu + \delta\mu)\frac{\delta a}{a} - 2\delta\mu] \simeq \frac{4mc}{\hbar|e|}\delta a\ n_1 \tag{6.42}$$

Now that we have the critical fields H_c and H_{c2} in hand, we can compare the two in order to determine the type-I/II nature. If $H_c < H_{c2}$ this means that it is energetically favourable for microscopic regions of the superconducting

state to be nucleated as H is decreased. This is type-II behavior, and this nucleation manifests itself in the form of an vortex lattice. If $H_c > H_{c2}$, then it is energetically favorable for macroscopic regions of the superconducting state to be present as H is decreased. This is a type-I superconductor and the superconducting state persists everywhere in the material when $H < H_c$, as opposed to a type-II superconductor where it is localized in regions of space in between the vortices. From Eqs. (6.5,6.39,6.41,6.42) we see that

$$\frac{H_{c2}}{H_c} \simeq \sqrt{2}\frac{mc}{\sqrt{\pi}\hbar}\frac{\sqrt{\delta a}}{e} = \sqrt{2}\ \kappa_{np}. \tag{6.43}$$

This agrees with the parametrical behavior given in Eq. (6.35) obtained from the vortex interaction calculation of the previous section. To estimate H_c numerically, it is convenient to represent H_c as

$$H_c = \frac{\varphi_0}{2\pi\lambda\xi}\sqrt{\frac{\delta a}{a}}, \quad \varphi_0 = \frac{2\pi\hbar c}{e} = 2\times 10^7 \mathrm{G}\cdot\mathrm{cm}^2, \tag{6.44}$$

where φ_0 is the quantum of the fundamental flux. If we substitute $\lambda = 80$ fm and $\xi = 30$ fm (typical values) in the expression for the critical magnetic field (6.39), H_c is estimated to be the $H_c \simeq 10^{15}$ G, which is smaller than the "naive" estimate by a factor of $\sqrt{\delta a/a} \sim 10^{-1}$. It is quite amazing that very different calculations of the critical magnetic fields (6.43) lead exactly to the same conclusion which was derived from the analysis of the vortex-vortex interaction (6.35).

6.7 Conclusion

In this chapter we have demonstrated using various calculations that the proton superfluid present inside a neutron star may in fact be a type-I super-

conductor. This supports the observation made by Link [56] that the conventional picture of type-II superconductivity may be inconsistent with the observations of long period precession in isolated pulsars [91]. The most important consequence of this chapter is that whether the proton superconductor is type-I or type-II depends strongly on the magnitude of the $SU(2)$ asymmetry parameter ϵ. Specifically, we find that the superconductor is type-I when $\kappa_{np} = \sqrt{\epsilon}\lambda/\xi < 1/\sqrt{2}$, and type-II otherwise. This result is quite generic, and not very sensitive to the specific details of the interaction potential V. In particular, when $\epsilon \to 0$ the superconductor is type-I. The parameter ϵ is not known precisely; the corresponding microscopical calculation would require the analysis of the scattering lengths of Cooper pairs for different species. We can roughly estimate this parameter as being related to the original $SU(2)$ isospin symmetry breaking $\epsilon \sim (m_n - m_p)/m_n \sim 10^{-2}$. If we assume a typical value for $\lambda/\xi \sim 3$ and $\epsilon \sim 10^{-2}$, we estimate $\kappa_{np} = \sqrt{\epsilon}\lambda/\xi \sim 0.3 < 1/\sqrt{2}$, which corresponds to a type-I superconductor. From these crude estimates, we see that it is very likely that neutron stars are type-I superconductors with the superconducting region devoid of any magnetic flux, as was originally suggested in [56] to resolve the inconsistency with observations of long period precession [91] in isolated pulsars. If the proton superfluid exhibits type-I superconductivity then some explanations of glitches [75] that assume type-II superconductivity would have to be reconsidered, as suggested in Ref. [56]. It might be interesting to consider how the presence of a nonzero proton condensate affects the characteristics of the neutron vortices that carry angular momentum. In particular, we have demonstrated the for magnetic flux tubes, the neutron vortices might have an enhanced proton superfluid

density inside, as well as a coherence length ξ_n (the approximate size of the vortex core) which is much larger than originally expected. In this case, the pinning force that is related to the size of the vortex core [57] could be very different from the simple estimates when the strong interaction the neutron and proton Cooper pairs is ignored.

If the core is indeed a type-I superconductor, the magnetic field could exist in macroscopically large regions where there are alternating domains of superconducting (type-I) matter and normal matter. In this case, neutron stars could have long period precession. This structure follows from a few different arguments. First of all, it has been estimated [9] that it takes a very long time to expel magnetic flux from the neutron star core. Therefore, if the magnetic field existed before the neutron star became a type-I superconductor, it is likely that magnetic field will remain there. Another argument suggesting the same outcome follows from the fact that topology (magnetic helicity) is frozen in the environment with high conductivity; therefore, the magnetic field must remain in the bulk of the neutron star. The last argument supporting the same picture is due to Landau [52] who argued that if a body of arbitrary shape (being a type-I superconductor) is placed under influence of the external magnetic field with strength $H < H_c$, then the magnetic field in some parts of the body may reach the critical value H_c, while in other parts of the body it may remain smaller than the critical value, $H < H_c$. In this case, a domain structure will be formed, similar to ferromagnetic systems. Specifically, on a macroscopic distance scale, the magnetic flux must be embedded in the superconductor. This would mean that the superconductor is in an intermediate state as opposed to the vortex

state of the type-II superconductor, which was assumed to be realized up to this point. The intermediate state is characterized by alternating domains of superconducting and normal matter. The superconducting domains will then exhibit the Meissner effect, while the normal domains will carry the required magnetic flux. The pattern of these domains is usually strongly related to the geometry of the problem. The simplest geometry, originally considered by Landau [52], is a laminar structure of alternating superconducting and normal layers. However, it has been also argued [78] that due to the geometry of the neutron vortex lattice, the normal proton domains will be in the shape of cylinders concentric with rotational neutron vortices.

While some precise calculations are required for understanding the magnetic field structure in this case, one can give a simple estimate of the size of the domains using the calculations Landau presented for a different geometry. His formula [52] suggests that the typical size of a domain is

$$a \sim 10\sqrt{R\Delta}, \tag{6.45}$$

where R is a typical external size identified with a neutron star core ($R \sim$ 10 km), while Δ is a typical width of the domain wall separating normal and superconducting states. We estimate $\Delta \sim \delta = \xi/\sqrt{\epsilon}$ as the largest microscopical scale of the problem. Numerically, $a \sim 10^{-1}$ cm which implies that a domain of the normal matter will have a size on the order of $\sim 10^{-1}$ cm. The number of neutron vortices in a neutron star can easily be estimated using the total angular velocity of the superfluid and the angular momentum carried by a single neutron vortex. The number of vortices per cm^2 is given as $n = 2m_n\Omega_n/\pi\hbar \simeq 10^4 P(s)$ cm^{-2}, where m_n is the neutron mass, Ω_n is the angular velocity of the superfluid, and $P(s)$ is the spin period in

seconds. Given this estimate, we see that the average intervortex spacing is $l = n^{-1/2} \sim 10^{-2}$ cm for a period of 1 s, and we can accommodate ~ 10 neutron vortices in one of these domains of normal matter of size $a \sim 10^{-1}$ cm. The consequences of this picture still remain to be explored. In particular, it might be important in the explanation of glitches and in the analysis of the cooling properties of neutron stars.

Chapter 7

Vortons in the $SO(5)$ Model of High T_C Superconductivity

7.1 Motivation

As we have seen in the last few chapters of this thesis, the study of topological defects may prove to be important when studying the physics of neutron stars. In the following we will introduce the vortons discussed in Chapter 5 in the context of Zhang's $SO(5)$ theory of high temperature superconductivity. The study of vortons in high temperature superconductivity is an interesting problem as these materials are far from well understood both theoretically and experimentally. The introduction of a new type of quasiparticles may help explain some of the mysterious properties of the high temperature superconductors [29, 46, 50, 51, 64, 66, 67, 92, 94].

In the last twenty years there has been a large amount of interest in the study of topological defects that may have been created in the early universe. It is well known that defects such as domain walls and monopoles created at a certain epoch would exceed the critical density and lead to a closed universe, which contradicts our present knowledge of the universe. However, this problem of exceeding the critical density does not rule out

the possibility of strings that are left over from the early universe. The study of defects in cosmology is useful for a variety of reasons. If topological defects can be detected in our universe, the nature of these objects may provide clues as to the underlying particle physics models at high energies. Conversely, certain particle physics models which possess topological defects may be ruled out according to current cosmological observations (such as the density of our universe compared with the expected density of defects). In addition, it has been suggested that vortons formed in the early universe may provide an explanation for the high energy cosmic rays [15]. The main difficulty is that the neutron stars and the early universe are far from a controlled environment in which experiments can be performed. Fortunately, it is possible to study topological defects in a controlled environment on Earth by performing experiments in various condensed matter systems, such as superfluid He. This is the idea behind the recently established "Cosmology in the Laboratory" program (COSLAB) [48, 49, 97]. This program was initiated in order to shed some light on the the issues of defect formation, the interactions between defects, among other things. The study of vortices and vortons in the $SO(5)$ model of high T_c superconductivity may provide an interesting link between condensed matter and matter at high densities, as well as another system which can be studied in the spirit of the COSLAB program. To begin, we will give a very brief overview of some of the properties of the high temperature superconductors in the next section.

7.2 High Temperature Superconductivity

Since the discovery of the first high temperature superconducting materials, the theoretical description remains a mystery. The original cuprate superconductor ($La_{2-x}Sr_xCuO_4$ or simply La/Sr cuprate) was discovered in 1986 by Bednorz and Muller [13], with a superconducting temperature of $T_c = 30$ K. A large number of other cuprate superconductors (also known as high temperature superconductors) were subsequently discovered with much larger transition temperatures. Some of the more familiar examples are YBCO ($YBa_2Cu_3O_{6-x}$) with a T_c of 93 K and Bi ($Bi_2Sr_2CaCu_2O_{8+x}$) with a T_c of 94 K. A review of conventional superconductivity in metals and high temperature superconductivity in the cuprates can be found in the book by Waldram [98]. For a more recent review of the field of high temperature superconductivity, we refer to the reader to [69].

The high T_c cuprate superconductors share a number of common characteristics. These materials are layered compounds, with the layers composed of the base compound CuO_2. The CuO_2 planes contain the mobile electrons and hence superconductivity is believed to originate here. The interaction between the layers is relatively weak, making these materials quasi two-dimensional and therefore anisotropic in their properties. The ratio κ of the penetration depth λ and the coherence length ξ is typically quite large in the cuprates, with $\kappa \sim 100$. This means that the cuprate superconductors exhibit extreme type-II superconductivity, since $\kappa \gg 1/\sqrt{2}$. For zero doping, the cuprate superconductors are antiferromagnetic insulators with the spins of neighboring electrons antiparallel, with one hole per unit cell in the CuO_2 planes. The temperature at which the antiferromagnetic order

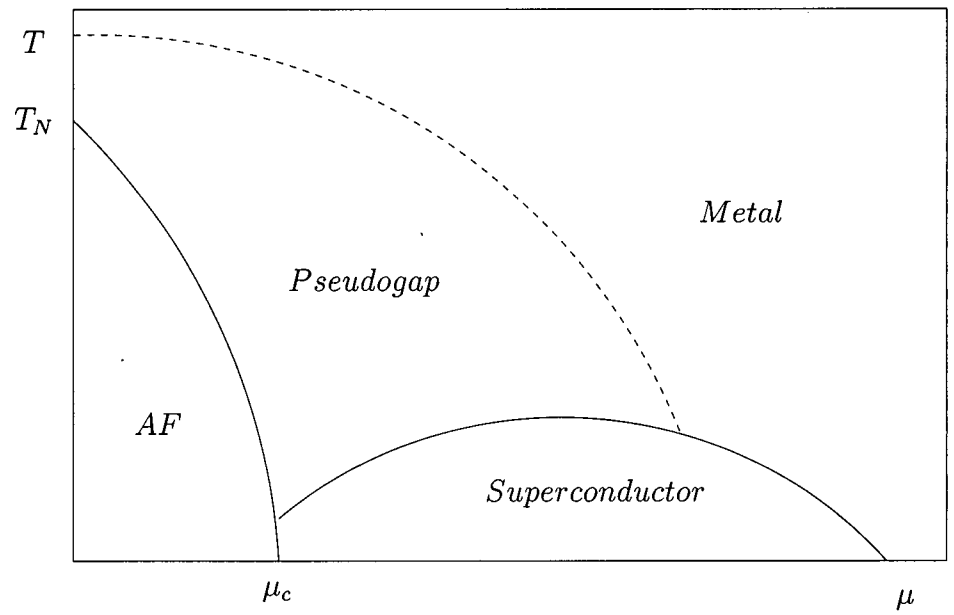

Figure 7.1: In this figure we give a possible picture of the phase diagram of the high T_c cuprates as a function of hole doping μ and temperature T.

is destroyed, called the Neel temperature T_N, is on the the order of hundreds of degrees K. As the system is doped (holes are added to the planes) the Neel temperature decreases with the antiferromagnetic order eventually disappearing completely as the doping is further increased. When antiferromagnetism (AF) is destroyed, superconductivity appears in its place, with a relatively low value for T_c . This region of the phase diagram is far from well understood, and it still remains an unresolved issue of whether there is a gap as function of doping μ when the AF state is destroyed and the superconducting state appears. As we will demonstrate in this chapter, if vortons are present in the high temperature superconductors we would expect this tran-

sition to be gapless and the onset of superconductivity is immediate. As the doping is increased further, the value of T_c also increases, eventually reaching its maximum at optimal doping and then decreases to zero as the doping is increased further. In Fig. 7.1 we show the possible phase diagram for the cuprate superconductors as a function of temperature T and hole doping μ. On this phase diagram we also show the so called pseudogap phase that is reached at higher temperatures. Although the nature of this phase is not clear, various experiments seem to indicate there is a gap that is a precursor to the superconducting gap. In other words, the pseudogap phase is characterized by the formation of pairs without long range phase order [35]. In this chapter we will be discussing physics in the underdoped region of the superconducting phase ($T < T_c$ and $\mu \gtrsim \mu_c$), slightly above the point where antiferromagnetic order is destroyed and superconductivity is realized.

One of the many features that distinguish the high temperature superconductors from conventional metallic superconductors is the nature of the order parameter or gap in the quasiparticle excitation spectrum, Δ. Experiments have shown that the superconducting objects have a charge $2e$, and therefore Cooper pairs are formed as in the BCS theory of superconductivity. In the conventional BCS theory of metallic superconductors the symmetry of the gap is s-wave. Therefore, as one traverses the Fermi surface in momentum space the gap remains constant and nonzero. This leads to all quasiparticle excitations having a gap. In contrast, it is well established that the symmetry of the gap in the high temperature superconductors is d-wave As one goes around the Fermi surface, the gap vanishes at the four nodes ($\hat{k}_x = \pm\hat{k}_y$) resulting in gapless excitations. In other words, as a function of momentum

$\vec{k}$ the gap Δ is given as

$$\Delta(\vec{k}) = \Delta_0(\hat{k}_x^2 - \hat{k}_y^2) = \Delta_0 \cos 2\phi,$$

where Δ_0 is the maximum value of the gap and ϕ is the azimuthal angle in $\vec{k}$-space. The presence of gapless excitations at the four nodes $\hat{k}_x = \pm\hat{k}_y$ alters various properties such as the penetration depth, in the s-wave case the temperature dependence is $\sim e^{-\Delta_0/T}$ while the penetration depth in a d-wave superconductor has a linear temperature dependence. The d-wave symmetry of the order parameter has been verified experimentally by measuring the linear temperature dependence of $\lambda(T)$ [40]. In addition, angle resolved photoemission measurements [80] also provided direct evidence for nodes in the gap. Now that we have given a very basic introduction to the cuprate superconductors, will now proceed in the next section by reviewing one of the current theories of the high temperature superconductors, the $SO(5)$ theory of high-temperature superconductivity. In addition, we will discuss the properties of the vortices that are present in these type-II superconductors.

7.3 Vortices in the $SO(5)$ theory of high-temperature superconductivity

In the pursuit of a unified theory of high temperature superconductivity and antiferromagnetism, Zhang proposed the $SO(5)$ theory of antiferromagnetism (AF) and d-wave superconductivity (dSC) in the high T_c cuprates [103]. The order parameter for antiferromagnetism is the Neel vector $\vec{m}$ which is a vector under the action of the group $SO(3)$, the group of 3-d spatial rotations. On

the superconducting side, the relevant order parameter is the complex superconducting order parameter ψ, which describes the gap in the electron spectrum. The effective Lagrangian for ψ is invariant under the group $U(1)$. The big step that Zhang originally proposed is that the two symmetry groups can be combined within a larger symmetry group, namely, $SO(5)$. This means that the three component vector $\vec{m}$ and the complex order parameter ψ can be combined to form a "superspin" vector $\vec{n} = (\psi_1, m_1, m_2, m_3, \psi_2)$ which transforms under the group $SO(5)$. The presence of doping in the cuprates actually breaks this symmetry down to $SO(3) \times U(1)$. At low doping, the AF phase is favored, corresponding to nonzero expectation value for $|\vec{m}|$, ($\langle|\psi|\rangle = 0$ and $\langle|\vec{m}|\rangle \neq 0$). As the doping is increased eventually the dSC phase becomes energetically favorable with $\langle|\psi|\rangle \neq 0$ and $\langle|\vec{m}|\rangle = 0$. As Zhang originally discussed in [103], the region of intermediate doping (near the AF-dSC phase boundary) should be characterized by conventional superconducting vortices, but possessing antiferromagnetic cores. This suggestion was verified by various groups who looked for numerical solutions of the classical equations of motion for different parameters [1, 7, 59]. Furthermore, there has been recent experimental evidence that suggests this theoretical picture may be correct [29, 50, 51, 64, 66, 67, 94].

The effective Lagrangian which describes the $SO(5)$ theory of high temperature superconductivity is very similar to the one used in Chapters 4 and 5, aside from numerical constants of course. We will make use of the results given in Chapters 4 and 5 throughout this chapter. In the present chapter we will show that is it possible to have loops of dSC vortices with AF cores that are classically stable objects (vortons). The source of this stabil-

ity is the presence of conserved charges trapped on the vortex core, leading to nonzero angular momentum as discussed in Chapter 5. Conservation of angular momentum prevents the vortex loops from shrinking and eventually disappearing. The presence of the AF condensate is crucial, as it is what allows the vortons to carry angular momentum and become classically stable quasiparticles.

We will now review the work of [1, 7, 59, 103], where it was shown that vortices with nontrivial core structure similar to the ones discussed in Chapter 4 for high density QCD are present within the $SO(5)$ theory of high T_c superconductivity. This will be beneficial in order to make analogies between condensed matter physics and particle physics. The effective Lagrangian which describes the Neel vector $\vec{m}$ and dSC order parameter ψ in the presence of a zero external electromagnetic field is given by [103]

$$\begin{aligned}\mathcal{L} &= \frac{\chi}{2}(|\partial_t\vec{m}|^2+|\partial_t\psi|^2)-\frac{\rho}{2}(|\nabla\vec{m}|^2+|\nabla\vec{m}|^2)\\ &+ (\tilde{g}-a)|\vec{m}|^2-a|\psi|^2-\frac{1}{2}b|\vec{m}|^4-\frac{1}{2}b|\psi|^4-b|\vec{m}|^2|\psi|^2, \qquad (7.2)\end{aligned}$$

where we have neglected the electromagnetic contribution to the vortex structure. Actually, one can show that the electromagnetic field does not change the qualitative effects which are the subject of the present chapter, and therefore, will be ignored in what follows. We will also assume that the d-wave symmetry of the order parameter ψ can safely be neglected as in the original proposal of the $SO(5)$ model [103] (only the magnitude of the order $|\psi|$ is important in what follows). Here χ is the susceptibility and $\rho=\hbar^2/m^*$ is the stiffness parameter. In reality, we know that the properties of χ and ρ are different in different directions. However, when we discuss the topological

properties of the configuration this difference can change the quantitative results but cannot change the qualitative picture. The Neel vector has three spatial components $\vec{m} = (m_1, m_2, m_3)$ and the superconducting order parameter is a complex field $\psi = \psi_1 + i\psi_2$. The parameters of the above effective Lagrangian are given by:

$$a < 0, \quad b > 0, \tag{7.3}$$

$$\tilde{g} = 4\chi(\mu_c^2 - \mu^2). \tag{7.4}$$

$$\xi = \sqrt{\frac{\rho}{2|a|}} \tag{7.5}$$

where μ is the chemical potential (or doping, not to be confused with the chemical potential for QCD in the previous section), μ_c is the critical chemical potential which defines the AF-dSC phase boundary, and ξ is the coherence length. The anisotropy $\tilde{g}$ is included which explicitly breaks the $SO(5)$ symmetry in the following fashion, $SO(5) \to SO(3) \times U(1)$. If $\tilde{g} = 0$ then the $SO(5)$ symmetry is restored and the order parameters $\vec{m}$ and ψ can be organized into a superspin order parameter $\vec{n} = (\psi_1, m_1, m_2, m_3, \psi_2)$ which transforms in the vector representation of $SO(5)$, as Zhang originally proposed in [103]. In the following we will consider $\mu > \mu_c$ and $\tilde{g} < 0$ so that we are in the dSC phase and $\langle|\psi|\rangle = \sqrt{|a|/b}$ and $\langle|\vec{m}|\rangle = 0$ in the bulk. One immediately notices that the form of the Lagrangian for the $SO(5)$ theory is very similar to the Lagrangian used to describe K-strings in high density QCD (4.20) in Chapter 4. In particular, the key element in the construction of the vortices with nonzero condensate in the core, the asymmetry parameter, is determined by the magnitude of δm^2 in Eq. (4.20). For the $SO(5)$ theory it is replaced by the parameter of anisotropy $\tilde{g}$ in Eq. (7.4).

A nonzero vacuum expectation value for ψ signals the onset of superconductivity and the breaking of the $U(1)$ symmetry. It is well known that stable vortices can form since the topology of the vacuum manifold is that of a circle. Analogous to the situation for high density QCD, for a certain range of the anisotropy parameter $\tilde{g}$ these vortices should have an antiferromagnetic core ($\langle|\vec{m}(\vec{r}=0)|\rangle \neq 0$). This was originally pointed out by Zhang [103] when he introduced the $SO(5)$ model and further studied in [1, 7, 59]. Similar to the K vortex/condensate solution given by Eq. (5.11), these vortices are described by the following static field configurations:

$$\psi = \sqrt{\frac{|a|}{b}} f(r)\, e^{i\phi}, \tag{7.6}$$

$$\vec{m} = \sigma \sqrt{\frac{|a|}{b}} g(r)\, \hat{m}, \tag{7.7}$$

where ϕ is the azimuthal angle in cylindrical coordinates, σ is the parameter obeying the relation $0 \leq \sigma < 1$, and $\hat{m}$ is an arbitrary unit vector. As before, $f(r)$ and $g(r)$ are solutions to the classical equations of motion satisfying the boundary conditions $f(0) = 0, f(\infty) = 1$ and $g'(0) = 0,\ g(\infty) = 0,$ and $g(0) = 1$. The width of the vortex determined by the profile function f is approximately given by the coherence length (7.5), $\delta_\psi \approx \xi$. The width of the condensate in the core (if it forms) is estimated to be of the order of $\delta_m \approx 1/\sqrt{|\tilde{g}|} \sim 1/\sqrt{(\mu^2 - \mu_c^2)}$ and becomes very large at the phase boundary.

Using what we have already learned from QCD and the results from earlier work on these vortices [1, 7, 59], we can immediately summarize the main features of these objects. Numerical calculations in [1] confirm that as the anisotropy parameter $|\tilde{g}|$ is decreased, the size and width of the condensate in the core increases. We will support these numerical calculations using some

analytical arguments given below.

The free energy (per unit length) obtained from the Lagrangian (7.2) is:

$$\begin{aligned}\frac{\mathcal{F}}{l} &= \int d^2r \left[\frac{\chi}{2}\left(|\partial_t\vec{m}|^2+|\partial_t\psi|^2\right)+\frac{\rho}{2}(|\nabla\vec{m}|^2+|\nabla\psi|^2)\right. \\ &- \left.(|a|+\tilde{g})|\vec{m}|^2-|a||\psi|^2+\frac{1}{2}b|\vec{m}|^4+\frac{1}{2}b|\psi|^4+b|\vec{m}|^2|\psi|^2\right]. \quad (7.8)\end{aligned}$$

If anisotropy $\tilde{g}\equiv 0$ we know from topological arguments that this theory does not possess any vortices since the vacuum manifold is that of a 4-sphere and therefore does not have noncontractible loops. If $|\tilde{g}|$ is relatively large, then the residual symmetry group has a subgroup $U(1)$ and the vacuum manifold is that of circle, leading to the formation of classically stable global vortex solution described in terms of ψ field with a typical profile function when $|\psi(r=0)|=0$ and $|\psi(r=\infty)|=\sqrt{|a|/b}$. From these two limiting cases, as discussed in Chapter 4, it is clear that there should be some intermediate region that somehow interpolates (as a function of $\tilde{g}$) between the two cases. The way this interpolation works is as follows (see Chapter 4 where the physical picture is quite analogous to the present case). At some finite magnitude of $\tilde{g}$, an instability arises through the condensation of $\vec{m}$-field inside of the core of the vortex. As the magnitude of $\tilde{g}$ decreases, the size of the core becomes larger and larger with nonzero values of both $\vec{m}$ and ψ condensates inside the core. Finally, at $\tilde{g}=0$ the core of the string (with nonzero condensates $\vec{m}$ and ψ) fills the entire space, in which case the meaning of the string is completely lost, and we are left with the situation when the $SO(5)$ symmetry is exact: no stable strings are possible.

In order to estimate that critical value of the parameter $\tilde{g}=\tilde{g}_{\rm crit}$ where an AF core forms inside the vortex, the same method can be applied as

described for the QCD color superconductor in Chapter 4. We will use the following change of variables in order to express the free energy in terms of dimensionless variables only:

$$\psi = \sqrt{\frac{|a|}{b}}\psi', \quad \vec{m} = \sqrt{\frac{|a|}{b}}\vec{m}', \quad \vec{r} \;=\; \xi\vec{r}'. \tag{7.9}$$

Expanding the expression for the change in the free energy (7.8) in the background of a ψ vortex solution given by Eq. (7.6) and keeping only quadratic terms in $\vec{m}$, we have:

$$\frac{\delta\mathcal{F}}{l} = \sigma^2\frac{\rho|a|}{2b}\int d^2r'\, g(r')[\hat{H}+\epsilon]g(r'), \tag{7.10}$$

where

$$\hat{H} \;=\; -\frac{1}{r'}\frac{d}{dr'}(r'\frac{d}{dr'}) - [1-f^2(r')], \tag{7.11}$$

$$\epsilon \;=\; \frac{|\tilde{g}|}{|a|} = 4\frac{\chi(\mu^2-\mu_c^2)}{|a|}. \tag{7.12}$$

Since we are working in the dSC phase $\tilde{g} < 0$ the perturbation $\epsilon > 0$. We have now cast the change in the free energy in the exact same form as we did for the QCD vortices in Chapter 4. The problem is now reduced to the analysis of the two-dimensional Schrödinger equation for a particle in an attractive potential $V(r') = -[1-f^2(r')]$. As before, this potential is negative everywhere and approaches zero at infinity. This means that the ground state eigenfunction $\hat{H}g_0 = \hat{E}g_0$ has a negative eigenvalue $\hat{E}$. The instability with respect to the formation of the AF condensate in the core occurs not for an arbitrarily small negative eigenvalue $\hat{E}$, but when the absolute value of $|\hat{E}|$ is large enough to overcome the positive contribution due to ϵ. Therefore, we immediately see that an AF core forms if $\hat{E}+\epsilon \leq 0$. If $|\tilde{g}|$ is greater than some critical

value $\tilde{g}_{\rm crit}$ then it is not energetically favorable for an antiferromagnetic core to form, and dSC vortices will possess a normal core where the symmetry is restored. Following the same procedure as in the QCD case, we have:

$$\frac{|\tilde{g}_{crit}|}{|a|} = 4\frac{\chi(\mu^2 - \mu_c^2)}{|a|} \simeq 0.2. \tag{7.13}$$

where for numerical estimates we used the variational approach developed in [42].

Above we have reviewed the basic properties of superconducting vortices with an antiferromagnetic core within the $SO(5)$ theory of superconductivity. We should emphasize once more that all results presented above are not new and have been discussed previously from a different perspective. Let us repeat the main results of this section once again: If $\tilde{g} = 0$ then the dSC vortices are unstable. If $0 < |\tilde{g}| < \tilde{g}_{\rm crit}$ then an AF core will form inside the dSC vortices. The width of the AF core in this case becomes larger and larger when we approach the phase transition line, *i.e.* $\tilde{g} \to 0$. Finally, if $|\tilde{g}| > \tilde{g}_{\rm crit}$ then the dSC vortices will have a normal core when symmetry is restored and $|\vec{m}|(r=0) = |\psi|(r=0) = 0$. In what follows we will always be working in the region of the phase diagram where $0 < |\tilde{g}| < \tilde{g}_{\rm crit}$ and dSC vortices have an AF core (which will be referred to as dSC/AF vortices). Now we will proceed to the next section and introduce vortons, loops of dSC/AF vortices which are stabilized by angular momentum.

7.4 Vortons in high temperature superconductivity

We will now consider the interesting possibility that loops of the dSC/AF vortices (vortons) can exist as classically stable objects (and at least metastable quantum mechanically). Vortons are also present within high density QCD as discussed in Chapter 5 of this thesis.

As Davis and Shellard originally pointed out in [30, 32, 33], if one has a theory which contains vortices with a condensate trapped on the core then loops of such vortices can form which are stabilized by angular momentum alone. We will consider a large loop of string of radius $R \gg \delta$, where δ is the vortex thickness, so that curvature effects can be neglected. The z-axis is defined along the length of the string, varying from 0 to $L = 2\pi R$ as one goes around the loop. Although we are considering a circular loop for simplicity at the moment, we realize that this is probably not the relevant physical case. The results we will discuss in this section should not depend on the geometry of the loop, the important point is the presence of conserved charges which are trapped on the vortex leading to stability. In reality, the final stable configuration of these vortex loops is probably a more complicated shape because of the quasi two-dimensional nature of the high temperature superconductors. In particular, we have neglected the difference between the transverse and tangential spatial directions in our treatment of the problem. The appropriate calculations would include this difference and lead to an asymmetric shape. However, we neglect these complications at this stage.

In order to make an analogy with the QCD case where the condensate on

the core is described by a complex field, we are free to represent two degrees of freedom represented by a unit Neel vector $\hat{m}$, $\hat{m}^2 = 1$ defined by Eq. (7.7) in terms of a single complex field Φ as,

$$\hat{m} = \left(\frac{\Phi + \Phi^*}{1 + |\Phi|^2}, \frac{\Phi - \Phi^*}{i(1 + |\Phi|^2)}, \frac{1 - |\Phi|^2}{1 + |\Phi|^2} \right), \tag{7.14}$$

where $\Phi = |\Phi| e^{i\alpha}$ (this is simply the projection of the unit sphere onto the complex plane). At this point we are free to pick the direction of the Neel vector. For a background classical field describing a vortex defined along the z direction, we will pick $\vec{m}$ to lie in the xy-plane so that $m_z = 0$. We should note that all calculations and results which follow do not depend on the particular choice of $\vec{m}$ that we have made above. However, we do expect that this will turn out to be the lowest energy configuration when higher order derivative terms are included in the free energy (see below). We neglect fluctuations of the absolute value $|\Phi|$ in the description of the classical background and only consider variation of its phase α. In this case, we have $|\Phi| = 1$ for the classical background field as it follows from the transformation (7.14), and $\vec{m}$ simplifies to:

$$\hat{m} = \frac{1}{2} (\Phi + \Phi^*, i(\Phi^* - \Phi), 0) . \tag{7.15}$$

with $|\Phi| = 1$ fixed. The condensate $|\Phi| \neq 0$ can carry currents and charges along the string so we will represent it by the following ansatz which describes the dependence of these excitations on z and t:

$$\Phi = |\Phi| e^{i\alpha(z,t)} = |\Phi| e^{i(kz - \omega t)}. \tag{7.16}$$

With this redefinition of the fields, the kinetic term acquires two additional

terms due to the (z,t) dependence of the phase in the core:

$$\frac{\chi}{2}\left[|\partial_0\vec{m}|^2 - v_s^2|\partial_z\vec{m}|^2\right] \rightarrow \tag{7.17}$$
$$\frac{\chi}{2}m^2(r)\left[(\partial_0\alpha(z,t))^2 - v_s^2(\partial_z\alpha(z,t))^2\right],$$

where $v_s^2 \equiv \rho/\chi$. As in Chapter 5, we will define a charge N which is topologically conserved:

$$N = \oint_C \frac{dz}{2\pi}\left(\frac{d\alpha}{dz}\right) = kR, \tag{7.18}$$

where the path C is defined along the vortex loop and we assume that ω and k are some constants along the loop. Since α can change by multiples of 2π in circling the vortex loop, N must be an integer. This is required in order for the condensate m to remain single valued.

In addition to the topologically conserved winding number N, there also exist the standard Noether charges and currents which can be trapped on the vortex core associated with the parameter ω, k included in the phase α above. In our case, the relevant symmetry, $SO(3)$, implies a conservation of three Noether charges:

$$Q_k = \int d^3r j_k^0 = i\chi \int d^3r[(\partial_0 m_a)\ (S_k)_{ab}\ m_b], \tag{7.19}$$

while the corresponding three currents are:

$$J_k^z = \int d^3r j_k^z, = -i\rho \int d^3r[(\partial_z m_a)\ (S_k)_{ab}\ m_b], \tag{7.20}$$

where S_k are the three generators of $SO(3)$.

A vortex loop with nonzero Noether charges Q_k and topological charge N trapped on the core is described by an ansatz of the following form which

depends on the position $\vec{r} = (r, \phi, z)$ and time t as (using Eqs. (7.6), (7.7), (7.14), and (7.16)):

$$\psi = \sqrt{\frac{|a|}{b}} f(r)\ e^{i\phi}, \tag{7.21}$$

$$\vec{m} = \sigma \sqrt{\frac{|a|}{b}} g(r)\,(\cos(kz - \omega t),\ \sin(kz - \omega t),\ 0)\,, \tag{7.22}$$

where as in the previous section $f(r), g(r)$ are solutions to the classical equations of motion obeying the appropriate boundary conditions.

For the solution given by Eq. (7.22) we have a nonzero Noether charge Q_z which is trapped on the vortex core:

$$Q_z = \chi L \omega \Sigma, \tag{7.23}$$

where Σ is defined as as the integral of $|\vec{m}|^2$ over the vortex cross section:

$$\Sigma = \int_{\times} d^2r\ |\vec{m}|^2. \tag{7.24}$$

We should note that for a different choice of the direction of Neel vector $\hat{m}$. the conserved charge which is nonzero would be different. The important point is that a nonzero charge will always be present independent of the of the Neel direction $\hat{m}$.

As discussed in Chapter 5, these vortons are spinning and carry angular momentum. The vortons are stable against shrinking due to the conservation of the angular momentum. To calculate the angular momentum of a vorton with nonzero charges N and Q_z trapped on the core, we use the standard formula for the angular momentum expressed in terms of the energy-momentum tensor:

$$M_{ij} = \int d^3r (T_{0i} x_j - T_{0j} x_i), \tag{7.25}$$

which can be approximated for a large vorton in the plane as

$$\begin{aligned} M &\simeq 2\pi\chi R^2\sigma^2\frac{|a|}{b}\int d^2r g(r)^2\omega k, \\ &= 2\pi\chi R^2\omega\ k\ \Sigma. \end{aligned} \tag{7.26}$$

The angular momentum points in the direction normal to the surface formed by the vorton. Angular momentum M [Eq. (7.26)], which is essentially the product of two charges N and Q_z is also nonzero when both charges N and Q_z are nonzero. In the discussion above we neglected the higher order derivative terms. In particular, there will be some correlation between the charge Q_i (7.19) and the momentum along the vorton $P_i = T_{0i}$ in the expression for the free energy ($\sim T_{0i}Q_i$). Such a correlation implies that the ansatz (7.15) will represent the lowest energy configuration if the angular momentum $\vec{M}$ (7.26) points in the direction normal to the surface formed by the vorton.

We will assume that we now have a vorton configuration with nonzero values of N and Q_z. In order to assign specific numbers for these quantities one must look at the mechanism of formation. We will not address such complex issues in this chapter and simply assume that there is some nonzero probability for a vorton to form. For recent work on the issue of vorton formation we refer the reader to [62]. The free energy of a vorton can be obtained by substituting Eqs. (7.21) and (7.22) into Eq. (7.8):

$$\begin{aligned} \mathcal{F} &= \int d^3r \left[\frac{\chi}{2}\left((\omega^2 + v_s^2n^2)m^2 + v_s^2(\nabla_r m)^2 + v_s^2|\nabla\psi|^2\right)\right. \\ &- \left.(|a| + \tilde{g})m^2 - |a||\psi|^2 + \frac{1}{2}b(m^4 + |\psi|^4 + 2m^2|\psi|^2)\right], \end{aligned} \tag{7.27}$$

where $m = \sigma\sqrt{|a|/b}\ g(r)$. We can simplify this expression further by using the fact that m is a solution to the equation of motion and represent the free

energy in the following way:

$$\mathcal{F} = L\left(\rho\pi\frac{|a|}{b}\ln(\Lambda/\xi) - \frac{b}{2}\Sigma_4 + \chi\omega^2\Sigma\right), \tag{7.28}$$

where we have defined the quantity Σ_4 for brevity:

$$\Sigma_4 = \int_\times d^2r|\vec{m}|^4. \tag{7.29}$$

The first term in Eq. (7.28) is simply the energy from the dSC vortex with no condensate present in the core (to logarithmic accuracy). Here Λ is the long distance cutoff which must be included to regulate the logarithmic divergence of the normal global string. The long distance cutoff is typically the distance between vortices, so in our case we will take $\Lambda = L$ where L is the length the vortex loop. The second term is negative, reflecting the fact that it is energetically favorable to have an AF core. And the third term is the additional contribution to the energy due to nonzero Q_z (N).

There are various cases which must be considered, $v_sk > \omega, v_sk < \omega$, and $v_sk = \omega$. Notice that the effect of having nonzero k and ω is the addition of a masslike term for $\vec{m}$ to the Lagrangian:

$$\delta\mathcal{L} = \frac{\chi}{2}(\omega^2 - v_s^2k^2)m^2. \tag{7.30}$$

If $v_sk > \omega$ then the effect of a nonzero v_sk, ω is to add a positive mass term for $|m|$ to the Lagrangian. This counteracts the effects of the negative mass term in the original Lagrangian (7.2). Since $k \sim 1/L$ quenching occurs and the size of the condensate Σ decreases as the vortex loop gets smaller. Conversely, if $\omega > v_sk$ one has the opposite situation and anti-quenching occurs. As the vortex loop shrinks, the size of the condensate Σ gets larger

as one would expect. The different cases have been examined using numerical calculations in [30, 32]. Recall, Eq. (7.23), where ω is given as

$$\omega = \frac{Q_z}{\chi L}\Sigma^{-1}. \tag{7.31}$$

As Davis and Shellard point out in [32] if ω starts out less than $v_s k$ quenching occurs and forces ω increase faster than Q_z/L. In the opposite case where $\omega > v_s k$ antiquenching occurs and therefore ω increases more slowly than Q_z/L. The important conclusion that was drawn from this analysis is that $\omega/(v_s k) \to 1$ is an attractor [32]. As a loop shrinks $\omega/(v_s k)$ approaches 1 and the quenching (or antiquenching) slows and the eventually stops leaving a classically stable vorton behind. Therefore, for simplicity we will focus on the so called chiral case when $\omega = v_s k$ which is the most stable configuration. Realistically, we know that the periodic structure of the material of the superconductor breaks the rotational symmetry, leading to non-conservation of angular momentum (it can be transferred to the material). However, the topological charge N is still a conserved quantity. Therefore, for the chiral vortons, $Q \sim N$ is also conserved due to relations (7.18) and (7.23). For such configurations, stability is ensured. When $\omega \neq v_s k$, the transfer of angular momentum to the lattice is possible, eventually settling to the chiral case with $\omega = v_s k$.

In the chiral case the size of the condensate Σ is independent of N, Q_z, L and the free energy (7.28) can be written as:

$$\begin{aligned} \mathcal{F} &= L\alpha_{\rm str} + (2\pi)^2 \rho \frac{N^2 \Sigma}{L}, \\ \alpha_{\rm str} &= \rho\pi \frac{|a|}{b} \ln(\Lambda/\xi) - \frac{b}{2}\Sigma_4, \end{aligned} \tag{7.32}$$

where $\alpha_{\rm str}$ is the string tension of the bare dSC/AF vortex with $Q_z = N = 0$ and k is expressed in terms of the conserved winding number N according to Eq. (7.18). Written in this form, it is immediately obvious that for a given nonzero value of N the free energy has a minimum at $L = L_0$:

$$\frac{N}{L_0} = \frac{1}{2\pi}\sqrt{\frac{\alpha_{\rm str}}{\rho\Sigma}}. \tag{7.33}$$

We can give a crude estimate of the winding number density, $n_0 \equiv N/L_0$, of a stable vorton configuration,

$$\Sigma \sim \sigma^2 \frac{|a|}{b}\delta_m^2, \tag{7.34}$$

$$\alpha_{\rm str} \sim \rho\frac{|a|}{b}, \tag{7.35}$$

where δ_m is the width of the condensate. This gives us:

$$n_0 \equiv \frac{N}{L_0} \sim \frac{1}{\delta_m} \sim \sqrt{|\tilde{g}|} \sim \sqrt{4\chi(\mu^2 - \mu_c^2)}, \tag{7.36}$$

which is approximately the inverse width of the condensate. As expected, the winding number density n_0 does not depend on the large number N, but depends only on the internal structure of the vorton, *i.e.* on the width of AF condensate in dSC vortex core. Equation (7.36) tells us that as one goes around a vorton the direction of the Neel vector $\hat{m}$ varies over a distance scale $\sim \delta_m$, the width of the condensate. As the doping is decreased and the AF-dSC phase boundary is approached from above the width of the condensate increases. For a given value of $N(Q_z)$ (determined at the time of formation) the size of a stable vorton increases as one approaches the AF-dSC phase boundary.

The discussion above has shown that vortons are indeed classically stable. This would imply that on the quantum mechanical level such quasiparticles

are at least metastable. As we have mentioned in Chapter 5, the issue of quantum stability of vortons was addressed in a recent paper [14]. In this paper they calculated the lifetime of a vorton with $Q = 0, N \neq 0$ (pure current case). The mechanism of decay is some quantum mechanical tunneling process where the condensate instantaneously goes to zero on the core, allowing the winding number to decrease by one unit from N to $N - 1$.

7.5 Conclusion

In this chapter we have reviewed the dSC vortices which have an antiferromagnetic core within the $SO(5)$ theory of high temperature superconductivity [1, 7, 59, 103]. We have compared these dSC/AF vortices with similar vortices which arise in a completely different context, high density QCD (as discussed in Chapter 4).

The main point that was presented in this chapter is that loops of dSC/AF vortices, called vortons, can exist as classically stable objects in the absence of an external magnetic field. The source of the stability of these vortons is the conservation of angular momentum that counteracts the string tension, which "prefers" to minimize the length of the vortex loop. The fact that there is a condensate trapped on the vortex core is crucial for the stability of vortons. It is the condensate which allows nonzero charges to be trapped on the core, leading to the presence of nonzero angular momentum. It remains to be seen if such quasiparticles will be important for the physics of the high T_c superconductors. In what follows, we will provide arguments supporting the idea that the vortons can play a key role in AF-dSC phase transition. At

this point we consider the vorton mechanism driving AF-dSC phase transition as a conjecture.

The first argument goes as follows. As we have shown above, for a given value of N there exists classically stable vorton configurations with size L and fixed ratio $N/L_0 \sim 1/\delta_m$, where δ_m is the width of the condensate that is trapped on the vortex core. As one decreases the doping parameter and approaches the AF-dSC phase boundary, the width of the condensate δ_m increases. This is the direct consequence of the fact that the asymmetry parameter $|\tilde{g}|$ becomes smaller and smaller when the phase boundary is approached. From the relation $L_0/N \sim \delta_m$ given above, this would imply that L_0, the length of a classically stable vorton, must increase. Decreasing the asymmetry parameter $|\tilde{g}| \sim 4\chi(\mu^2 - \mu_c^2)$ further would result in a large vorton with a large core size. The volume of the regions filled with the AF state behaves like $V_{\rm AF} \sim L_0\delta_m^2 \sim |\tilde{g}|^{-3/2}$. When the phase transition line is approached, the regions with the AF state fill the entire sample. At this point the AF-dSC phase transition occurs. Our approximations are no longer valid at this point, because our description assumes that the vorton core size is much smaller than L and the interaction between strings can be neglected (plus many other assumptions that we have made). These assumptions certainly fail in the vicinity of the phase transition. Nevertheless, the fact that the size of the AF regions inside of the dSC phase increases rapidly when the AF-dSC phase transition is approached should be considered as a strong argument in favor of the vorton mechanism driving the AF-dSC phase transition.

We would also like to make the observation that on the other side of the

phase transition boundary, in the AF state, there are quasiparticles (hedgehogs) whose cores are in dSC phase [39]. Therefore, one can imagine a situation where one type of quasiparticles (dSC vortices with an AF core) becomes a different type of quasiparticles (AF hedgehogs with a dSC core) when the doping parameter decreases and the phase transition line is crossed.

The next natural question to ask is as follows: let us assume that vortons are the relevant quasiparticles which drive AF-dSC phase transition at small temperatures. Can the same vortons be an essential part of the dynamics when the temperature T (rather than the chemical potential μ) crosses the superconducting phase transition at T_c? If the answer is positive, we would have a nice unified picture for two different phase transitions on the (T, μ) plane. We believe the answer is positive as the arguments given below suggest.

We start by reminding the reader that the pseudogap phase is characterized by the temperature $T_c < T < T^*$, when the Cooper pairs are already formed but the long-range phase coherence sets in only at the much lower temperature $T_c \ll T^*$. It is believed that in this regime the phase order is destroyed by fluctuating vortices of the Cooper pair field ψ above T_c [28, 102]. It is quite natural to *identify* our vortons (loops of vortices) sliced by a two dimensional plane with vortex-antivortex pairs with distinct experimental signatures from Ref. [28, 102]. In this case, since underdoped cuprates are effectively two-dimensional, at finite temperature the loss of phase order may be expected to proceed via the Berezinsky-Kosterlitz-Thouless phase transition. In this case, the vortons discussed in the present chapter, being sliced by the two-dimensional plane, become the vortex-antivortex pairs an-

alyzed in Ref. [28, 102] and could be responsible for the phase transition at T_c. However, the picture of the phase transition here is quite different from what we previously discussed regarding the AF-dSC phase boundary. In the present case, when T crosses T_c the transition happens because the vortex-antivortex interaction potential is proportional to $\rho\pi|a|/b\ln(x_1 - x_2)$ and not because the seeds of a new phase (the vorton cores) fill the entire space. This is the typical two dimensional form due to the global nature of the vortices (local strings do not possess this feature). The volume occupied by the vortex cores at this point is still much smaller than the volume of the system. It is well known that such a logarithmic interaction is a key element for understanding the Berezinsky-Kosterlitz-Thouless phase transition.

Encouraged by the argument given above, we extend our conjecture and assume that the same quasiparticles, vortons, are responsible not only for the AF-dSC phase transition but also for the phase transition separating the pseudogap and dSC phases at temperature T_c when $\mu > \mu_c$. The natural question to ask is: how does the critical temperature $T_c(\mu)$ depend on the chemical potential μ within this conjecture? To answer this question we recall that the critical temperature T_c for the Berezinsky-Kosterlitz-Thouless phase transition is proportional to the strength of the logarithmic interaction mentioned above. In our case it is nothing but the string tension determined (mainly) by the vacuum expectation value of the ψ field, Eq. (7.32), *i.e.* $T_c \sim \alpha_{\rm str}$. When $\mu = \mu_c$ the asymmetry parameter is zero and $\langle\psi^2\rangle = |a|/b$ is determined by the unperturbed coefficients a, b. The simplest way to determine how the expectation value of the field ψ varies when μ increases is to introduce the asymmetry parameter in the "symmet-

ric" manner[1] $\mathcal{F}_{asym} = -\tilde{g}(\vec{m}^2 - |\psi|^2)$ such that negative $\tilde{g}$ corresponds to the condensation of the ψ field, and positive $\tilde{g}$ corresponds to the condensation of the $\vec{m}$ field. This asymmetry parameter enters the string tension in dSC phase as follows, $\alpha_{\rm str} \sim (|a| - \tilde{g})/b$, $\tilde{g} < 0$. From this expression one can immediately deduce that $\alpha_{\rm str}$ (and therefore, T_c) will increase with μ when $\tilde{g}$, being negative, becomes larger and larger in magnitude. It is interesting to note that the very same conclusion has been reached in the original paper [103], where the increase of T_c with chemical potential was explained as a result of mass increase of the π triplet (see [103] for details).

Having presented our arguments supporting the conjecture that vortons might be the relevant degrees of freedom in the dSC phase at zero external magnetic field, we now conclude with a few remarks on how this picture can be experimentally tested. First, the possible experimental methods (such as μSR and inelastic neutron scattering) for observing AF vortex cores were discussed in Ref. [7] and we shall not repeat their analysis. However, we should mention that the fact that the AF cores do appear in the vortices [29, 50, 51, 64, 66, 67, 94] suggests that the $SO(5)$ model of high T_c superconductivity may be correct. Our original remark here is that the AF vortex core size is on the order of dSC coherence length far away from the point $\tilde{g} = 0$, and becomes larger when the chemical potential approaches μ_c at zero external magnetic field. We expect that the average size $\langle L \rangle$ of vortons grows with temperature, and therefore, correlations between AF cores will grow with temperature as well. Similar behavior is expected to occur when μ approaches μ_c at a fixed temperature. In this case the effect is expected

[1] This definition of asymmetry is different from what we used in the rest of the chapter.

to be even more pronounced because the volume occupied by the AF cores grows as $|\tilde{g}|^{-3/2}$, as discussed above, and therefore the correlations as well as the magnitude of the local electron magnetic fields should scale accordingly. This picture suggests that the AF correlation length is proportional to L and could be very large, much larger than any other scale of the problem. Apparently, such large AF correlation lengths have already been observed in [50, 51] and we would like to argue that this correlation is related to our vortons. One should remark here that such a large correlation length cannot be simply explained by the interaction between vortices (which have size $\xi \sim 20$ Å) because it would lead to a strong dependence on the Neel temperature as a function of the intervortex spacing controlled by the external magnetic field, while observations suggest that the Neel temperature is field independent [50, 51].

All the effects previously mentioned require the existence of the AF core in the vortex and they are not specifically sensitive to the existence of vortons, which is the subject of this work. The main feature of the vortons is that they can carry angular momentum [see Eq. (7.26)] and provide large AF correlation lengths (see discussion above). Therefore, these excitations should be present if a dSC sample is rotated with nonzero angular momentum. The situation is very similar to the ^3He and ^4He systems where superfluid vortices can be studied by rotating liquid helium in a can. In many respects our vortons are similar to rotons, and presumably can be studied in a similar way using the technique developed for these systems.

Chapter 8

Summary and Outlook

In this thesis we have presented various topological defects in the context of high density baryonic matter and high temperature superconductivity. In QCD at large baryon density the condensates (qq, K^0) that are formed spontaneously break various symmetries of the QCD Lagrangian that are respected at low baryon density. A consequence of this symmetry breaking is the formation of various topological defects. The domain walls, strings, and vortons that are present in high density QCD (discussed in Chapters 3, 4, and 5 of this thesis) may prove to be important for the physics of the interior of a neutron star, where the color superconducting phase of QCD may be realized. The application of these topological defects to neutron star physics is an interesting direction for future research, requiring extensive analytical calculations and numerical computations. We will briefly outline some of the outstanding problems below:

- *Glitches.* The rotational rate of a neutron star decreases over time as a result of magnetic torque. Glitches are periodic jumps in the rotational frequency, with $\Delta\Omega/\Omega \sim 10^{-8} - 10^{-6}$. The origin of these glitches is presently unknown, and they are thought to originate in the core of neutron stars, where the CFL+K^0 phase of high density QCD may be the correct ground state. As our estimates given in Chapter 5

indicate, K-vortons may carry angular momentum more efficiently than the usual way of carrying angular momentum in a superfluid state, which is straight vortices. The glitches may occur when a vorton(s) collides with the crust of the neutron star, resulting in the transfer of angular momentum and the observed increase in the rotational rate. In order to make a more definitive statement one must study the vorton dynamics. Specifically, it would be interesting to understand the the rate of formation, the interaction with the environment (such as the electric and magnetic fields), and an estimate of the lifetime (due to electromagnetic and weak interactions).

- *Cooling.* The conventional picture of the way a neutron star cools is through the emission of neutrinos. In the CFL+K^0 phase of high density QCD, the presence of K-vortons could alter the mean free path, as the cross section for neutrino-vorton scattering may be quite large, similar to the Aharonov-Bohm interaction of cosmic strings with matter [5].

- *Magnetic Fields.* The K-vortons discussed in this thesis are macroscopically large (compared with other scales) electrically charged objects due to the presence of the K^+ condensate that is trapped on the core of the vortons. These defects could alter the electromagnetic fields present in the core of neutron stars. In addition, the $U(1)_A$ strings that are attached to the $U(1)_A$ domain walls of Chapter 3 could also prove to be important. Although, they are not electrically charged, they couple to electromagnetism due to the "rotated" electromagnetism that

remains unbroken in high density QCD [38].

In Chapter 6 we have studied aspects of nuclear matter at densities slightly below the critical density where the color superconducting phase occurs. This phase is mainly composed of neutrons, with a small amount of protons and electrons. The neutrons form $^3P_2$ Cooper pairs and Bose condense to a superfluid state, while the protons form $^1S_0$ Cooper pairs and Bose condense to give a superconductor. We have shown that contrary to the standard picture, the proton superconductor may exhibit type-I rather than type-II superconductivity. This result could have various implications:

- *Glitches.* As mentioned above, glitches are sudden jumps that are observed in the rotational rates of neutron stars. In the superfluid core, it is the neutron vortices that carry angular momentum. The conventional picture is that the core is also characterized by a proton condensate that exhibits type-II superconductivity. The magnetic flux tubes that are present (due to the magnetic field) pin the neutron vortices [75]. As the the neutron star's rotational frequency decreases, the density of vortices in the superfluid core must also decrease, since the number of quantized vortices is proportional to the total angular momentum. However, if the neutron vortices (that carry angular momentum in the superfluid state) are pinned by the presence of magnetic flux tubes, there cannot be a continuous release of the neutron vortices as the period increases. As the rotation rate decreases, the stress on the vortices increases eventually overcoming the pinning forces holding them in place. The release of a large number of vortices leads to the transfer of angular momentum from the core to the crust, resulting in

a glitch in the rotational rate of the star. We have demonstrated in Chapter 6 that the proton superconductor may actually be a type-I superconductor. If this is the case, models for glitches that rely on neutron vortex-magnetic flux tube interactions [75] would have to be reconsidered. It would be interesting to consider the effect the presence of a nonzero proton condensate would have on the structure of the neutron vortices that carry angular momentum. In particular, the pinning force that is related to the size of the neutron vortex core [57] could be very different from the usual estimates.

- *Magnetic Field Structure.* If the inner core of a neutron star exhibits type-I superconductivity it may drastically alter the magnetic field structure. In this case the interior of a neutron star could consist of alternating domains of normal matter and superconducting (type-I) matter. This intermediate state of type-I superconductors was originally proposed by Landau [52]. The domains of normal matter support the magnetic field while the superconducting states exhibit the Meissner effect. The specific domain structure depends on various properties, such as the geometry. A complete understanding of the magnetic field structure in the interior of a neutron star would require detailed calculations. It would also be interesting to consider how the presence of a color superconducting core (which is not an electromagnetic superconductor) would affect the magnetic field structure when it is embedded in a type-I (proton) superconductor.

In Chapter 7 of this thesis we have also introduced a new type of topological defect in condensed matter physics, vortons in the $SO(5)$ model of high

temperature superconductivity in the cuprates. There are also a number of outstanding problems in understanding the high T_c superconductors where vortons may prove to be important degrees of freedom:

- *Coexistence of Antiferromagnetism and Superconductivity.* The vortons that are present in the $SO(5)$ model of high temperature superconductivity may provide an explanation of the coexistence of antiferromagnetism and superconductivity in the underdoped cuprates. In particular, experiments have suggested that up to 40% of the volume of the superconductors may be magnetically ordered regions that are $15 - 50$ Å in size, even in the presence of zero external magnetic field [46]. As discussed in Chapter 7, our estimates indicate that the volume of the superconducting state that is antiferromagnetic scales with the doping parameter μ as $V_{AF} \sim |\tilde{g}|^{-3/2}$, where $\tilde{g} = 4\chi(\mu^2 - \mu_c^2)$.

- *Large Scale Magnetic Correlations.* Recent experimental observations seem to indicate that the underdoped cuprate superconductors possess magnetism that is correlated over very large length scales ($\zeta > 400$ Å), much larger than any length scale that is present in the system [51]. These large magnetic correlation lengths may be explained by the presence of vortons, as the interaction between the vortons is nontrivial due to the presence of the charges trapped on the core. These charges may lead to an attractive interaction between vortons. For a network of vortons, this attractive interaction could produce the observed large scale magnetic correlation lengths.

- *Thermal Conductivity.* The anomalous behavior of the thermal conductivity in the cuprates remains a mystery up to this point. In the underdoped regime, the thermal conductivity of these materials increases when an external magnetic field is applied, contrary to the result in the overdoped samples [92]. It would be interesting to investigate if the addition of a new type of quasiparticles, vortons, could explain this result.

It is known that the CFL+K^0 phase may be realized in nature in neutron star interiors [36, 68, 101] and in the violent events associated with collapse of massive stars or collisions of neutron stars. It has been recently argued [70, 105] that such conditions may also occur in early universe during the QCD phase transition. In this case it might be important for cosmological problems, such as the dark matter problem and baryogenesis [70, 105]. It would be very interesting to test some of the ideas outlined in this thesis by doing laboratory experiment in the spirit of the Cosmology in the Laboratory (COSLAB) program. In particular, if vortons are indeed the relevant degrees of freedom in the high T_c superconductors, it provides a unique opportunity to study cosmology and astrophysics by doing laboratory experiments in condensed matter physics. Over the last few years several experiments have been done to test ideas drawn from cosmology (see the review papers [48, 49, 97] for further details). The study of topological defects in various systems is interesting as the applications seem to be wide, as we have eluded to above. We hope that the work done in this thesis will eventually help solve some of the problems listed above.

Bibliography

[1] S. Alama, A. J. Berlinsky, L. Bronsard, and T. Giorgi. Vortices with antiferromagnetic cores in the SO(5) theory of high temperature superconductivity. *Phys. Rev.*, B60:6901, 1999.

[2] M. G. Alford. Color superconducting quark matter. *Ann. Rev. Nucl. Part. Sci.*, 51:131–160, 2001.

[3] M. G. Alford, K. Rajagopal, and F. Wilczek. QCD at finite baryon density: Nucleon droplets and color superconductivity. *Phys. Lett.*, B422:247–256, 1998.

[4] M. G. Alford, K. Rajagopal, and F. Wilczek. Color-flavor locking and chiral symmetry breaking in high density QCD. *Nucl. Phys.*, B537:443–458, 1999.

[5] M. G. Alford and F. Wilczek. Aharonov-Bohm interaction of cosmic strings with matter. *Phys. Rev. Lett.*, 62:1071, 1989.

[6] A. F. Andreev and E. P. Bashkin. Three-velocity hydrodynamics of superfluid solutions. *Sov. Phys. JETP*, 42:164, 1975.

[7] D. Arovas, J. Berlinsky, C. Kallin, and S. C. Zhang. Superconducting vortex with antiferromagnetic core. *Phys. Rev. Lett.*, 79:2871, 1997.

[8] M. Balbo *et al.* $^3P_2 - {}^3F_2$ pairing in neutron matter with modern nucleon-nucleon potentials. *Phys. Rev.*, C58:1921, 1998.

[9] G. Baym, C. Pethick, and D. Pines. Superfluidity in neutron stars. *Nature*, 224:673–674, 1969.

[10] S. R. Beane, P. F. Bedaque, and M. J. Savage. Meson masses in high density QCD. *Phys. Lett.*, B483:131–138, 2000.

[11] P. F. Bedaque. Charged kaon condensation in high density quark matter. *Phys. Lett.*, B524:137–143, 2002.

[12] P. F. Bedaque and T. Schafer. High density quark matter under stress. *Nucl. Phys.*, A697:802–822, 2002.

[13] J. G. Bednorz and K. A. Muller. Possible high T_c superconductivity in the Ba-La-Cu-O system. *Z. Phys.*, B64:189, 1986.

[14] J. J. Blanco-Pillado, K. D. Olum, and A. Vilenkin. Quantum tunneling of superconducting string currents. *Phys. Rev.*, D66:023506, 2002.

[15] S. Bonazzola and P. Peter. Can high energy cosmic rays be vortons? *Astropart. Phys.*, 7:161–172, 1997.

[16] J. A. Bowers and K. Rajagopal. The crystallography of color superconductivity. *Phys. Rev.*, D66:065002, 2002.

[17] W. E. Brown, J. T. Liu, and H. Ren. The transition temperature to the superconducting phase of QCD at high baryon density. *Phys. Rev.*, D62:054016, 2000.

[18] K. B. W. Buckley. Classical stability of $U(1)_A$ domain walls in dense matter QCD. *Phys. Rev.*, D65:125011, 2002.

[19] K. B. W. Buckley, M. A. Metlitski, and A. R. Zhitnitsky. Drum vortons in high density QCD. *Phys. Rev.*, D68:105006, 2003.

[20] K. B. W. Buckley, M. A. Metlitski, and A. R. Zhitnitsky. Neutron stars as type-I superconductors. *arXiv:astro-ph/0308148*, 2003.

[21] K. B. W. Buckley and A. R. Zhitnitsky. Superconducting K strings in high density QCD. *JHEP*, 08:013, 2002.

[22] K. B. W. Buckley and A. R. Zhitnitsky. Vortons in the SO(5) model of high temperature superconductivity. *Phys. Rev.*, B67:174522, 2003.

[23] B. Carter, R. H. Brandenberger, and A. C. Davis. Thermal stabilisation of superconducting sigma strings and their drum vortons. *Phys. Rev.*, D65:103520, 2002.

[24] R. Casalbuoni and R. Gatto. Effective theory for color-flavor locking in high density QCD. *Phys. Lett.*, B464:111–116, 1999.

[25] S. R. Coleman. Q balls. *Nucl. Phys.*, B262:263, 1985.

[26] S. R. Coleman and E. Weinberg. Radiative corrections as the origin of spontaneous symmetry breaking. *Phys. Rev.*, D7:1888–1910, 1973.

[27] E. J. Copeland, N. Turok, and M. Hindmarsh. Dynamics of superconducting cosmic strings. *Phys. Rev. Lett.*, 58:1910–1913, 1987.

[28] J. Corson *et al.* Vanishing of phase coherence in underdoped $Bi_2Sr_2CaCu_2O_{8+d}$. *Nature*, 398:221, 1999.

[29] P. Dai *et al.* The connection between superconducting phase correlations and spin excitations in $YBa_2Cu_3O_{6.6}$: A magnetic field study. *Nature (London)*, 406:965, 2000.

[30] R. L. Davis. Semitopological solitons. *Phys. Rev.*, D38:3722, 1988.

[31] R. L. Davis and E. P. S. Shellard. The physics of vortex superconductivity. *Phys. Lett.*, B207:404, 1988.

[32] R. L. Davis and E. P. S. Shellard. The physics of vortex superconductivity. 2. *Phys. Lett.*, B209:485, 1988.

[33] R. L. Davis and E. P. S. Shellard. Cosmic vortons. *Nucl. Phys.*, B323:209–224, 1989.

[34] R. L. Davis and E. P. S. Shellard. Global strings and superfluid vortices. *Phys. Rev. Lett.*, 63:2021, 1989.

[35] J. Ding and et. al. Spectroscopic evidence for a pseudogap in the normal state of underdoped high-T_c superconductors. *Nature*, 382:51, 1996.

[36] J. J. Drake *et al.* Is RX J185635-375 a quark star? *Astrophys. J.*, 572:996–1001, 2002.

[37] M. M. Forbes and A. R. Zhitnitsky. Domain walls in QCD. *JHEP*, 10:013, 2001.

[38] M. M. Forbes and A. R. Zhitnitsky. Global strings in high density QCD. *Phys. Rev.*, D65:085009, 2002.

[39] P. M. Goldbart and D. E. Sheehy. Antiferromagnetic hedgehogs with superconducting cores. *Phys. Rev.*, B58:5731, 1998.

[40] W. N. Hardy, D. A. Bonn, D. C. Morgan, R. Liang, and K Zhang. Precision measurements of the temperature dependence of lambda in $YBa_2Cu_3O_6$.95: Strong evidence for nodes in the gap function. *Phys. Rev. Lett.*, 70:3999, 1993.

[41] H. Heiselberg and V. Pandharipande. Recent progress in neutron star theory. *arXiv:astro-ph/0003276*, 2000.

[42] C. T. Hill, H. M. Hodges, and M. S. Turner. Bosonic superconducting cosmic strings. *Phys. Rev.*, D37:263, 1988.

[43] M. James, L. Perivolaropoulos, and T. Vachaspati. Detailed stability analysis of electroweak strings. *Nucl. Phys.*, B395:534–546, 1993.

[44] D. B. Kaplan and S. Reddy. Charged and superconducting vortices in dense quark matter. *Phys. Rev. Lett.*, 88:132302, 2002.

[45] D. B. Kaplan and S. Reddy. Novel phases and transitions in quark matter. *Phys. Rev.*, D65:054042, 2002.

[46] B. Khaykovich *et al.* Enhancement of long-range magnetic order by magnetic field in superconducting La_2CuO_{4+y}. *arXiv:cond-mat/0112505*, 2001.

[47] T. W. B. Kibble. Topology of cosmic domains and strings. *J. Phys.*, A9:1387–1398, 1976.

[48] T. W. B. Kibble. Testing cosmological defect formation in the laboratory. *arXiv:cond-mat/0111082*, 2001.

[49] T. W. B. Kibble. Symmetry breaking and defects. *arXiv:cond-mat/0211110*, 2002.

[50] B. Lake *et al.* Spins in the vortices of a high temperature superconductor. *Science*, 291:1759, 2001.

[51] B. Lake *et al.* Antiferromagnetic order induced by an applied magnetic field in a high-temperature superconductor. *Nature (London)*, 415:299, 2002.

[52] L. D. Landau. *Sov. Phys. JETP*, 13:377, 1937.

[53] L. D. Landau and E. M. Lifshitz. *Quantum Mechanics: Non-relativistic Theory*, volume 3 of *Course of Theoretical Physics*. Pergamon Press, Oxford; New York, third edition, 1989, c1977.

[54] Y. Lemperiere and E. P. S. Shellard. On the behaviour and stability of superconducting currents. *Nucl. Phys.*, B649:511–525, 2003.

[55] Y. Lemperiere and E. P. S. Shellard. Vorton existence and stability. *arXiv:hep-ph/0305156*, 2003.

[56] B. Link. Constraining hadronic superfluidity with neutron star precession. *Phys. Rev. Lett.*, 91:101101, 2003.

[57] B. Link and C. Cutler. Vortex unpinning in precessing neutron stars. *arXiv:astro-ph/0108281*, (2001).

[58] U. Lombardo and H.-J. Schulze. Superfluidity in neutron stars. *Lect. Notes Phys.*, 578:30–53, 2001.

[59] R. MacKenzie and J. M. Cline. Solitons in SO(5) superconductivity. In A. Astbury, B. A. Campbell, F. C. Khanna, J. Pinfold, and M.G. Vincter, editors, *Electroweak Physics. Proceedings of the 1999 Lake Louise Winter Institute.* World Scientific, Singapore, 2000.

[60] R. Mackenzie, M. A. Vachon, and U. F. Wichoski. Interaction between vortices in models with two order parameters. *Phys. Rev.*, D67:105024, 2003.

[61] C. Manuel and M. H. G. Tytgat. Masses of the goldstone modes in the CFL phase of QCD at finite density. *Phys. Lett.*, B479:190–200, 2000.

[62] C. J. A. P. Martins and E. P. S. Shellard. Vorton formation. *Phys. Rev.*, D57:7155–7176, 1998.

[63] M. A. Metlitski and A. R. Zhitnitsky. Vortex rings in two component Bose-Einstein condensates. *arXiv:cond-mat/0307559*, 2003.

[64] R. I. Miller *et al.* Evidence for static magnetism in the vortex cores of ortho-II $YBa_2Cu_3O_{6.5}$. *Phys. Rev. Lett*, 88:137002, 2002.

[65] V. A. Miransky, I. A. Shovkovy, and L. C. R. Wijewardhana. The effective potential of composite diquark fields and the spectrum of resonances in dense QCD. *Phys. Lett.*, B468:270–278, 1999.

[66] V. F. Mitrovic *et al.* Spatially resolved electronic structure inside and outside the vortex cores of a high-temperature superconductor. *Nature (London)*, 413:501, 2001.

[67] V. F. Mitrovic *et al.* Antiferromagnetism in the vortex cores of $YBa_2Cu_3O_{7-\delta}$. *Phys. Rev.*, B67:220503, 2003.

[68] NASA Press Release. Cosmic X-rays reveal evidence for new form of matter. *see http://chandra.nasa.gov, http://chandra.harvard.edu*, April 10, 2002.

[69] M. R. Norman and C. Pepin. The electronic nature of high temperature cuprate superconductors. *arXiv:cond-mat/0302347*, 2003.

[70] D. H. Oaknin and A. R. Zhitnitsky. Baryon asymmetry, dark matter and quantum chromodynamics. *arXiv:hep-ph/0309086*, 2003.

[71] R. D. Pisarski and D. H. Rischke. Gaps and critical temperature for color superconductivity. *Phys. Rev.*, D61:051501, 2000.

[72] K. Rajagopal and F. Wilczek. The condensed matter physics of QCD. In M. Shifman, editor, *At the Frontier of Particle Physics / Handbook of QCD*. World Scientific, Singapore, 2001.

[73] R. Rapp, T. Schafer, E. V. Shuryak, and M. Velkovsky. Diquark bose condensates in high density matter and instantons. *Phys. Rev. Lett.*, 81:53–56, 1998.

[74] R. Rapp, T. Schafer, E. V. Shuryak, and M. Velkovsky. High-density QCD and instantons. *Annals Phys.*, 280:35–99, 2000.

[75] M. Ruderman, T. Zhu, and K. Chen. Neutron star magnetic field evolution, crust movement, and glitches. *Astrophys. J.*, 492:267–280, 1998.

[76] M. M. Salomaa and G. E. Volovik. Quantized vortices in superfluid ^3He. *Rev. Mod. Phys.*, 59:533–613, 1987.

[77] T. Schafer. Kaon condensation in high density quark matter. *Phys. Rev. Lett.*, 85:5531–5534, 2000.

[78] D. M. Sedrakian, A. Sedrakian, and G. F. Zharkov. Type I superconductivity in neutron stars. *Mon. Not. Roy. Astron. Soc.*, 290:203, 1997.

[79] S. L. Shapiro and S. A. Teukolsky. *Black Holes, White Dwarfs, and Neutron Stars-The Physics of Compact Objects.* John Wiley and Sons, Toronto, 1983.

[80] Z.-X. Shen and et. al. Anomalously large gap anisotropy in the a-b plane of $Bi_2Sr_2CaCu_2O_8$ + *delta*. *Phys. Rev. Lett.*, 70:1553, 1993.

[81] M. A. Shifman, A. I. Vainshtein, and V. I. Zakharov. Instanton density in a theory with massless quarks. *Nucl. Phys.*, B163:46, 1980.

[82] M. A. Shifman, A. I. Vainshtein, and V. I. Zakharov. Instantons in non-perturbative QCD vacuum. *Nucl. Phys.*, B165:45, 1980.

[83] E. V. Shuryak and A. R. Zhitnitsky. Domain wall bubbles in high energy heavy ion collisions. *Phys. Rev.*, C66:034905, 2002.

[84] D. T. Son. Superconductivity by long-range color magnetic interaction in high density quark matter. *Phys. Rev.*, D59:094019, 1999.

[85] D. T. Son. Light Goldstone boson and domain walls in the K^0-condensed phase of high density quark matter. *arXiv:hep-ph/0108260*, 2001.

[86] D. T. Son and M. A. Stephanov. Inverse meson mass ordering in color-flavor-locking phase of high density QCD. *Phys. Rev.*, D61:074012, 2000.

[87] D. T. Son and M. A. Stephanov. Inverse meson mass ordering in color-flavor-locking phase of high density QCD: Erratum. *Phys. Rev.*, D62:059902, 2000.

[88] D. T. Son, M. A. Stephanov, and A. R. Zhitnitsky. Domain walls of high-density QCD. *Phys. Rev. Lett.*, 86:3955–3958, 2001.

[89] D. T. Son, M. A. Stephanov, and A. R. Zhitnitsky. Instanton interactions in dense-matter QCD. *Phys. Lett.*, B510:167–172, 2001.

[90] J. M. Speight. Static intervortex forces. *Phys. Rev.*, D55:3830, 1997.

[91] I. H. Stairs, A. G. Lyne, and S. L. Shemar. Evidence for free precession in a pulsar. *Nature*, 406:484, 2000.

[92] X. F. Sun *et al.* Magnetic-field-induced localization of quasiparticles in underdoped $La_{2-x}Sr_xCuO_4$. *arXiv:cond-mat/0301339*, 2003.

[93] G. 't Hooft. Computation of the quantum effects due to a four- dimensional pseudoparticle. *Phys. Rev.*, D14:3432–3450, 1976.

[94] D. Vaknin, J. L. Zaretsky, and L. L. Miller. On the possibility of antiferromagnetic vortex cores in superconducting $Ba_2Cu_3O_{7-\delta}$,. *Physica*, C329:109, 2000.

[95] J. J. P. Veerman, D. Bazeia, and F. Moraes. Soliton stability in a Z(2) field theory. *J. Math. Phys.*, 40:3925, 1999.

[96] A. Vilenkin and E. P. S. Shellard. *Cosmic Strings and Other Topological Defects.* Cambridge University Press, Cambridge, 1994.

[97] G. E. Volovik. Superfluid analogies of cosmological phenomena. *Phys. Rept.*, 351:195–348, 2001.

[98] J. R. Waldram. *Superconductivity of Metals and Cuprates.* Institute of Physics Publishing, London, 1996.

[99] F. M. Walter and J. Lattimer. A revised parallax and its implications for RX J185635-3754. *Astrophys. J.*, 576:L145–L148, 2002.

[100] E. Witten. Superconducting strings. *Nucl. Phys.*, B249:557–592, 1985.

[101] R. X. Xu. Thermal featureless spectrum: Evidence for bare strange stars. *Astrophys. J.*, 570:L65–L68, 2002.

[102] Z. A. Xu *et al.* Vortex-like excitations and the onset of superconducting phase fluctuation in underdoped $La_{2-x}Sr_xCuO_4$. *Nature*, 406:486, 2000.

[103] S. C. Zhang. SO(5) quantum nonlinear sigma model theory of the high T_c superconductivity. *Science*, 275:1089, 1997.

[104] X. Zhang, T. Huang, and R. H. Brandenberger. Pion and eta strings. *Phys. Rev.*, D58:027702, 1998.

[105] A. R. Zhitnitsky. "Nonbaryonic" dark matter as baryonic color superconductor. *arXiv:hep-ph/0202161*, 2002.